

Doctoral Dissertation

**Analysis of Electromagnetic Scattering  
by Multiple Spheres Configuration  
and Its Applications**

学位論文：博士(工学) 甲第437号

By

Nguyen Tien Dong

SUBMITTED IN PARTIAL FULFILLMENT OF THE  
REQUIREMENTS FOR THE DEGREE OF  
DOCTOR OF PHILOSOPHY IN ENGINEERING

AT  
GIFU UNIVERSITY  
GIFU, JAPAN

March 2013

©Copyright by Nguyen Tien Dong, 2013

# Abstract

This dissertation presents the study of electromagnetic scattering by multiple spheres configuration and its two applications on the study of Scanning Near-field Optical Microscopy (SNOM) phenomenon and on the calculation of specific rain attenuation.

In this dissertation, exact solution to multiple scattering of electromagnetic waves by multiple spheres configuration is discussed. The solution is the result of the analysis method which builds upon the multipole expansions of electromagnetic fields, and the superposition of Mie theory. In this analysis, the scattering field is expressed as a superposition of vector harmonic expansions written about each sphere in the configuration. One of the most intractable problems in electromagnetic scattering by multiple spheres configuration is the evaluation of addition coefficients introduced by the addition theorems for vector spherical harmonics. The derivation of the analytical expressions for the addition coefficients is lengthy and complex while the computation of the addition coefficients is annoyingly time-consuming even with the reasonably fast computers available nowadays. This dissertation presents an efficient algorithm for calculating addition coefficients which is based on the recursive relation of scalar addition coefficients. Numerical results from the formulation derived in this dissertation agree with those of previous published results but the algorithm proposed here reduces the computational time considerably. This dissertation also discusses the strengths and limitations of other formulations and numerical techniques found in the literature.

Since this analytical method can be applied to multiple spheres of any size, even when they are in contact, we use it for studying the physical mechanism of the interaction between the probe tip and the sample in scanning near-field optical microscopy (SNOM) models. In these models, the probe tip is approximated to a sphere while the sample is approximated to a group of spheres with various sizes.

The method is also used to calculate the rain attenuation via the scattering and absorption of electromagnetic waves by multiple raindrops with sphere shape. In this dissertation, we focus on the quantitative evaluations considering the change of temperature, frequency and the existence of multiple scattering effects with three raindrop-size distributions: the negative exponential, the lognormal and Weibull distribution models.

*This page is intentionally left blank.*

# Acknowledgements

There are many people without whom this work would not have been possible.

First of all, I would like to express my deepest appreciation to my academic advisor, Associate Professor Masahiro Tanaka, who guided my studies on the field of computational electromagnetics. He deserves for a very special thank for his valuable instruction, and constant encouragement during my period of study at Gifu University.

I am also grateful to Professor Kazuo Tanaka for his valuable instruction during his course and the time at the Tanaka Laboratory.

I would like to thank Professor Yoshihiro Kawase at the same department for his helps and valuable instruction I received to complete my dissertation.

I would also like to thank Mr. Hirokazu Murakami for his helpful discussions during the time in Tanaka Laboratory at Gifu University.

My great thanks are due to Vietnamese and Japanese friends for their kind help and concern in many ways.

Thanks to the Japanese Government for the Monbukagakusho Scholarship during my study in Japan.

Finally, my warmest and most grateful thanks are due to my family. I would like to express my deep thanks to my parents, who made every effort to provide me with the excellent basic education, on which all of my progress is based. Last but not least, I would like to thank my wife Ngo Thi Hong Xiem for her understanding and love during the past few years. Her support and encouragement was in the end what made this dissertation possible.

Nguyen Tien Dong

Gifu, Japan

March 25, 2013



*This page is intentionally left blank.*

# Contents

<b>Abstract</b>	<b>i</b>
<b>Acknowledgements</b>	<b>iii</b>
<b>1 Introduction</b>	<b>1</b>
1.1 Overview of Electromagnetic Scattering by Multiple Spheres Configuration	1
1.2 Simulation and Experiment . . . . .	2
1.3 Motivation . . . . .	2
1.4 Organization of this Dissertation . . . . .	3
<b>2 Basic Theory of Electromagnetic Scattering</b>	<b>5</b>
2.1 Introduction . . . . .	5
2.2 Maxwell's Equations . . . . .	5
2.3 Boundary Conditions . . . . .	6
2.4 Vector Spherical Harmonics . . . . .	7
2.5 Multipole expansions of the incident field . . . . .	8
<b>3 Electromagnetic Scattering by Multiple Spheres Configuration</b>	<b>11</b>
3.1 Introduction . . . . .	11
3.2 One Sphere Configuration . . . . .	11
3.2.1 Mie theory . . . . .	11
3.2.2 Truncation number for Mie theory . . . . .	13
3.3 Multiple spheres configuration . . . . .	13
3.3.1 Formulation of Problem . . . . .	13
3.3.2 Incident coefficients . . . . .	15
3.3.3 Scattered coefficients . . . . .	16
3.3.4 Internal coefficients . . . . .	19
3.4 Scattering properties . . . . .	20
3.4.1 Near-field . . . . .	20
3.4.2 Far-field . . . . .	20
3.5 Comparison with previous articles . . . . .	23
3.5.1 Comparison the Efficiencies with Mackowski's results . . . . .	23

3.5.2	Comparison the Intensity Phase Function with Fuller and Kattawar's results . . . . .	24
3.5.3	Comparison the Radar Cross Sections with Bruning and Lo's results	24
3.6	Conclusion . . . . .	24
<b>4</b>	<b>Addition theorems and Addition coefficients</b>	<b>27</b>
4.1	Introduction . . . . .	27
4.2	Addition theorems . . . . .	28
4.2.1	Scalar addition theorems . . . . .	28
4.2.2	Vector addition theorems . . . . .	29
4.3	Explicit formula for addition coefficients . . . . .	29
4.4	Rotation coefficients . . . . .	30
4.5	Axial translation coefficients . . . . .	30
4.5.1	GX method . . . . .	31
4.5.2	VM method . . . . .	32
4.5.3	SM method . . . . .	33
4.6	SD method . . . . .	34
4.7	Results and Discussion . . . . .	35
4.7.1	Number of coefficients . . . . .	35
4.7.2	Execution time . . . . .	37
4.7.3	Numerical results . . . . .	39
4.8	Conclusion . . . . .	39
<b>5</b>	<b>Scanning Near-field Optical Microscopy</b>	<b>43</b>
5.1	Introduction . . . . .	43
5.2	Analysis method . . . . .	45
5.2.1	Formulation of problem . . . . .	45
5.2.2	Simulation of scanning . . . . .	46
5.2.3	Optimization of Computation . . . . .	46
5.3	Numerical Results . . . . .	46
5.3.1	One sphere sample . . . . .	47
5.3.2	Two and three spheres sample . . . . .	50
5.4	Conclusion . . . . .	50
<b>6</b>	<b>Rain Attenuation</b>	<b>53</b>
6.1	Introduction . . . . .	53
6.2	Raindrop Distribution Models . . . . .	54
6.2.1	Negative Exponential Distribution . . . . .	54
6.2.2	Lognormal Distribution . . . . .	55
6.2.3	Weibull Distribution . . . . .	55

6.3	Specific rain attenuation . . . . .	56
6.4	Numerical Results and Discussions . . . . .	56
6.4.1	Negative Exponential Distribution . . . . .	57
6.4.2	Lognormal Distribution . . . . .	57
6.4.3	Weibull Distribution . . . . .	57
6.4.4	Discussions . . . . .	58
6.5	Conclusion . . . . .	58
<b>7</b>	<b>Summary</b>	<b>65</b>
<b>Appendix A Vector Analysis</b>		<b>67</b>
A.1	Coordinate systems . . . . .	67
A.1.1	Rectangular Cartesian coordinates . . . . .	67
A.1.2	Spherical coordinates . . . . .	67
A.1.3	Conjugate coordinates . . . . .	68
A.1.4	Rotation of coordinates . . . . .	69
A.2	Vector Transformations . . . . .	70
A.2.1	Rectangular to Spherical (and vice versa) . . . . .	70
A.2.2	Rectangular to Conjugate (and vice versa) . . . . .	70
A.3	Vector differential operators . . . . .	71
A.3.1	Rectangular coordinates . . . . .	71
A.3.2	Spherical coordinates . . . . .	71
A.3.3	Conjugate coordinates . . . . .	72
A.4	Vector identities . . . . .	73
A.4.1	Addition and Multiplication . . . . .	73
A.4.2	Differentiation . . . . .	73
<b>Appendix B Special functions and their properties</b>		<b>75</b>
B.1	Associated Legendre functions . . . . .	75
B.1.1	Definition . . . . .	75
B.1.2	Properties . . . . .	75
B.2	Spherical Bessel functions . . . . .	76
B.2.1	Definition . . . . .	76
B.2.2	Properties . . . . .	77
<b>Appendix C Recursive relations of spherical harmonics</b>		<b>79</b>
C.1	Scalar spherical harmonics $u_{mn}$ . . . . .	79
C.2	Vector spherical harmonics $\mathbf{M}_{mn}$ . . . . .	79
C.3	Vector spherical harmonics $\mathbf{N}_{mn}$ . . . . .	80

<b>Bibliography</b>	<b>81</b>
<b>List of Publications by the Author</b>	<b>85</b>

# Chapter 1

## Introduction

### 1.1 Overview of Electromagnetic Scattering by Multiple Spheres Configuration

The Mie theory [1] is well-known to be the first approach to the electromagnetic scattering from homogeneous spheres endowed with all the accuracy of the Maxwell electromagnetic theory. As a consequence, after the publication of the Mie theory in 1908, several scattering objects were described in terms of equivalent spherical scatterers (multiple spheres configuration). It soon became evident, however, that the morphological details of the actual particles were often too important to be neglected, especially in some wavelength ranges. On the other hand, setting aside some particular cases in which the predictions of the Mie theory were acceptable, no viable alternative for the description of scattering from particles of arbitrary shape was at hand.

In the last few decades, progress has been made in developing light scattering theory for interacting spheres. The development of the addition theorems (by Friedman & Russek [2] in 1954, Stein [3] in 1961, and Cruzan [4] in 1962) opened up a new area in the theoretical study of multiple spheres scattering problems.

The first step toward the solution of the multiple spheres problem using the method of modal analysis is to solve the boundary conditions for the interactive scattering coefficients of each sphere in a spherical coordinate system with its origin at the center of the sphere. Bruning & Lo [5] (1971) were the first to publish such a solution for two interacting spheres. This solution given by Bruning & Lo is simple enough to deal with two spheres problem, but it is getting more and more complicated when the number of spheres increases. Later, in 1988, Fuller & Kattawar [6] extended Bruning & Lo's solution pair-wise to the case of an arbitrary ensemble of spheres. This solution was also independently obtained by Borghese et al. [7] in 1979 using Debye potentials. In 1991, Mackowski [8] proposed a new method to calculate the addition coefficients using recursive relations. After that, Xu [9] (1995) also proposed a different method to calculate the addition coefficients. Mackowski [10] (1999) and Xu [11] (2003) completed their solutions

of electromagnetic scattering by multiple spheres configurations with different methods. These solutions are real improvement over the Mie theory because several processes that occur, e.g., in the atmospheric aerosols and in the interstellar medium, can be interpreted in terms of clustering of otherwise spherical scatterers.

## 1.2 Simulation and Experiment

The scattering properties of multiple spheres configuration can be either computed theoretically or measured experimentally, and both approaches have their strengths and weaknesses. Theoretical modeling does not involve expensive instrumentation, can be used to compute any scattering characteristic, and often allows switching to another shape, size, refractive index, or orientation by changing a few lines in a code. However, accurate computations for realistic polydispersions of irregular particles can be very costly, if at all possible, and often have to be replaced by computations for simplified model shapes. Experimental measurements using visible or infrared light can deal with real particles, either natural or artificial. However, these experiments use complex and expensive hardware, are often incapable of simultaneously and accurately measuring all scattering characteristics, and traditionally suffer from the inability to characterize the sample precisely. The microwave analog technique allows a much greater degree of sample characterization and enables true controlled laboratory measurements, but involves even costlier equipment and cannot be readily applied to realistic particle polydispersions. It is thus clear that only a combination of various theoretical and experimental approaches can lead to a much improved knowledge of electromagnetic scattering by multiple spheres configuration.

## 1.3 Motivation

There are various mathematical methods that can be used to obtain a solution for the multiple spheres problem. Based on solving Maxwell's equation either analytically or numerically, these methods roughly fall into two categories: analytical methods and numerical methods.

Numerical methods use appropriate algorithms with a digital computer to obtain solution to Maxwell's equations. The solution are a set of numbers, such as numerical values for the electric field at points on a grid space for a particular set of times. Such solutions are not always useful for obtaining general physic understanding of electromagnetic phenomena. Nevertheless, numerical methods have an advantage in that they can be used to solve problems involving complicated geometries that are not solvable by standard analytical methods.

In the other hand, analytical methods use the separation of variables technique in

one of the few coordinate systems in which this equation is separable to search for the solution. Analytical methods provide solutions that are closed-form expressions for the electromagnetic field. These solutions can be examined to obtain physical understanding of electromagnetic phenomena.

From the above discussions, we use the analytical method to study the electromagnetic scattering by multiple spheres configuration.

## 1.4 Organization of this Dissertation

This dissertation contains seven chapters, including this introduction. Below is a summary of the major contents of each chapter.

In chapter 2, brief explanation about fundamentals of the electromagnetic scattering theory which are relevant in the analysis of electromagnetic scattering by multiple spheres configuration. We begin with a brief discussion on the physical background of Maxwells equations and boundary conditions. We then establish vector spherical wave expansions (or multipole expansions) for the incident field.

In chapter 3, the analysis of electromagnetic scattering by multiple spheres configuration is described. We review Mie theory as the simplest case with one sphere configuration and discuss about the truncation number of Mie theory. We then discuss about the formulation of multiple sphere configuration problem, and how to determine the incident, scattered and internal expansion coefficients. Near-field and far-field properties which are needed for this work are derived. We also shows the comparison between our method and the previous articles.

Because of the importance of the addition theorems and the complexity of the determination of addition coefficients, chapter 4 is used to discuss about the method to calculate the addition coefficients. We review three modern methods and propose the new method which reduces the required number of intermediate coefficients that improves considerably the computation speed, especially in case of large truncation number.

In chapter 5, we apply the proposed method discussed above to study the electromagnetic scattering in scanning near-field optical microscopy (SNOM) models. In these models, the probe tip and the sample approximates as sphere-based shapes with various size. Electromagnetic scattering field by these models should be analyzed and computed in both near-field and far-field.

In chapter 6, we apply the proposed method discussed above to study the electromagnetic scattering by rain. We calculate the rain attenuation via the scattering and absorption of electromagnetic waves by multiple raindrops with sphere shape. In this dissertation, we focus on the quantitative evaluations considering the change of temperature, frequency and the existence of multiple scattering effects with three raindrop-size distributions: the negative exponential, the lognormal and Weibull distribution models.



Chapter 7 is the summary of all this dissertation.

There are 3 appendices in this dissertation.

In appendix 1, a basic background about vector analysis used in this dissertation is provided. It contains the definition of coordinate systems, especially the conjugate coordinate system, and vector transformations between these coordinate systems.

In appendix 2, some special functions, such as associated Legendre functions and Bessel functions, and their recursive relations are summarized.

In appendix 3, we derive the recursive relations of scalar and vector spherical harmonics by using the recursive relations of Bessel and associated Legendre functions in conjugate coordinates.

# Chapter 2

## Basic Theory of Electromagnetic Scattering

### 2.1 Introduction

This chapter is devoted to present the fundamentals of the electromagnetic scattering theory which are relevant in the analysis of electromagnetic scattering by multiple spheres configuration. We begin with a brief discussion on the physical background of Maxwells equations and boundary conditions. We then establish vector spherical wave expansions (or multipole expansions) for the incident field.

### 2.2 Maxwell's Equations

The behavior of the macroscopic field at interior points in material media is governed by Maxwells equations [12]:

$$\nabla \times \mathbf{E} = -\frac{\partial \mathbf{B}}{\partial t} \quad (\text{Faraday's induction law}), \quad (2.1)$$

$$\nabla \times \mathbf{H} = \mathbf{J} + \frac{\partial \mathbf{D}}{\partial t} \quad (\text{Maxwell-Ampere law}), \quad (2.2)$$

$$\nabla \cdot \mathbf{D} = \rho \quad (\text{Gauss' electric field law}), \quad (2.3)$$

$$\nabla \cdot \mathbf{B} = 0 \quad (\text{Gauss' magnetic field law}), \quad (2.4)$$

where  $t$  is time,  $\mathbf{E}$  the electric field,  $\mathbf{H}$  the magnetic field,  $\mathbf{B}$  the magnetic flux density,  $\mathbf{D}$  the electric flux density and  $\rho$  and  $\mathbf{J}$  the electric charge density and current density, respectively.

The first three equations in Maxwells theory are independent, because the Gauss' magnetic field law can be obtained from Faradays law by taking the divergence and by setting the integration constant with respect to time equal to zero. Analogously, taking the divergence of Maxwell-Ampere law and using the Gauss' electric field law we obtain the continuity equation:

$$\nabla \cdot \mathbf{J} + \frac{\partial \rho}{\partial t} = 0, \quad (2.5)$$

which expresses the conservation of electric charge. The Gauss' magnetic field law and the continuity equation should be treated as auxiliary or dependent equations in the entire system of equations (2.1)–(2.5). The charge and current densities are associated with the so-called free charges, and for a sourcefree medium,  $\mathbf{J} = 0$  and  $\rho = 0$ . In this case, the Gauss' electric field law can be obtained from Maxwell-Ampere law and only the first two equations in Maxwell's theory are independent.

In our analysis we will assume that all fields and sources are time harmonic. With  $\omega$  being the circular frequency and  $i = \sqrt{-1}$ , we write

$$\mathbf{E}(\mathbf{r}, t) = \text{Re} \{ \mathbf{E}(\mathbf{r}) e^{-i\omega t} \} \quad (2.6)$$

and similarly for other field quantities. The vector field  $\mathbf{E}(\mathbf{r})$  in the frequency domain is a complex quantity, while  $\mathbf{E}(\mathbf{r}, t)$  in the time domain is real. The harmonic time factor  $e^{-i\omega t}$  is assumed throughout this work and is suppressed hereafter.

Since the problem of multiple spheres configuration deals with a source free homogeneous medium (electric permittivity  $\varepsilon$  and magnetic permeability  $\mu$ ) of each sphere, the Maxwell's equations become:

$$\nabla \times \mathbf{E} = i\omega\mu\mathbf{H}, \quad (2.7a)$$

$$\nabla \times \mathbf{H} = -i\omega\varepsilon\mathbf{E}. \quad (2.7b)$$

## 2.3 Boundary Conditions

A boundary condition is associated with each of Maxwell's equations. We a surface boundary joining two different media 1 and 2 and let  $\mathbf{n}$  be the surface normal pointing toward medium 2 (Fig. 2.1). The boundary conditions corresponding to Maxwell's equations are as follows. The tangential component of  $\mathbf{E}$  is continuous:

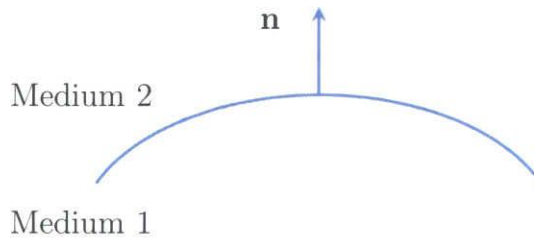


**Figure 2.1:** A surface boundary between two different media.

$$\mathbf{n} \times (\mathbf{E}_2 - \mathbf{E}_1) = 0, \quad (2.8)$$

The discontinuity in tangential component of  $\mathbf{H}$  equals surface current density  $\mathbf{J}_s$ :

$$\mathbf{n} \times (\mathbf{H}_2 - \mathbf{H}_1) = \mathbf{J}_s, \quad (2.9)$$

The normal component of  $\mathbf{B}$  is continuous:

$$\mathbf{n} \cdot (\mathbf{B}_2 - \mathbf{B}_1) = 0, \quad (2.10)$$

The discontinuity in tangential component of  $\mathbf{D}$  equals surface charge density  $\rho_s$ :

$$\mathbf{n} \cdot (\mathbf{D}_2 - \mathbf{D}_1) = \rho_s. \quad (2.11)$$

Since the problem of multiple spheres configuration deals with a source free homogeneous medium of each sphere, the boundary conditions become:

$$\mathbf{n} \times (\mathbf{E}_2 - \mathbf{E}_1) = 0, \quad (2.12a)$$

$$\mathbf{n} \times (\mathbf{H}_2 - \mathbf{H}_1) = 0, \quad (2.12b)$$

## 2.4 Vector Spherical Harmonics

Time-harmonic fields scattered by a sphere must satisfy the vector Helmholtz equation

$$\nabla \times \nabla \times \mathbf{F} - \tilde{k}^2 \mathbf{F} = 0, \quad (2.13)$$

where  $\mathbf{F}$  is the vector field  $\mathbf{E}$  or  $\mathbf{H}$ ,  $\tilde{k}^2 = \omega^2 \mu \varepsilon$  is the wave number,  $\mu$  and  $\varepsilon$  are the magnetic permeability and electric permittivity, respectively. Stratton (1941) [12] shows that there are two independent vector solutions to equation (2.13),

$$\mathbf{M}_{mn}^{(J)} = \nabla u_{mn}^{(J)} \times \mathbf{r}, \quad (2.14a)$$

$$\mathbf{N}_{mn}^{(J)} = \frac{1}{\tilde{k}} \nabla \times \mathbf{M}_{mn}^{(J)}, \quad (2.14b)$$

where  $\mathbf{r}$  is the position vector for the spherical coordinate system  $O$  with coordinates  $(r, \theta, \phi)$  and the scalar potentials  $u_{mn}^{(J)}$  are characteristic solutions of the scalar wave equation,

$$\nabla^2 u + \tilde{k}^2 u = 0, \quad (2.15)$$

and are given by,

$$u_{mn}^{(J)} = z_n^{(J)} (\tilde{k}r) P_n^m(\cos \theta) e^{im\phi}; \quad 0 \leq n \leq \infty, -n \leq m \leq n. \quad (2.16)$$

$z_n^{(J)}$  is the appropriate kind of spherical Bessel or Hankel functions  $j_n, y_n, h_n^{(1)}$ , and  $h_n^{(2)}$ , for  $J = 1, 2, 3$ , and  $4$ , respectively; we use only the value of  $J = 1$  and  $J = 3$  in our work.  $P_n^m$  is the associated Legendre function without phase factor  $(-1)^m$  (see Appendix B). From (2.14) and (2.16), the vector spherical harmonics<sup>†</sup> can be written in the explicit

---

<sup>†</sup>We denote  $\mathbf{M}_{mn}^{(J)}(\rho, \theta, \phi)$  and  $\mathbf{N}_{mn}^{(J)}(\rho, \theta, \phi)$  as  $\mathbf{M}_{mn}^{(J)}, \mathbf{N}_{mn}^{(J)}$ , respectively where  $\rho = \tilde{k}r$  is the normalized distance from the observation point to the origin  $O$ .

forms,

$$\mathbf{M}_{mn}^{(J)} = [\hat{\mathbf{e}}_\theta i\pi_{mn}(\theta) - \hat{\mathbf{e}}_\phi \tau_{mn}(\theta)] z_n^{(J)}(\rho) \exp(im\phi), \quad (2.17a)$$

$$\begin{aligned} \mathbf{N}_{mn}^{(J)} = & \left\{ \hat{\mathbf{e}}_r n(n+1) P_n^m(\cos\theta) \frac{z_n^{(J)}(\rho)}{\rho} \right. \\ & \left. + [\hat{\mathbf{e}}_\theta \tau_{mn}(\theta) + \hat{\mathbf{e}}_\phi i\pi_{mn}(\theta)] \frac{[\rho z_n^{(J)}(\rho)]'}{\rho} \right\} \exp(im\phi), \end{aligned} \quad (2.17b)$$

where  $(\hat{\mathbf{e}}_r, \hat{\mathbf{e}}_\theta, \hat{\mathbf{e}}_\phi)$  are the unit vectors in the spherical coordinates, The prime denotes differentiation with respect to argument. The functions  $\pi_{mn}(\theta)$  and  $\tau_{mn}(\theta)$  are defined by

$$\pi_{mn}(\theta) = \frac{m}{\sin\theta} P_n^m(\cos\theta), \quad (2.18a)$$

$$\tau_{mn}(\theta) = \frac{d}{d\theta} P_n^m(\cos\theta). \quad (2.18b)$$

Clearly  $\mathbf{M}_{mn}^{(J)}$  has no radial component and hence all radial fields must be represented by  $\mathbf{N}_{mn}^{(J)}$  alone. Therefore, H modes (TE) which have only a magnetic radial component, have the magnetic field  $\mathbf{H}$  represented by  $\mathbf{N}_{mn}^{(J)}$  and the electric field  $\mathbf{E}$  by  $\mathbf{M}_{mn}^{(J)}$ ; for E modes (TM), the opposite is true.

## 2.5 Multipole expansions of the incident field

An arbitrary incident electromagnetic field, which generally involves both types of modes, can be written as [12],

$$\mathbf{E}_{inc} = - \sum_{n=1}^{\infty} \sum_{m=-n}^n i E_{mn} [p_{mn} \mathbf{N}_{mn}^{(1)} + q_{mn} \mathbf{M}_{mn}^{(1)}], \quad (2.19a)$$

$$\mathbf{H}_{inc} = - \frac{\tilde{k}}{\omega\mu} \sum_{n=1}^{\infty} \sum_{m=-n}^n E_{mn} [q_{mn} \mathbf{N}_{mn}^{(1)} + p_{mn} \mathbf{M}_{mn}^{(1)}]. \quad (2.19b)$$

This is usually referred to as a multipole, modal, or partial wave expansion.  $(p_{mn}, q_{mn})$  is the expansion coefficients for the incident field,  $\omega$  and  $\mu$  are the circular frequency and magnetic permeability, respectively. The prefactor  $E_{mn}$  is introduced as a normalization constant to maintain numerical stability,

$$E_{mn} = E_0 i^n \left[ \frac{(2n+1)(n-m)!}{n(n+1)(n+m)!} \right]^{1/2}, \quad (2.20)$$

where  $E_0$  is the magnitude of the incident wave.

The incident coefficients  $p_{mn}$  and  $q_{mn}$  are determined by

$$p_{mn} = \frac{i \int_0^{2\pi} \int_0^\pi \mathbf{E}_{inc} \cdot \mathbf{N}_{mn}^{(1)*} \sin \theta d\theta d\phi}{E_{mn} \int_0^{2\pi} \int_0^\pi |\mathbf{N}_{mn}^{(1)}|^2 \sin \theta d\theta d\phi}, \quad (2.21a)$$

$$q_{mn} = \frac{i \int_0^{2\pi} \int_0^\pi \mathbf{E}_{inc} \cdot \mathbf{M}_{mn}^{(1)*} \sin \theta d\theta d\phi}{E_{mn} \int_0^{2\pi} \int_0^\pi |\mathbf{M}_{mn}^{(1)}|^2 \sin \theta d\theta d\phi}. \quad (2.21b)$$

*This page is intentionally left blank.*

# Chapter 3

## Electromagnetic Scattering by Multiple Spheres Configuration

### 3.1 Introduction

This chapter describes the analysis of electromagnetic scattering by multiple spheres configuration. In Section 3.2, we review Mie theory as the simplest case with one sphere configuration. We also discuss about the truncation number and how to expand the limit range of Mie theory. Section 3.3 shows the formulation of problem, and how to determine the incident, scattered and internal expansion coefficients. Near-field and far-field properties which are needed for this work are derived and some numerical results to demonstrate our work are described in Section 3.4. Section 3.5 shows the comparison between our method and the previous articles.

### 3.2 One Sphere Configuration

#### 3.2.1 Mie theory

The complete solution to the problems of light scattering by single, isotropic, and homogeneous sphere was found by Gustav Mie (1908) with the well known Mie theory [1]. The given sphere has the size parameter of  $x = \tilde{k}a$  ( $a$  is the radius of the sphere) and the refractive index of  $m$ . Without loss of generality, we assume the incident plane wave propagates in the  $z$ -direction ( $\tilde{\mathbf{k}}_{inc} = \tilde{k}\hat{\mathbf{e}}_z$ ) and is polarized in the  $x$ -direction (see Fig. 3.1).

$$\mathbf{E}_{inc} = E_0 \exp(i\tilde{k}z)\hat{\mathbf{e}}_x \quad (3.1)$$

where  $(\hat{\mathbf{e}}_x, \hat{\mathbf{e}}_y, \hat{\mathbf{e}}_z)$  are the orthonormal unit vectors in the Cartesian coordinate system.

Multipole expansions for the incident, scattered and internal electromagnetic fields



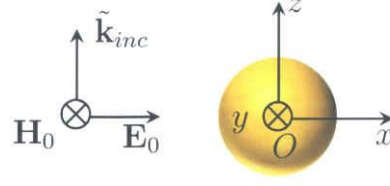


**Figure 3.1:** One sphere configuration.

are given by,

$$\mathbf{E}_{inc} = - \sum_{n=1}^{\infty} i E_{1n} \left[ p_{1n} \mathbf{N}_{1n}^{(1)} + q_{1n} \mathbf{M}_{1n}^{(1)} \right], \quad (3.2a)$$

$$\mathbf{H}_{inc} = - \frac{\tilde{k}}{\omega \mu} \sum_{n=1}^{\infty} E_{1n} \left[ q_{1n} \mathbf{N}_{1n}^{(1)} + p_{1n} \mathbf{M}_{1n}^{(1)} \right]. \quad (3.2b)$$

$$\mathbf{E}_{sca} = \sum_{n=1}^{\infty} i E_{1n} \left[ a_{1n} \mathbf{N}_{1n}^{(3)} + b_{1n} \mathbf{M}_{1n}^{(3)} \right], \quad (3.3a)$$

$$\mathbf{H}_{sca} = \frac{\tilde{k}}{\omega \mu} \sum_{n=1}^{\infty} E_{1n} \left[ b_{1n} \mathbf{N}_{1n}^{(3)} + a_{1n} \mathbf{M}_{1n}^{(3)} \right]. \quad (3.3b)$$

$$\mathbf{E}_{int} = - \sum_{n=1}^{\infty} i E_{1n} \left[ d_{1n} \mathbf{N}_{1n}^{(1)} + c_{1n} \mathbf{M}_{1n}^{(1)} \right], \quad (3.4a)$$

$$\mathbf{H}_{int} = - \frac{\tilde{k}}{\omega \mu_{int}} \sum_{n=1}^{\infty} E_{1n} \left[ c_{1n} \mathbf{N}_{1n}^{(1)} + d_{1n} \mathbf{M}_{1n}^{(1)} \right]. \quad (3.4b)$$

where  $(p_{1n}, q_{1n})$ ,  $(a_{1n}, b_{1n})$  and  $(d_{1n}, c_{1n})$  are the incident, scattered and incident coefficients, respectively;  $\tilde{k}$  is the wave number,  $\tilde{k} = \frac{2\pi}{\lambda}$  ( $\lambda$  is the wavelength of the incident radiation);  $\omega$  is the circular frequency,  $\mu$  and  $\mu_{int}$  are the magnetic permeability outside and inside the sphere, respectively. The factor  $E_{1n}$  is given by Eqn. (2.20) when  $m = 1$ ,

$$E_{1n} = E_0 i^n \frac{\sqrt{2n+1}}{n(n+1)}. \quad (3.5)$$

The incident coefficients  $(p_{1n}, q_{1n})$  are determined by,

$$p_{1n} = q_{1n} = \frac{\sqrt{2n+1}}{2}. \quad (3.6)$$

Across the surface of the sphere, the tangential components of the electric and magnetic fields are continuous,

$$(\mathbf{E}_{inc} + \mathbf{E}_{sca} - \mathbf{E}_{int}) \times \hat{\mathbf{e}}_r = 0, \quad (\mathbf{H}_{inc} + \mathbf{H}_{sca} - \mathbf{H}_{int}) \times \hat{\mathbf{e}}_r = 0. \quad (3.7)$$

### 3.3. MULTIPLE SPHERES CONFIGURATION

By applying the above boundary conditions and utilizing the orthogonality properties of the spherical harmonics, the scattered coefficients  $(a_{1n}, b_{1n})$  can be expressed in terms of the incident coefficients  $(p_{1n}, q_{1n})$  by,

$$a_{1n} = \alpha_n p_{1n}, \quad b_{1n} = \beta_n q_{1n}, \quad (3.8)$$

where  $(\alpha_n, \beta_n)$  are the Mie coefficients given by,

$$\alpha_n = \frac{m\psi'_n(x)\psi_n(mx) - \psi_n(x)\psi'_n(mx)}{m\xi'_n(x)\psi_n(mx) - \xi_n(x)\psi'_n(mx)}, \quad (3.9)$$

$$\beta_n = \frac{\psi'_n(x)\psi_n(mx) - m\psi_n(x)\psi'_n(mx)}{\xi'_n(x)\psi_n(mx) - m\xi_n(x)\psi'_n(mx)}, \quad (3.10)$$

where  $\psi_n(\rho) = \rho j_n(\rho)$  and  $\xi_n(\rho) = \rho h_n^{(1)}(\rho)$ ,  $j_n$  and  $h_n^{(1)}$  are the spherical Bessel and spherical Hankel function of the first kind, respectively; the prime denotes differentiation with respect to argument.

The internal coefficients  $(d_{1n}, c_{1n})$  are related to the scattering coefficients by

$$d_{1n} = \frac{im}{m\psi'_n(x)\psi_n(mx) - \psi_n(x)\psi'_n(mx)} a_{1n}, \quad (3.11a)$$

$$c_{1n} = \frac{im}{\psi'_n(x)\psi_n(mx) - m\psi_n(x)\psi'_n(mx)} b_{1n}. \quad (3.11b)$$

#### 3.2.2 Truncation number for Mie theory

The index  $n$  in Mie coefficients  $(\alpha_n, \beta_n)$  runs from 1 to  $\infty$ , but the infinite series occurring in Mie formulas can be truncated at a maximum  $N_{max}$ . There are a relation between the normalized radius  $x$  and the truncation number  $N_{max}$  suggested by Wiscombe [13],

$$N_{max} = \begin{cases} x + 4x^{1/3} + 1, & 0.02 \leq x \leq 8, \\ x + 4.05x^{1/3} + 2, & 8 < x < 4200, \\ x + 4x^{1/3} + 2, & 4200 \leq x \leq 20000. \end{cases} \quad (3.12)$$

Since the normalized radius  $x = \tilde{k}a$  depends on the wave number  $\tilde{k} = \frac{2\pi}{\lambda}$  and sphere radius  $a$ , the truncation number and the wavelength are in inverse ratio.

## 3.3 Multiple spheres configuration

### 3.3.1 Formulation of Problem

We solve the electromagnetic scattering problem of a multiple spheres configuration with  $N_s$  spheres, each characterized by a normalized radius  $x^i = \tilde{k}a^i$ , a relative refractive index  $m^i$ , and a normalized position  $O^i(X^i, Y^i, Z^i)$  in the global coordinates  $OXYZ$ , where  $\tilde{k} = \frac{2\pi}{\lambda}$  is the wave number,  $\lambda$  is the incident wavelength in the surrounding

medium (see Fig. 3.2). We use harmonic time dependence  $\exp(-i\omega t)$  for all field quantities, where  $\omega$  is the circular frequency,  $i = \sqrt{-1}$ . In  $O^i$  coordinate system centered on sphere  $i$ , the expansion of incident, scattered and internal fields are given by

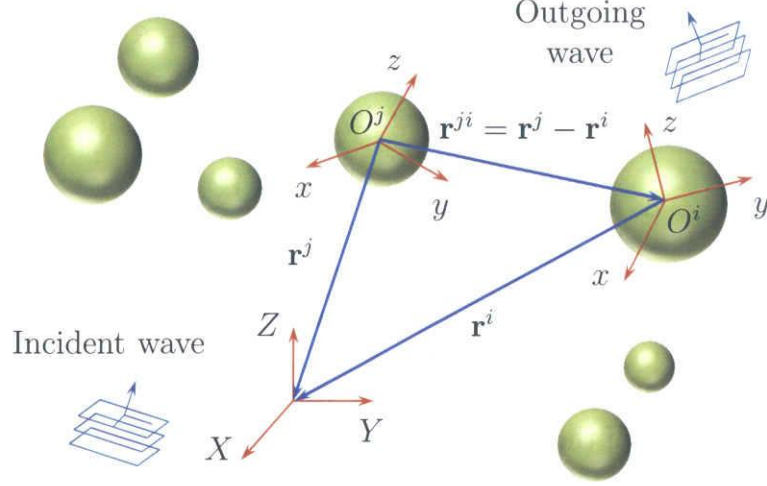


**Figure 3.2:** Multiple spheres configuration.

$$\mathbf{E}_{inc}^i = - \sum_{n=1}^{\infty} \sum_{m=-n}^n i E_{mn} [p_{mn}^i \mathbf{N}_{mn}^{(1)} + q_{mn}^i \mathbf{M}_{mn}^{(1)i}], \quad (3.13a)$$

$$\mathbf{H}_{inc}^i = - \frac{\tilde{k}}{\omega \mu} \sum_{n=1}^{\infty} \sum_{m=-n}^n E_{mn} [q_{mn}^i \mathbf{N}_{mn}^{(1)} + p_{mn}^i \mathbf{M}_{mn}^{(1)i}], \quad (3.13b)$$

$$\mathbf{E}_{sca}^i = \sum_{n=1}^{\infty} \sum_{m=-n}^n i E_{mn} [a_{mn}^i \mathbf{N}_{mn}^{(3)i} + b_{mn}^i \mathbf{M}_{mn}^{(3)i}], \quad (3.14a)$$

$$\mathbf{H}_{sca}^i = \frac{\tilde{k}}{\omega \mu} \sum_{n=1}^{\infty} \sum_{m=-n}^n E_{mn} [b_{mn}^i \mathbf{N}_{mn}^{(3)i} + a_{mn}^i \mathbf{M}_{mn}^{(3)i}], \quad (3.14b)$$

$$\mathbf{E}_{int}^i = - \sum_{n=1}^{\infty} \sum_{m=-n}^n i E_{mn} [d_{mn}^i \mathbf{N}_{mn}^{(1)i} + c_{mn}^i \mathbf{M}_{mn}^{(1)i}], \quad (3.15a)$$

$$\mathbf{H}_{int}^i = - \frac{\tilde{k}}{\omega \mu_{int}^i} \sum_{n=1}^{\infty} \sum_{m=-n}^n E_{mn} [c_{mn}^i \mathbf{N}_{mn}^{(1)i} + d_{mn}^i \mathbf{M}_{mn}^{(1)i}], \quad (3.15b)$$

where  $(p_{mn}^i, q_{mn}^i)$ ,  $(a_{mn}^i, b_{mn}^i)$  and  $(d_{mn}^i, c_{mn}^i)$  are the expansion coefficients for the incident, scattered and internal fields, respectively.  $\mu$  and  $\mu_{int}^i$  are magnetic permeability outside the spheres and inside sphere  $i$ , respectively. The prefactor  $E_{mn}$  is defined (as in Eqn. 2.20) by,

$$E_{mn} = E_0 i^n \left[ \frac{(2n+1)(n-m)!}{n(n+1)(n+m)!} \right]^{1/2}, \quad (3.16)$$

where  $E_0$  is the magnitude of the incident wave.

### 3.3.2 Incident coefficients

#### Arbitrary incident plane wave:

The incident plane wave propagates in the direction  $\tilde{\mathbf{k}}_{inc}$  defined by the polar angle  $\beta_p$  and the azimuth angle  $\alpha_p$  with respect to the coordinate system. The incident wave is linear polarized, with the electric vector  $\mathbf{E}_0$  at the angle  $\gamma_p$  from the  $\tilde{\mathbf{k}}_{inc}$ - $Z$  plane (see Fig. 3.3).  $(\alpha_p, \beta_p, \gamma_p)$  are also the ZYZ Euler angles which can be defined in Fig. 3.4. The incident electric field of sphere  $i$  can be expressed by [14],

$$\mathbf{E}_{inc}^i = \mathbf{E}_0 \exp(i\tilde{\mathbf{k}}_{inc} \cdot \mathbf{r}^i). \quad (3.17)$$

The incident coefficients are given by

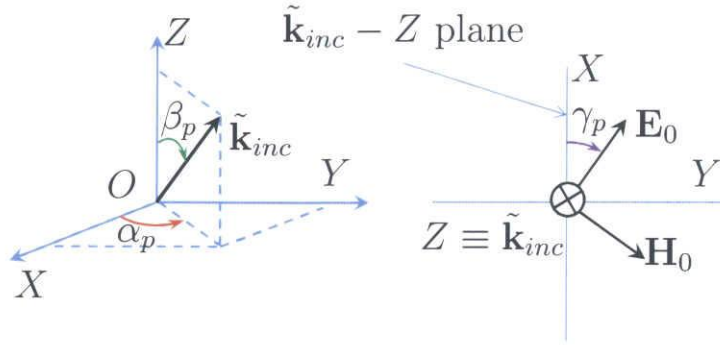


**Figure 3.3:** Illustration of arbitrary incident wave.

$$\begin{bmatrix} p_{mn}^i \\ q_{mn}^i \end{bmatrix} = \begin{bmatrix} p_{mn}^0 \\ q_{mn}^0 \end{bmatrix} \exp \left\{ i\tilde{k} \left[ Z^i \cos \beta_p + \sin \beta_p (X^i \cos \alpha_p + Y^i \sin \alpha_p) \right] \right\}, \quad (3.18)$$

$$p_{mn}^0 = C_{mn} [\tau_{mn}(\beta_p) \cos \gamma_p - i\pi_{mn}(\beta_p) \sin \gamma_p] \exp(-im\alpha_p), \quad (3.19a)$$

$$q_{mn}^0 = C_{mn} [\pi_{mn}(\beta_p) \sin \gamma_p - i\tau_{mn}(\beta_p) \cos \gamma_p] \exp(-im\alpha_p), \quad (3.19b)$$

where

$$C_{mn} = \left[ \frac{(2n+1)(n-m)!}{n(n+1)(n+m)!} \right]^{1/2} = i^{-n} \frac{E_{mn}}{E_0}. \quad (3.20)$$

#### Z propagation incident plane wave:

Without loss of generality, the incident plane wave vector always points to the positive  $Z$  direction. The incident wave has a linear polarization angle  $\alpha_p$  and is characterized by the wave vector  $\tilde{\mathbf{k}}_{inc} = \tilde{k}\hat{\mathbf{e}}_z$ , where  $\hat{\mathbf{e}}_z$  together with  $\hat{\mathbf{e}}_x, \hat{\mathbf{e}}_y$  are the orthonormal unit vectors in the Cartesian coordinate system.

$$p_{mn}^i = \exp(i\tilde{k}Z^i) m\delta_{|m|,1} \frac{\sqrt{2n+1}}{2} \exp(-im\alpha_p), \quad (3.21a)$$

$$q_{mn}^i = -\exp(i\tilde{k}Z^i) \delta_{|m|,1} \frac{\sqrt{2n+1}}{2} \exp(-im\alpha_p), \quad (3.21b)$$

where Kronecker delta  $\delta_{|m|,1} = 1$  if  $|m| = 1$  and  $\delta_{|m|,1} = 0$  if  $|m| \neq 1$ .

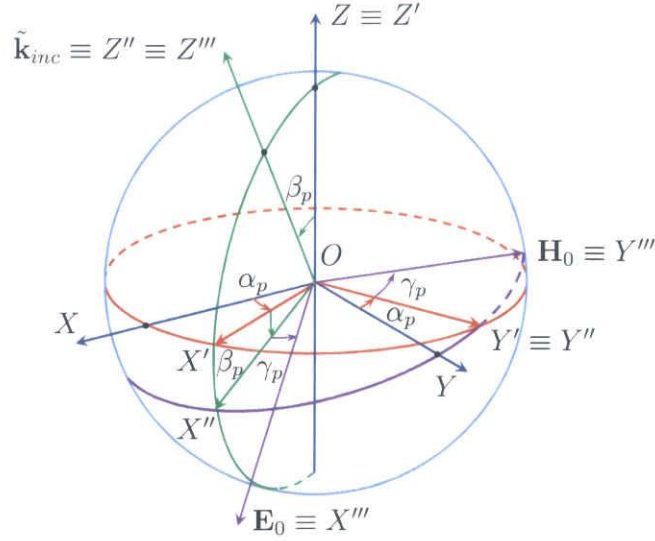


**Figure 3.4:** Illustration of arbitrary incident wave with ZYZ Euler angles  $(\alpha_p, \beta_p, \gamma_p)$ .

### 3.3.3 Scattered coefficients

#### Superposition of Mie theory

The complete scattered electric field is given by a sum over all  $N_s$  spheres

$$\mathbf{E}_{sca} = \sum_{i=1}^{N_s} \mathbf{E}_{sca}^i. \quad (3.22)$$

By using the superposition of Mie theory, electric field of sphere  $i$  can be expressed as

$$\mathbf{E}_{sca}^i = \mathcal{M} \left( \mathbf{E}_{inc}^i + \sum_{\substack{j=1 \\ j \neq i}}^{N_s} \mathbf{E}_{sca}^j \right), \quad (3.23)$$

where the symbol  $\mathcal{M}$  denotes the application of Mie theory. The Mie coefficients for sphere  $i$  depend on the normalized radius  $x^i$  and the relative refractive index  $m^i$  as

$$\alpha_n^i = \frac{m^i \psi'_n(x^i) \psi_n(m^i x^i) - \psi_n(x^i) \psi'_n(m^i x^i)}{m^i \xi'_n(x^i) \psi_n(m^i x^i) - \xi_n(x^i) \psi'_n(m^i x^i)}, \quad (3.24a)$$

$$\beta_n^i = \frac{\psi'_n(x^i) \psi_n(m^i x^i) - m^i \psi_n(x^i) \psi'_n(m^i x^i)}{\xi'_n(x^i) \psi_n(m^i x^i) - m^i \xi_n(x^i) \psi'_n(m^i x^i)}, \quad (3.24b)$$

where  $\psi_n(z) = z j_n(z)$  and  $\xi_n(z) = z h_n^{(1)}(z)$ ,  $j_n$  and  $h_n^{(1)}$  are the spherical Bessel and spherical Hankel functions of the first kind, respectively.

In the case of sphere  $i$  is a perfect conductor, equation (3.24) is reduced to:

$$\alpha_n^i = \frac{\psi'_n(x^i)}{\xi'_n(x^i)}, \quad \beta_n^i = \frac{\psi_n(x^i)}{\xi_n(x^i)}. \quad (3.25)$$

Imposing the standard boundary conditions for electromagnetic fields at the surface of the spheres gives a set of inhomogeneous linear equation for the coefficients  $(a_{mn}^i, b_{mn}^i)$



$$a_{mn}^i = \alpha_n^i \left[ p_{mn}^i - \sum_{\substack{j=1 \\ j \neq i}}^{N_s} \sum_{l=1}^{\infty} \sum_{k=-l}^l (A_{mn}^{kl} a_{kl}^j + B_{mn}^{kl} b_{kl}^j) \right], \quad (3.26a)$$

$$b_{mn}^i = \beta_n^i \left[ q_{mn}^i - \sum_{\substack{j=1 \\ j \neq i}}^{N_s} \sum_{l=1}^{\infty} \sum_{k=-l}^l (A_{mn}^{kl} b_{kl}^j + B_{mn}^{kl} a_{kl}^j) \right], \quad (3.26b)$$

where  $(a_{mn}^i, b_{mn}^i)$  are scattered coefficients,  $(p_{mn}^i, q_{mn}^i)$  are incident coefficients,  $(\alpha_n^i, \beta_n^i)$  are Mie coefficients for sphere  $i$ ,  $(A_{mn}^{kl}, B_{mn}^{kl})$  are addition coefficients<sup>†</sup>. The addition theorems for vector spherical harmonics, which transform harmonics from one coordinate system into another are used to calculate the addition coefficients.

### 'Order of scattering' solution

Armed with the recursive relations developed above, the scattered coefficients  $a_{mn}, b_{mn}$  for each sphere can be calculated from equation (3.26) using an appropriate linear equation solution technique.

An efficient solution technique is the 'order of scattering' method developed by Fuller & Kattawar [6]. This method, which is essentially an iterative scheme, is based upon the physical concept of multiple reflections. The external field of a given sphere can always be decoposed into the incident field plus the field arising from first, second, third, and higher reflections off of neighboring spheres. The scattered coefficients for this sphere can thus be expressed as a series of 'partial' scattered coefficients, each corresponding to the particular reflection order of the external field. Using this approach, the system of equation for the scattered coefficients, equation (3.26), can be written,

$$a_{mn}^i = \sum_{p=1}^{\infty} a_{mn}^{i,p}, \quad (3.27a)$$

$$b_{mn}^i = \sum_{p=1}^{\infty} b_{mn}^{i,p}, \quad (3.27b)$$

$$a_{mn}^{i,p+1} = -\alpha_n^i \sum_{\substack{j=1 \\ j \neq i}}^{N_s} \sum_{l=1}^{\infty} \sum_{k=-l}^l [A_{mn}^{kl} a_{kl}^{j,p} + B_{mn}^{kl} b_{kl}^{j,p}], \quad (3.28a)$$

$$b_{mn}^{i,p+1} = -\beta_n^i \sum_{\substack{j=1 \\ j \neq i}}^{N_s} \sum_{l=1}^{\infty} \sum_{k=-l}^l [A_{mn}^{kl} b_{kl}^{j,p} + B_{mn}^{kl} a_{kl}^{j,p}], \quad (3.28b)$$

---

<sup>†</sup>We use  $A_{mn}^{kl}, B_{mn}^{kl}$  instead of  $A_{mn}^{kl}(\tilde{k}\mathbf{r}^{ji}), B_{mn}^{kl}(\tilde{k}\mathbf{r}^{ji})$ .

$$a_{mn}^{i,0} = \alpha_n^i p_{mn}^i, \quad (3.29a)$$

$$b_{mn}^{i,0} = \beta_n^i q_{mn}^i. \quad (3.29b)$$

We denote  $(a_{mn}^{ji,p}, b_{mn}^{ji,p})$  as the 'translated' scattered coefficients,

$$a_{mn}^{ji,p+1} = \alpha_n^i \sum_{l=1}^{\infty} \sum_{k=-l}^l [A_{mn}^{kl} a_{kl}^{j,p} + B_{mn}^{kl} b_{kl}^{j,p}], \quad (3.30a)$$

$$b_{mn}^{ji,p+1} = \beta_n^i \sum_{l=1}^{\infty} \sum_{k=-l}^l [A_{mn}^{kl} b_{kl}^{j,p} + B_{mn}^{kl} a_{kl}^{j,p}]. \quad (3.30b)$$

Equation (3.28) can be rewritten,

$$a_{mn}^{i,p+1} = - \sum_{\substack{j=1 \\ j \neq i}}^{N_s} a_{mn}^{ji,p}, \quad (3.31a)$$

$$b_{mn}^{i,p+1} = - \sum_{\substack{j=1 \\ j \neq i}}^{N_s} b_{mn}^{ji,p}. \quad (3.31b)$$

### Three-step technique

We use Mackowski's the three-step technique [8] which decomposes addition coefficients  $(A_{mn}^{kl}, B_{mn}^{kl})$  into rotation coefficients  $R_{mn}^k$  and axial translation coefficients  $(A_{mn}^{ml}, B_{mn}^{ml})$  as

$$A_{mn}^{kl} \equiv (R_{mn}^k)^{-1} (\theta^{ji}, \phi^{ji}, 0) A_{mn}^{ml} (\rho^{ji}) R_{mn}^k (\theta^{ji}, \phi^{ji}, 0), \quad (3.32)$$

$$B_{mn}^{kl} \equiv (R_{mn}^k)^{-1} (\theta^{ji}, \phi^{ji}, 0) B_{mn}^{ml} (\rho^{ji}) R_{mn}^k (\theta^{ji}, \phi^{ji}, 0). \quad (3.33)$$

where  $(A_{mn}^{ml}, B_{mn}^{ml})$  are the special case of  $(A_{mn}^{kl}, B_{mn}^{kl})$  when  $k = m$  ( $\theta^{ji} = 0, \phi^{ji} = 0$ ). The calculation of axial translation coefficients  $(A_{mn}^{ml}, B_{mn}^{ml})$  and rotation coefficients  $R_{mn}^k$  are described in chapter 4.

By using recursive relations, we can calculate the 'translated' scattered coefficients with 3 steps (see Fig. 3.5).

**Step 1:** The coordinate system of sphere  $j$  is rotated so that the  $z$ -axis of sphere  $j$  points towards the origin of sphere  $i$ . The Euler angles for this rotation are  $\alpha = \phi^{ji}, \beta = \theta^{ji}$  and  $\gamma = 0$ , and the transformation yields,

$$a_{mn}^{j,p+1} = \sum_{k=-n}^n D_{mn}^k (\theta^{ji}) \exp ik\phi^{ji} a_{kn}^{j,p}, \quad (3.34a)$$

$$b_{mn}^{j,p+1} = \sum_{k=-n}^n D_{mn}^k (\theta^{ji}) \exp ik\phi^{ji} b_{kn}^{j,p}. \quad (3.34b)$$

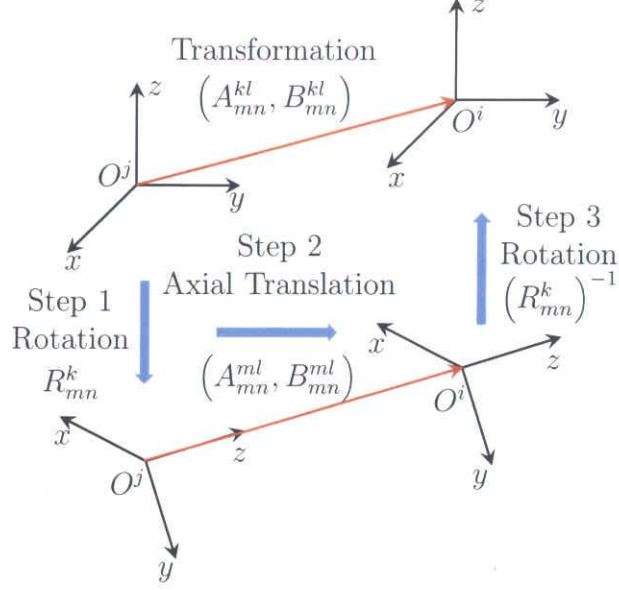


**Figure 3.5:** Three steps to calculate scattered coefficients.

**Step 2:** The rotated coefficients at sphere  $j$  are axially translated to the origin of sphere  $i$ ,

$$a_{mn}^{'ji,p+1} = \alpha_n^i \sum_{l=1}^{\infty} \left[ A_{mn}^{ml} \left( \tilde{k}r^{ji} \right) a_{ml}^{'j,p+1} + B_{mn}^{ml} \left( \tilde{k}r^{ji} \right) b_{ml}^{'j,p+1} \right], \quad (3.35a)$$

$$b_{mn}^{'ji,p+1} = \beta_n^i \sum_{l=1}^{\infty} \left[ A_{mn}^{ml} \left( \tilde{k}r^{ji} \right) b_{ml}^{'j,p+1} + B_{mn}^{ml} \left( \tilde{k}r^{ji} \right) a_{ml}^{'j,p+1} \right]. \quad (3.35b)$$

**Step 3:** The coefficients are rotated back to the original orientation. For this rotation, the Euler angles are  $\alpha = \pi, \beta = \phi^{ji}$  and  $\gamma = \pi - \phi^{ji}$ . This completes the translation transformation,

$$a_{mn}^{ji,p+1} = (-1)^m \exp(-im\phi^{ji}) \sum_{k=-n}^n (-1)^k D_{mn}^k(\theta^{ji}) a_{kn}^{'ji,p+1}, \quad (3.36a)$$

$$b_{mn}^{ji,p+1} = (-1)^m \exp(-im\phi^{ji}) \sum_{k=-n}^n (-1)^k D_{mn}^k(\theta^{ji}) b_{kn}^{'ji,p+1}. \quad (3.36b)$$

In these equations,  $D_{mn}^k(\beta)$  is the  $\beta$ -rotation coefficient, and is defined in section 4.4.

### 3.3.4 Internal coefficients

Similarly to one sphere problem, the internal coefficients  $(d_{mn}^i, c_{mn}^i)$  are related to the scattering coefficients by

$$d_{mn}^i = \frac{im^i}{m^i \psi_n'(x^i) \psi_n(m^i x^i) - \psi_n(x^i) \psi_n'(m^i x^i)} a_{mn}^i, \quad (3.37a)$$

$$c_{mn}^i = \frac{im^i}{\psi_n'(x^i) \psi_n(m^i x^i) - m^i \psi_n(x^i) \psi_n'(m^i x^i)} b_{mn}^i. \quad (3.37b)$$

If sphere  $i$  is a perfect conductor, the internal coefficients  $d_{mn}^i = 0$  and  $c_{mn}^i = 0$ .



## 3.4 Scattering properties

### 3.4.1 Near-field

We suppose that the point  $F$  has  $(r^{iF}, \theta^{iF}, \phi^{iF})$  in the spherical coordinates of sphere  $i$ .

Once the scattered coefficients  $(a_{mn}^i, b_{mn}^i)$  are calculated, the total electric field at point  $F$  (outside of the spheres) can be calculated by,

$$\mathbf{E}_{out}^F = \mathbf{E}_{sca}^F + \mathbf{E}_{inc}^F, \quad (3.38)$$

where  $\mathbf{E}_{inc}^F$  is the incident electric field at point  $F$  and  $\mathbf{E}_{sca}^F$  is the total scattered electric field at point  $F$  caused by all spheres.

$$\begin{aligned} \mathbf{E}_{inc}^F = E_0 [ & \hat{\mathbf{e}}_x (\cos \alpha \cos \beta \cos \gamma - \sin \alpha \sin \gamma) + \hat{\mathbf{e}}_y (\sin \alpha \cos \beta \cos \gamma + \cos \alpha \sin \gamma) \\ & - \hat{\mathbf{e}}_z \sin \alpha \cos \gamma ] \exp \{ -i [ Z^F \cos \beta + \sin \beta (X^F \cos \alpha + Y^F \sin \alpha) ] \}, \end{aligned} \quad (3.39)$$

$$\mathbf{E}_{sca}^F = \sum_{i=1}^{N_s} \sum_{n=1}^{\infty} \sum_{m=-n}^n iE_{mn} [a_{mn}^i \mathbf{N}_{mn}^{(3)}(r^{iF}, \theta^{iF}, \phi^{iF}) + b_{mn}^i \mathbf{M}_{mn}^{(3)}(r^{iF}, \theta^{iF}, \phi^{iF})]. \quad (3.40)$$

The total electric field at point  $F$  (inside sphere  $i$ ) is

$$\mathbf{E}_{in}^F = - \sum_{n=1}^{\infty} \sum_{m=-n}^n iE_{mn} [d_{mn}^i \mathbf{N}_{mn}^{(1)i}(r^{iF}, \theta^{iF}, \phi^{iF}) + c_{mn}^i \mathbf{M}_{mn}^{(1)i}(r^{iF}, \theta^{iF}, \phi^{iF})], \quad (3.41)$$

where

$$\mathbf{M}_{mn}^{(J)} = [\hat{\mathbf{e}}_{i\theta} i\pi_{mn}(\theta^{iF}) - \hat{\mathbf{e}}_{i\phi} \tau_{mn}(\theta^{iF})] z_n^{(J)}(\rho^{iF}) \exp(im\phi^{iF}), \quad (3.42a)$$

$$\begin{aligned} \mathbf{N}_{mn}^{(J)} = & \left\{ \hat{\mathbf{e}}_{ir} n(n+1) P_n^m(\cos \theta^{iF}) \frac{z_n^{(J)}(\rho^{iF})}{\rho^{iF}} \right. \\ & \left. + [\hat{\mathbf{e}}_{i\theta} \tau_{mn}(\theta^{iF}) + \hat{\mathbf{e}}_{i\phi} i\pi_{mn}(\theta^{iF})] \frac{[\rho z_n^{(J)}(\rho)]'_{\rho=\rho^{iF}}}{\rho^{iF}} \right\} \exp(im\phi^{iF}), \end{aligned} \quad (3.42b)$$

$(\hat{\mathbf{e}}_{ir}, \hat{\mathbf{e}}_{i\theta}, \hat{\mathbf{e}}_{i\phi})$  are the unit vectors in spherical coordinate system of  $O^i$ ;  $\rho^{iF} = \tilde{k}r^{iF}$ ; the prime denotes differentiation with respect to argument. In order to calculate  $\mathbf{E}_{out}^F$  and  $\mathbf{E}_{in}^F$ , the spherical coordinate system of  $O^i$  should be converted to the global Cartesian coordinates  $OXYZ$  before taking the summation (see Appendix A).

### 3.4.2 Far-field

In the far-field region, by using the asymptotic limit of the Hankel function  $h_n^{(1)}$ , the  $r$  component of the far-field electromagnetic wave will be vanished  $\lim_{r \rightarrow \infty} \hat{\mathbf{e}}_r \cdot \mathbf{E}_{sca} = 0$ . The

$\theta$  and  $\phi$  components of this wave can be expressed in terms of a single coordinate system by the form

$$\mathbf{E}_{sca}^\theta = E_0 \frac{e^{i\tilde{k}r}}{-i\tilde{k}r} \sum_{n=1}^{\infty} \sum_{m=-n}^n C_{mn} [a_{mn}^T \tau_{mn}(\theta) + b_{mn}^T \pi_{mn}(\theta)] \exp(im\phi), \quad (3.43)$$

$$\mathbf{E}_{sca}^\phi = E_0 \frac{e^{i\tilde{k}r}}{-i\tilde{k}r} \sum_{n=1}^{\infty} \sum_{m=-n}^n iC_{mn} [a_{mn}^T \pi_{mn}(\theta) + b_{mn}^T \tau_{mn}(\theta)] \exp(im\phi), \quad (3.44)$$

where  $C_{mn}$  is defined in equation (3.20), and

$$a_{mn}^T = \sum_{i=1}^{N_s} a_{mn}^i \exp(-i\tilde{\mathbf{k}}_{sca} \cdot \Delta^i), \quad (3.45)$$

$$b_{mn}^T = \sum_{i=1}^{N_s} b_{mn}^i \exp(-i\tilde{\mathbf{k}}_{sca} \cdot \Delta^i), \quad (3.46)$$

with  $\tilde{\mathbf{k}}_{sca} \cdot \Delta^i = \tilde{k} (X^i \sin \theta \cos \phi + Y^i \sin \theta \sin \phi + Z^i \cos \theta)$ , and  $(X^i, Y^i, Z^i)$  is the Cartesian coordinates of the center of sphere  $i$  in the choosen global coordinate system.

#### (a) Amplitude matrix $\mathbb{S}$

The relation between incident and scattered amplitudes in far zone is written in matrix form

$$\begin{bmatrix} E_{sca}^\theta \\ -E_{sca}^\phi \end{bmatrix} = \frac{e^{i\tilde{k}r}}{-i\tilde{k}r} \mathbb{S} \begin{bmatrix} \cos \phi & -\sin \phi \\ \sin \phi & \cos \phi \end{bmatrix} \begin{bmatrix} E_{inc}^x \\ -E_{inc}^y \end{bmatrix}, \quad (3.47)$$

The  $x$  and  $y$  components of the incident wave with linear polarization angle  $\gamma_p$  (see Fig. 3.3) as follow,

$$E_{inc}^x = E_0 \cos(\gamma_p), \quad (3.48a)$$

$$E_{inc}^y = E_0 \sin(\gamma_p), \quad (3.48b)$$

The amplitude matrix  $\mathbb{S}$  is defined by

$$\mathbb{S} = \begin{bmatrix} S_2 & S_3 \\ S_4 & S_1 \end{bmatrix}, \quad (3.49)$$

$$S_2(\theta, \phi) = \sum_{n=1}^{\infty} \sum_{m=0}^n \sigma_m [f_{mn}^T(\theta) \exp(im\phi_m) + f_{-mn}^T(\theta) \exp(-im\phi_m)], \quad (3.50)$$

$$S_3(\theta, \phi) = \sum_{n=1}^{\infty} \sum_{m=0}^n i\sigma_m [f_{mn}^T(\theta) \exp(im\phi_m) - f_{-mn}^T(\theta) \exp(-im\phi_m)], \quad (3.51)$$

$$S_4(\theta, \phi) = -\sum_{n=1}^{\infty} \sum_{m=0}^n i\sigma_m [g_{mn}^T(\theta) \exp(im\phi_m) + g_{-mn}^T(\theta) \exp(-im\phi_m)], \quad (3.52)$$

$$S_1(\theta, \phi) = \sum_{n=1}^{\infty} \sum_{m=0}^n \sigma_m [g_{mn}^T(\theta) \exp(im\phi_m) - g_{-mn}^T(\theta) \exp(-im\phi_m)], \quad (3.53)$$

where  $\phi_m = (m-1)\phi + \gamma_p$ ,  $\sigma_m = \frac{1}{1 + \delta_{0m}}$ , the Kronecker delta  $\delta_{0m} = 1$  if  $m = 0$  and  $\delta_{0m} = 0$  if  $m \neq 0$ .  $f_{mn}^T(\theta)$  and  $g_{mn}^T(\theta)$  is determined by,

$$f_{mn}^T(\theta) = C_{mn} [a_{mn}^T \tau_{mn}(\theta) + b_{mn}^T \pi_{mn}(\theta)], \quad (3.54a)$$

$$g_{mn}^T(\theta) = C_{mn} [a_{mn}^T \pi_{mn}(\theta) + b_{mn}^T \tau_{mn}(\theta)]. \quad (3.54b)$$

### (b) Forward and back scattering cross section

Forward scattering cross section (FSCS) and back scattering cross section (BSCS) (or radar cross section RCS [5]) are given by the following formulas:

$$FSCS = \lim_{r \rightarrow \infty} \frac{4\pi r^2}{\tilde{k}^2} \frac{|\mathbf{E}_{sca}|^2}{|\mathbf{E}_{inc}|^2} \bigg|_{\theta=0} = 4\pi |A|^2 \bigg|_{\theta=0}, \quad (3.55)$$

$$RCS = BSCS = \lim_{r \rightarrow \infty} \frac{4\pi r^2}{\tilde{k}^2} \frac{|\mathbf{E}_{sca}|^2}{|\mathbf{E}_{inc}|^2} \bigg|_{\theta=\pi} = 4\pi |A|^2 \bigg|_{\theta=\pi}, \quad (3.56)$$

where

$$A \bigg|_{\theta=0} = \sum_{n=1}^{\infty} \frac{\sqrt{2n+1}}{2} [(a_{1n}^T + b_{1n}^T) \exp(i\gamma_p) - (a_{-1n}^T - b_{-1n}^T) \exp(-i\gamma_p)], \quad (3.57)$$

$$A \bigg|_{\theta=\pi} = \sum_{n=1}^{\infty} (-1)^{n+1} \frac{\sqrt{2n+1}}{2} [(a_{1n}^T - b_{1n}^T) \exp(i\gamma_p) - (a_{-1n}^T + b_{-1n}^T) \exp(-i\gamma_p)]. \quad (3.58)$$

### (c) Total cross sections

Total scattering, extinction and absorption cross sections of the configuration are given by

$$C_{ext} = \frac{4\pi}{\tilde{k}^2} \text{Re} \sum_{i=1}^{N_s} \sum_{n=1}^{\infty} \sum_{m=-n}^n (a_{mn}^i p_{mn}^{i*} + b_{mn}^i q_{mn}^{i*}), \quad (3.59)$$

$$C_{sca} = \frac{4\pi}{\tilde{k}^2} \text{Re} \sum_{i=1}^{N_s} \sum_{n=1}^{\infty} \sum_{m=-n}^n (a_{mn}^{i*} a_{mn}^{Ti} + b_{mn}^{i*} b_{mn}^{Ti}), \quad (3.60)$$

$$C_{abs} = \frac{4\pi}{\tilde{k}^2 |m^i|^2} \text{Re} \sum_{i=1}^{N_s} \sum_{n=1}^{\infty} \sum_{m=-n}^n i \psi'_n(m^i x^i) \psi_n^*(m^i x^i) (m^{i*} |d_{mn}^i|^2 + m^i |c_{mn}^i|^2), \quad (3.61)$$

where the asterisk denotes complex conjugate and

$$a_{mn}^{Ti} = \sum_{j=1}^{N_s} \sum_{l=1}^{\infty} \sum_{k=-l}^l (a_{kl}^j \tilde{A}_{mn}^{kl} + b_{kl}^j \tilde{B}_{mn}^{kl}), \quad (3.62)$$

$$b_{mn}^{Ti} = \sum_{j=1}^{N_s} \sum_{l=1}^{\infty} \sum_{k=-l}^l (a_{kl}^j \tilde{B}_{mn}^{kl} + b_{kl}^j \tilde{A}_{mn}^{kl}), \quad (3.63)$$

where  $\tilde{A}_{mn}^{kl}, \tilde{B}_{mn}^{kl}$  coefficients are calculated as  $A_{mn}^{kl}, B_{mn}^{kl}$ , but with spherical Hankel function  $h_n^{(1)}$  replaced by spherical Bessel function  $j_n$ .

#### (d) Total efficiencies

Relation between cross section and efficiency,

$$Q = \frac{C}{G}, \quad (3.64)$$

where  $G$  is the total surface area of the configuration,  $G = \pi \sum_{i=1}^{N_s} (a^i)^2$ ,  $Q$  is the efficiency and  $C$  is the total cross section.

#### (e) Intensity phase function

Scattered intensity phase function is given by

$$I_{sca}(\theta, \phi) = \frac{1}{2} \text{Re} \{ E_{sca}^\theta H_{sca}^{\phi*} - E_{sca}^\phi H_{sca}^{\theta*} \}. \quad (3.65)$$

### 3.5 Comparison with previous articles

#### 3.5.1 Comparison the Efficiencies with Mackowski's results

Fig. 3.6 illustrated extinction, absorption and scattering efficiencies for a closed-packed tetrahedral cluster of four identical spheres against cluster orientation angle  $\alpha$ . Four spheres has the same size of  $\tilde{k}r = 3.114$  and refractive index of  $m = 1.366 + 0.005i$ . This result agree well with Mackowski's result [8].

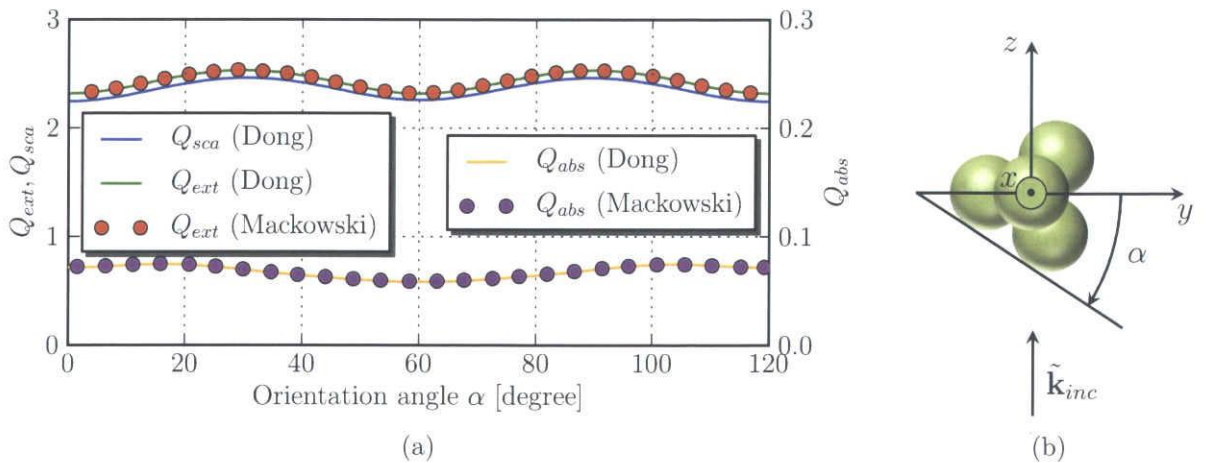


**Figure 3.6:** (a) Extinction, absorption and scattering efficiencies for a closed-packed tetrahedral cluster of four identical spheres against cluster orientation angle  $\alpha$ ; (b) Cluster orientation angle  $\alpha$ .

### 3.5.2 Comparison the Intensity Phase Function with Fuller and Kattawar's results

Scattered intensity phase function of four and five spheres configurations are illustrated in Fig. 3.7 and Fig. 3.8. In those figures all spheres have the same size of  $\tilde{k}r = 3.114$  and refractive index of  $m = 1.366 + 0.005i$ . These results also has the agreement with Fuller & Kattawar's results [6].

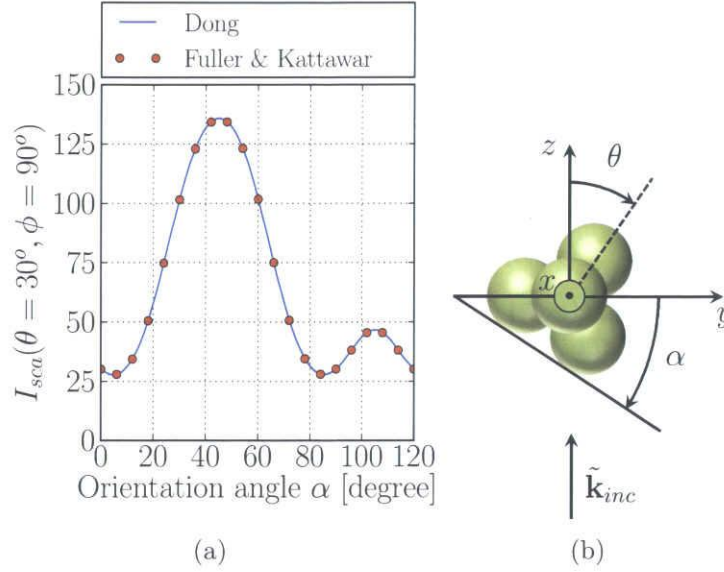


**Figure 3.7:** (a) Scattered intensity phase function at the scattering angle  $\theta = 30^\circ, \phi = 90^\circ$  against cluster orientation angle  $\alpha$ . Conditions are the same as in Fig. 3.6; (b) Cluster orientation angle  $\alpha$  and scattering angle  $\theta$ .

### 3.5.3 Comparison the Radar Cross Sections with Bruning and Lo's results

Fig. 3.9 illustrated the radar cross sections of two perfectly conductive spheres with the same size against the distance of them. The results of our calculation agree well with the results of Bruning & Lo's results. Note that the polarization angle  $\gamma$  defined in Bruning & Lo's article [5] is opposite sign with our definition (see section 3.3.2),  $\gamma_p = -\gamma$ .

## 3.6 Conclusion

In this chapter, the analysis of electromagnetic scattering by multiple spheres configuration is described. We have reviewed Mie theory as the simplest case with one sphere configuration and discuss about the truncation number of Mie theory. We then discuss about the formulation of multiple sphere configuration problem, and how to determine

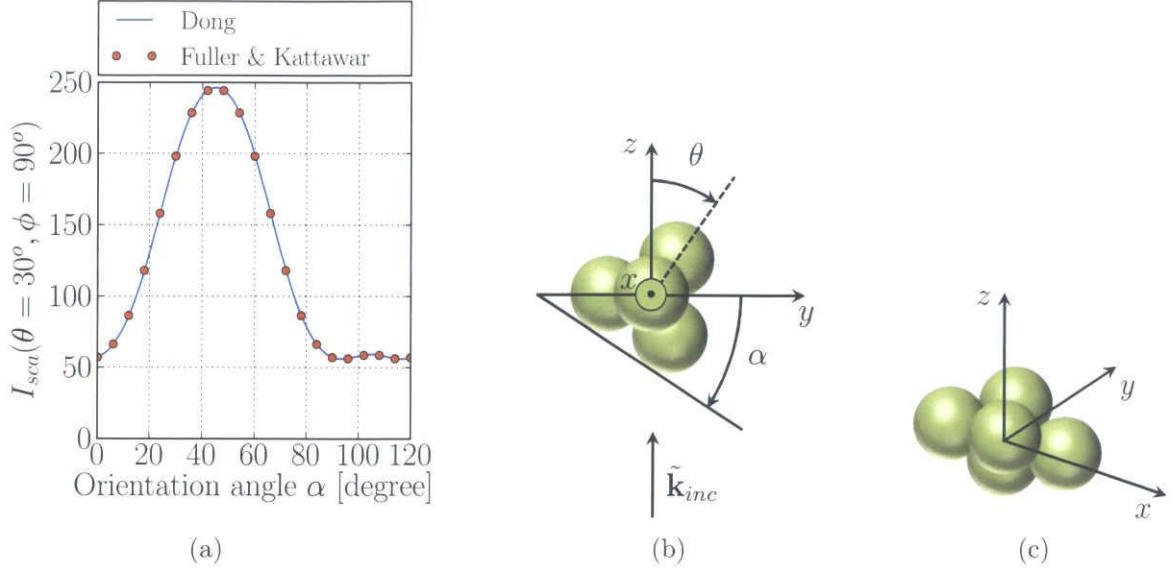


**Figure 3.8:** (a) Conditions are the same as Fig. 3.7 except that the cluster now is a hexahedron, with the fifth sphere located opposite the front sphere; (b) Cluster orientation angle  $\alpha$  and scattering angle  $\theta$ , the fifth sphere is invisible from the aspect shown in the inset; (c) The configuration from a specific view.

the incident, scattered and internal expansion coefficients. Near-field and far-field properties which are needed for this work were derived. We also show the comparison between our method and the previous articles.



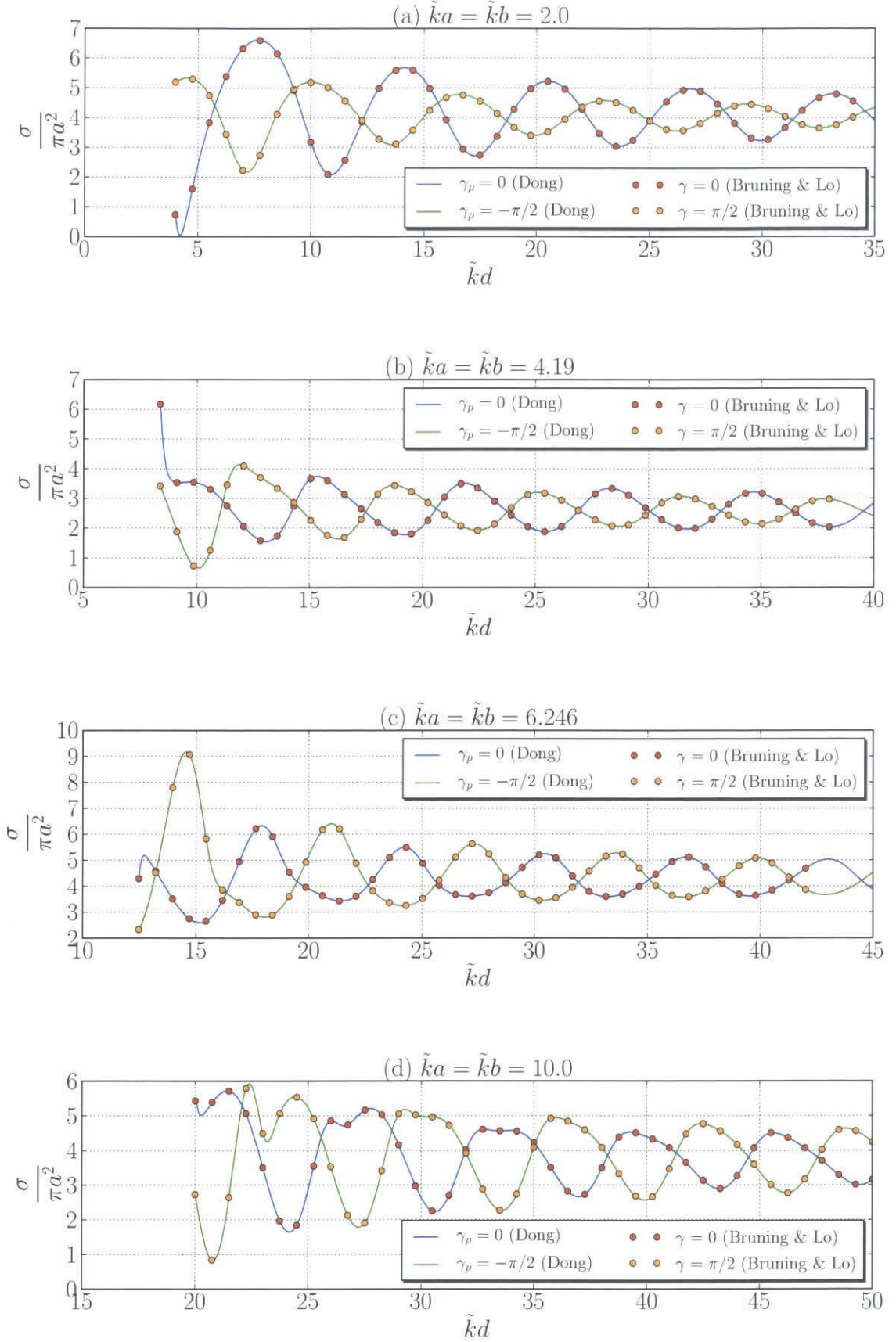


**Figure 3.9:** RCS of two equal perfectly conduction spheres at  $\gamma_p = 0$  and  $\gamma_p = \frac{\pi}{2}$  as spacing varied for  $\tilde{k}a = 2.0, 4.19, 6.246, 10.0$ .

# Chapter 4

## Addition theorems and Addition coefficients

### 4.1 Introduction

One of the most intractable problems in electromagnetic scattering by multiple spheres configuration is evaluation of addition coefficients  $(A_{mn}^{kl}, B_{mn}^{kl})$ . Addition coefficients are the key points to find the scattered coefficients  $(a_{mn}^i, b_{mn}^i)$ . Once the scattered coefficients are calculated, quantities of direct physical interest can be evaluated easily.

There are two ways to find the addition coefficients  $(A_{mn}^{kl}, B_{mn}^{kl})$ , direct and indirect ways. For the direct way, various methods were developed to calculate  $(A_{mn}^{kl}, B_{mn}^{kl})$  by using the addition theorems defined in Section 4.2. Friedman & Russek (1954) [2], Stein (1961) [3], Cruzan (1962) [4] and Xu (1996) [15] calculated the addition coefficients  $(A_{mn}^{kl}, B_{mn}^{kl})$  directly via general Gaunt coefficients. Among these methods, Xu's method [15] is the most effective method for calculating Gaunt coefficients.

Mackowski [8] was the first one who proposed the indirect way by using the three-step technique which decomposes addition coefficients  $(A_{mn}^{kl}, B_{mn}^{kl})$  into rotation coefficients  $R_{mn}^k$  and axial translation coefficients  $(A_{mn}^{ml}, B_{mn}^{ml})$  as

$$A_{mn}^{kl} \equiv (R_{mn}^k)^{-1} (\theta^{ji}, \phi^{ji}, 0) A_{mn}^{ml} (\rho^{ji}) R_{mn}^k (\theta^{ji}, \phi^{ji}, 0), \quad (4.1)$$

$$B_{mn}^{kl} \equiv (R_{mn}^k)^{-1} (\theta^{ji}, \phi^{ji}, 0) B_{mn}^{ml} (\rho^{ji}) R_{mn}^k (\theta^{ji}, \phi^{ji}, 0). \quad (4.2)$$

where  $(A_{mn}^{ml}, B_{mn}^{ml})$  are the special case of  $(A_{mn}^{kl}, B_{mn}^{kl})$  when  $k = m$  ( $\theta^{ji} = 0, \phi^{ji} = 0$ ).

There are several advantages of three-step technique over direct calculation. First of all, the three-step technique makes the calculation simpler. The derivation of the analytical expressions for the addition coefficients is lengthy and complex [2–4, 15] because  $(A_{mn}^{kl}, B_{mn}^{kl})$  which are the abbreviation for  $A_{mn}^{kl}(\tilde{k}\mathbf{r}^{ji}), B_{mn}^{kl}(\tilde{k}\mathbf{r}^{ji})$  depend on  $\tilde{k}\mathbf{r}^{ji} = (\rho^{ji}, \theta^{ji}, \phi^{ji})$ . In contrast, the rotation coefficients and the axial translation coefficients in the three-step technique can be calculated much easier. The rotation coefficients  $R_{mn}^k(\theta^{ji}, \phi^{ji}, 0)$  are well-developed by Mackowski [8, 10, 14, 16]. The axial translation coefficients are the special case of addition coefficients where  $k = m$ . In this case, the  $\theta$  and  $\phi$



components vanish  $\theta^{ji} = 0, \phi^{ji} = 0$ , and the addition coefficients  $A_{mn}^{kl}(\tilde{k}\mathbf{r}^{ji}), B_{mn}^{kl}(\tilde{k}\mathbf{r}^{ji})$  become the axial translation coefficients  $A_{mn}^{ml}(\rho^{ji}), B_{mn}^{ml}(\rho^{ji})$  which depend on only  $\rho^{ji} = \tilde{k}r^{ji}$  component.

In addition to this, the three-step technique calculates and stores only  $O(N^3)$  coefficients (rotation - axial translation - rotation coefficients) instead of  $O(N^4)$  addition coefficients directly (see table 4.1). Hence, the three-step technique requires less memory than the direct way.

As a result, Xu (2003) [11] changed his solution from the direct way to the indirect one. Later, Chien (2008) [17] used rotation coefficients developed by Edmonds [18] and axial translation coefficients developed by Brunning & Lo [5] for his work. This work also uses the indirect way with the rotation coefficients developed by Mackowski [8, 10, 14, 16] and the axial translation coefficients using SD method proposed by Dong et. al. [19].

GX, VM, SM, and SD stand for the methods which calculate Gaunt coefficients by Xus algorithm, Vector coupling coefficients by Mackowskis algorithm, Scalar addition coefficients by Mackowskis algorithm, and Scalar addition coefficients by Dongs algorithm, respectively.

## 4.2 Addition theorems

### 4.2.1 Scalar addition theorems

The potentials or scalar spherical harmonics are solutions of the Helmholtz equation in spherical coordinates,

$$\nabla^2 u + \tilde{k}^2 u = 0. \quad (4.3)$$

The scalar spherical harmonics  $u_{mn}^{(J)}$  are given by

$$u_{mn}^{(J)} = z_n^{(J)}(\rho) P_n^m(\cos \theta) \exp(im\phi), \quad (4.4)$$

where  $z_n^{(J)}$  is the appropriate kind of spherical Bessel or Hankel functions  $j_n, y_n, h_n^{(1)},$  and  $h_n^{(2)}$ , for  $J = 1, 2, 3,$  and  $4$ , respectively. Addition theorems for scalar harmonics which decompose the scalar harmonics about the origin  $O^j$  into the origin  $O^i$  can be written as [4]<sup>†</sup>

$$u_{kl}^{(3)j} = \sum_{l=1}^{\infty} \sum_{k=-l}^l C_{mn}^{kl} u_{mn}^{(1)i}, \quad r^{ji} \geq r^i, \quad (4.5)$$

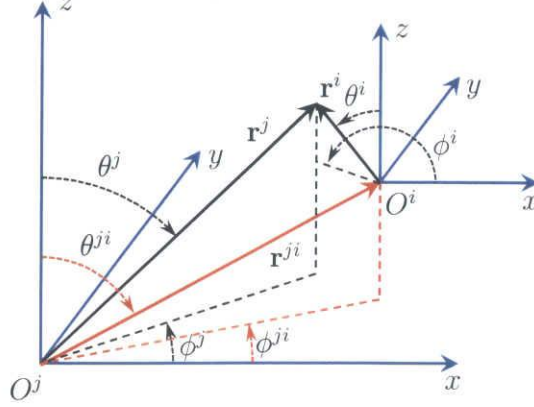
where  $C_{mn}^{kl}$  are the scalar addition coefficients which are used and calculated as the intermediate coefficients in SM and SD methods.

---

<sup>†</sup>We use  $u_{kl}^{(J)j}$  instead of  $u_{kl}^{(J)}(\tilde{k}\mathbf{r}^j)$  and  $C_{mn}^{kl}$  instead of  $C_{mn}^{kl}(\tilde{k}\mathbf{r}^{ji})$ .

**Table 4.1:** Number of coefficients required for calculation addition coefficients

Direct	Three-step technique		
$A_{mn}^{kl}, B_{mn}^{kl}$	$R_{mn}^k$	$A_{mn}^{ml}, B_{mn}^{ml}$	$(R_{mn}^k)^{-1}$
$[N(N+2)]^2$	$\frac{N(N+1)(2N+7)}{3} + N$	$\frac{N(N+1)(2N+1)}{3} + N^2$	$\frac{N(N+1)(2N+7)}{3} + N$


**Figure 4.1:** Translation of coordinates from origin  $O^j$  to  $O^i$ .

### 4.2.2 Vector addition theorems

Time-harmonic electric and magnetic fields  $\mathbf{E}$  and  $\mathbf{H}$  in a sourceless, isotropic, and homogeneous medium are divergence-free and must satisfy the vector wave equations

$$\nabla \times \nabla \times \mathbf{E} - \tilde{k}^2 \mathbf{E} = 0, \quad \nabla \times \nabla \times \mathbf{H} - \tilde{k}^2 \mathbf{H} = 0. \quad (4.6)$$

Addition theorems for vector harmonics which decompose the vector wave functions about the origin  $O^j$  into the origin  $O^i$  can be written as

$$\mathbf{M}_{mn}^{(3)j} = \sum_{l=1}^{\infty} \sum_{k=-l}^l \left[ A_{mn}^{kl} \mathbf{M}_{kl}^{(1)i} + B_{mn}^{kl} \mathbf{N}_{kl}^{(1)i} \right], \quad r^{ji} \geq r^i, \quad (4.7)$$

$$\mathbf{N}_{mn}^{(3)j} = \sum_{l=1}^{\infty} \sum_{k=-l}^l \left[ B_{mn}^{kl} \mathbf{M}_{kl}^{(1)i} + A_{mn}^{kl} \mathbf{N}_{kl}^{(1)i} \right], \quad r^{ji} \geq r^i, \quad (4.8)$$

where  $(A_{mn}^{kl}, B_{mn}^{kl})$  are addition coefficients.

## 4.3 Explicit formula for addition coefficients

From Cruzan [4], the vector addition coefficients for the translation from origin  $O^j$  to  $O^i$  illustrated in Fig. 4.1 is given as,

$$A_{mn}^{kl} (r^{ji}, \theta^{ji}, \phi^{ji}) = (-1)^m i^{n-l} \frac{2n+1}{2n(n+1)} \sum_p i^p [l(l+1) + n(n+1) - p(p+1)] \\ \times a(k, l; -m, n; p) h_p^{(1)}(r^{ji}) P_p^{k-m}(\cos \theta^{ji}) \exp[i(k-m)\phi^{ji}], \quad (4.9)$$

$$\begin{aligned}
 B_{mn}^{kl} (r^{ji}, \theta^{ji}, \phi^{ji}) = & -(-1)^m i^{n-l} \frac{2n+1}{2n(n+1)} \sum_p i^{p+1} \frac{2p+3}{2p+1} \\
 & \times \{ (n-m)(n+m+1) a(k, l; -m-1, n; p) \\
 & + 2m(p-k+m+1) a(k, l; -m, n; p) \\
 & - (p-k+m+1)(p-k+m) a(k, l; -m+1, n; p) \} \\
 & \times h_{p+1}^{(1)} P_{p+1}^{k-m} (\cos \theta^{ji}) \exp [i(k-m)\phi^{ji}].
 \end{aligned} \tag{4.10}$$

The quantity  $a(k, l; m, n; p)$  (so called Gaunt coefficient) is defined by the linearization expansion for Legendre functions,

$$P_l^k(\cos \theta) P_n^m(\cos \theta) = \sum_p a(k, l; m, n; p) P_p^{k+m}(\cos \theta). \tag{4.11}$$

The summation over  $p$  in equations (4.9)–(4.11) runs over the values  $p = |n-l|, |n-l|+2, \dots, n+l$ .

## 4.4 Rotation coefficients

The rotation coefficients of Euler angles  $(\alpha, \beta, \gamma)$  are defined as

$$R_{mn}^k(\alpha, \beta, \gamma) = e^{ik\gamma} D_{mn}^k(\beta) e^{im\alpha}, \tag{4.12}$$

$$(R_{mn}^k)^{-1}(\alpha, \beta, \gamma) = R_{mn}^k(\pi - \gamma, \beta, \pi - \alpha), \tag{4.13}$$

where  $(\alpha, \beta, \gamma)$  are the ZYZ Euler angles (see Fig. A.3 [18]). In this case,  $\alpha = \phi^{ji}, \beta = \theta^{ji}, \gamma = 0$ .  $D_{mn}^k(\beta)$  is the  $\beta$ -rotation coefficient first proposed by Edmonds [18] but then are well-developed by Mackowski [8, 10, 14, 16]. Recursive relations of  $D_{mn}^k(\beta)$  are given by

$$D_{mn}^0 = P_n^{-m}(\cos \beta), \tag{4.14}$$

$$D_{mn}^{k+1} = \cos^2 \frac{\beta}{2} D_{m-1n}^k - m \sin \beta D_{mn}^k - (n+m+1)(n-m) \sin^2 \frac{\beta}{2} D_{m+1n}^k, \tag{4.15}$$

$$\begin{aligned}
 D_{mn}^{k-1} = & \frac{1}{(n+k)(n-k+1)} \left[ -\sin^2 \frac{\beta}{2} D_{m-1n}^k - m \sin \beta D_{mn}^k \right. \\
 & \left. + (n+m+1)(n-m) \cos^2 \frac{\beta}{2} D_{m+1n}^k \right].
 \end{aligned} \tag{4.16}$$

## 4.5 Axial translation coefficients

The methods to calculate addition coefficients can be applied for the special case ( $k = m$ ), in order to obtain the axial translation coefficients. We can classify these methods into three groups according to the intermediate coefficients: Gaunt coefficients, Vector coupling coefficients and Scalar addition coefficients.

The methods developed by Friedman & Russek [2], Stein [3], Cruzan [4], Bruning & Lo [5] and Xu [11, 15] are in the Gaunt coefficients group. In these methods, Stein uses the scalar addition coefficients to express the formulas of addition coefficients but then he uses the Gaunt coefficients developed by Friedman & Russek to calculate these scalar addition coefficients. Based on Cruzan's method, Xu develops his new algorithm for calculating addition coefficients. For the special case of calculating axial translation coefficients, Xu's method is equivalent with Bruning & Lo's method. Xu's method (referred to as "GX method") is the most effective method in the Gaunt coefficients group (see [15]).

Mackowski's method [10, 16] is in Vector coupling coefficients group. We denote this method as "VM method".

In the scalar addition coefficients group, Mackowski's method [8] and the proposed method are denoted as "SM method" and "SD method", respectively.

The following symmetry properties of axial translation coefficients are used to minimize the storage requirements

$$A_{mn}^{ml} = A_{-mn}^{-ml} = A_{ml}^{mn} = A_{-ml}^{-mn}, \quad (4.17)$$

$$B_{mn}^{ml} = -B_{-mn}^{-ml} = B_{ml}^{mn} = -B_{-ml}^{-mn}. \quad (4.18)$$

### 4.5.1 GX method

GX method uses Gaunt coefficients  $a_q = a(-m, n, m, l, p)$  (where  $p = n + l - 2q$ ) as the intermediate coefficients to calculate axial translation coefficients  $(A_{mn}^{ml}, B_{mn}^{ml})$ . The details of GX method with general Gaunt coefficients  $a(m, n, k, l, p)$  are described on page 4-7 in reference [11]. For the special group of Gaunt coefficients  $a_q = a(-m, n, m, l, p)$ , the calculation reduces to Bruning & Lo's method [5]. GX method uses the following recursive relation

$$\alpha_{p+1}a_q - (4m^2 + \alpha_{p+2} + \alpha_{p+3})a_{q-1} + \alpha_{p+4}a_{q-2} = 0, \quad (4.19)$$

where

$$\alpha_p = \frac{[p^2 - (n-l)^2][p^2 - (n+l+1)^2]}{4p^2 - 1}. \quad (4.20)$$

Initial values are given by

$$a_{-1} = 0, \quad (4.21)$$

$$a_0 = \frac{(2n-1)!!(2l-1)!!}{(2n+2l-1)!!} \frac{(n+l)!}{(n-m)!(l+m)!}, \quad (4.22)$$

where  $(2k-1)!! = (2k-1)(2k-3)\cdots 3 \cdot 1$ ,  $(-1)!! \equiv 1$ .

Axial translation coefficients are calculated by

$$A_{mn}^{ml}(\rho) = C_0 \sum_{q=0}^{\min(n,l)} i^p C_p a_q h_p^{(1)}(\rho), \quad (4.23)$$

$$B_{mn}^{ml}(\rho) = \delta_{m,0} C_0 \sum_{q=1}^{\min(n,l)} i^{p+1} \frac{2p+3}{2m} (\alpha_{p+2} a_{q-1} - \alpha_{p+1} a_q) h_{p+1}^{(1)}(\rho), \quad (4.24)$$

where

$$C_0 = \frac{(-1)^m}{2} \left[ \frac{(2n+1)(2l+1)(n+m)!(l-m)!}{n(n+1)l(l+1)(n-m)!(l+m)!} \right]^{1/2}, \quad (4.25)$$

$$C_p = n(n+1) + l(l+1) - p(p+1). \quad (4.26)$$

### 4.5.2 VM method

VM method uses vector coupling coefficients  $\hat{C}_{-mn,ml}^p$  as the intermediate coefficients to calculate axial translation coefficients  $(A_{mn}^{ml}, B_{mn}^{ml})$ . The details of VM method with general vector coupling coefficients are described on page 2267-2268 in reference [16]. The  $\hat{C}_{-mn,ml}^p$  can be calculated by first defining

$$\hat{C}_{-mn,ml}^p = g_{nlp} (n-m)!(l+m)!p! S_{-mn,ml}^p, \quad (4.27)$$

where

$$g_{nlp} = \left( \frac{(2p+1)(n+l-p)!(p+n-l)!(p+l-n)!}{(n+l+p+1)!} \right)^{1/2}. \quad (4.28)$$

The  $S$  coefficients, in turn, obey the three-term downwards recursive relation

$$S_{-mn,ml}^{p-1} = b_p S_{-mn,ml}^p + c_p S_{-mn,ml}^{p+1}, \quad (4.29)$$

where

$$b_p = \frac{2mp(2p+1)}{(p+1)[p^2 - (n+l+1)^2]}, \quad (4.30)$$

$$c_p = \frac{p(p+1)[(p+1)^2 - (n-l)^2]}{p^2 - (n+l+1)^2}, \quad (4.31)$$

with initial values of

$$S_{-mn,ml}^{n+l+1} = 0, \quad (4.32)$$

$$S_{-mn,ml}^{n+l} = \frac{1}{(n+m)!(n-m)!(l+m)!(l-m)!}. \quad (4.33)$$

In VM method, the axial translation coefficients are expressed as [16]

$$A_{mn}^{ml}(\rho) = \frac{E_{ml}}{E_{mn}} \left\{ \rho \left[ \frac{n+m+1}{(n+1)(2n+3)} C_{mn+1}^{ml}(\rho) + \frac{n-m}{n(2n-1)} C_{mn-1}^{ml}(\rho) \right] + C_{mn}^{ml}(\rho) \right\}, \quad (4.34)$$

$$B_{mn}^{ml}(\rho) = \frac{E_{ml}}{E_{mn}} \left[ i \frac{m\rho}{n(n+1)} C_{mn}^{ml}(\rho) \right]. \quad (4.35)$$

where the scalar addition coefficients are obtained by the direct formula

$$C_{mn}^{ml}(\rho) = (-1)^m i^{l-n} (2n+1) \sum_p i^p a(-m, n, m, l, p) h_p(\rho), \quad (4.36)$$

$$a(-m, n, m, l, p) = (-1)^{n+l+p} \hat{C}_{-mn, ml}^p \hat{C}_{0n, 0l}^p, \quad (4.37)$$

where  $p$  takes on the values of  $p = |l-n|, |l-n|+2, \dots, l+n$ .

### 4.5.3 SM method

SM method uses Mackowski's strategy to derive the recursive relations of scalar and vector spherical harmonics by using the recursive relations of spherical Bessel and associated Legendre functions in conjugate coordinates  $(\hat{\mathbf{e}}_x + i\hat{\mathbf{e}}_y, \hat{\mathbf{e}}_x - i\hat{\mathbf{e}}_y, \hat{\mathbf{e}}_z)$  [8] (see Appendix B).

The axial translation coefficients are expressed by the scalar addition coefficients  $C_{mn}^{ml}$  as

$$A_{mn}^{ml}(\rho) = \frac{E_{ml}}{E_{mn}} \left\{ \rho \left[ \frac{n+m+1}{(n+1)(2n+3)} C_{mn+1}^{ml}(\rho) + \frac{n-m}{n(2n-1)} C_{mn-1}^{ml}(\rho) \right] + C_{mn}^{ml}(\rho) \right\}, \quad (4.38)$$

$$B_{mn}^{ml}(\rho) = \frac{E_{ml}}{E_{mn}} \left[ i \frac{m\rho}{n(n+1)} C_{mn}^{ml}(\rho) \right]. \quad (4.39)$$

The expression of axial translation coefficients given in Eqn. (4.38), (4.39) are the same as Eqn. (4.34), (4.35) in VM method. They are also Eqn. (70) and Eqn. (71) in reference [8] when  $k = m$  (note that Mackowski [8] defined  $E_{mn} = -1$  which causes  $\frac{E_{ml}}{E_{mn}} = 1$ ).

The scalar addition coefficients  $C_{mn}^{ml}$  can be obtained by the following recursive relations

$$C_{0n}^{00}(\rho) = (-1)^n (2n+1) h_n^{(1)}(\rho), \quad (4.40)$$

$$C_{ln}^{ll}(\rho) = \frac{2l-1}{2n+3} C_{l-1n+1}^{l-1l-1}(\rho) + \frac{2l-1}{2n-1} C_{l-1n-1}^{l-1l-1}(\rho), \quad (4.41)$$

$$C_{mn}^{ml}(\rho) = \frac{2l-1}{l-m} \left[ \frac{n-m}{2n-1} C_{mn-1}^{ml-1}(\rho) - \frac{n+m+1}{2n+3} C_{mn+1}^{ml-1}(\rho) + \frac{l+m-1}{2l-1} C_{mn}^{ml-2}(\rho) \right], \quad l \neq m. \quad (4.42)$$

Eqn. (4.41) and (4.42) are Eqn. (55) and (52) in reference [8] when decreasing  $l$  by 1 and  $k = m$ .

In these above formulas,  $C_{mn}^{ml} = 0$  if  $|m| > l$  or  $|m| > n$ .

## 4.6 SD method

Based on the Mackowski's strategy [8], we derive a new algorithm to calculate axial translation coefficients  $(A_{mn}^{ml}, B_{mn}^{ml})$  which is more effective than that of SM method (see section 4.7.1). The advantages of SD method over other methods are discussed in section 4.7.3. Axial translation coefficients  $(A_{mn}^{ml}, B_{mn}^{ml})$ , then, can be calculated by

$$A_{mn}^{ml}(\rho) = \frac{E_{ml}}{E_{mn}} \left\{ \frac{1}{2n(n+1)} \left[ (n-m)(n+m+1) C_{m+1n}^{m+1l}(\rho) + 2m^2 C_{mn}^{ml}(\rho) + (l+m)(l-m+1) C_{m-1n}^{m-1l}(\rho) \right] \right\}, \quad (4.43)$$

$$B_{mn}^{ml}(\rho) = \frac{E_{ml}}{E_{mn}} \left[ i \frac{m\rho}{n(n+1)} C_{mn}^{ml}(\rho) \right]. \quad (4.44)$$

Eqn. (4.43) and (4.44) in this dissertation are Eqn. (68) and (71) in reference [8] when  $k = m$  (note that Mackowski [8] defined  $E_{mn} = -1$  which causes  $\frac{E_{ml}}{E_{mn}} = 1$ ).

When  $k = m$ , Eqn. (50) and (61) in reference [8] become

$$\frac{1}{2l+1} (C_{mn}^{ml-1} + C_{mn}^{ml+1}) = \frac{C_{m-1n-1}^{m-1l}}{2n-1} + \frac{C_{m-1n+1}^{m-1l}}{2n+3}, \quad (4.45)$$

$$C_{m+1n}^{m+1l} = \rho \frac{C_{mn+1}^{ml}}{2n+3} + \rho \frac{C_{mn-1}^{ml}}{2n-1} + C_{mn}^{ml}. \quad (4.46)$$

Decreasing value of  $m$  in Eqn. (4.46) by 1 gives

$$C_{mn}^{ml} = \rho \frac{C_{m-1n+1}^{m-1l}}{2n+3} + \rho \frac{C_{m-1n-1}^{m-1l}}{2n-1} + C_{m-1n}^{m-1l}. \quad (4.47)$$

Eliminating  $C_{m-1n+1}^{m-1l}$  and  $C_{m-1n-1}^{m-1l}$  by subtracting Eqn. (4.45) to  $1/\rho$  times Eqn. (4.47) gives us

$$\frac{1}{2l+1} (C_{mn}^{ml-1} + C_{mn}^{ml+1}) - \frac{1}{\rho} C_{mn}^{ml} = \frac{1}{\rho} C_{m-1n}^{m-1l}. \quad (4.48)$$

Eqn. (4.48) can be rewritten as

$$C_{mn}^{ml+1}(\rho) = \frac{2l+1}{\rho} [C_{mn}^{ml}(\rho) - C_{m-1n}^{m-1l}(\rho)] - C_{mn}^{ml-1}(\rho). \quad (4.49)$$

By decreasing value of  $l$  in Eqn. (4.49) by 1, the recursive relations of  $C_{mn}^{ml}$  for  $m \geq 0$  are obtained

$$C_{mn}^{ml}(\rho) = \frac{2l-1}{\rho} [C_{mn}^{ml-1}(\rho) - C_{m-1n}^{m-1l-1}(\rho)] - C_{mn}^{ml-2}(\rho). \quad (4.50)$$

From Eqn. (51) and (62) in reference [8] in case of  $k = m$ , we do the same procedure as above and have the recursive relations of  $C_{mn}^{ml}$  for  $m < 0$

$$C_{mn}^{ml} = \frac{2l-1}{\rho} \left[ \frac{l+m}{l-m} C_{mn}^{ml-1} + \frac{(n-m)(n+m+1)}{(l-m)(l-m-1)} C_{m+1n}^{m+1l-1} \right] - \frac{(l+m-1)(l+m)}{(l-m-1)(l-m)} C_{mn}^{ml-2}. \quad (4.51)$$

From symmetry properties given in Eqn. (4.17), (4.18), and (4.43) and (4.44), we need to calculate the scalar addition coefficients in the range of  $-1 \leq m \leq l, 0 \leq l \leq n, l \leq n \leq N$  (where  $N$  is the truncation number). When  $m = -1$ , Eqn. (4.51) becomes

$$C_{-1n}^{-1l}(\rho) = \frac{2l-1}{\rho} \left[ \frac{l-1}{l+1} C_{-1n}^{-1l-1}(\rho) - \frac{n(n+1)}{l(l+1)} C_{0n}^{0l-1}(\rho) \right] - \frac{(l-2)(l-1)}{l(l+1)} C_{-1n}^{-1l-2}(\rho). \quad (4.52)$$

We apply Eqn. (4.50) and (4.52) for  $l \geq 2$  with initial values

$$C_{0n}^{00}(\rho) = (-1)^n (2n+1) h_n^{(1)}(\rho), \quad (4.53)$$

$$C_{-1n}^{-11}(\rho) = (-1)^{n+1} \frac{n(n+1)}{2} \frac{2n+1}{\rho} h_n^{(1)}(\rho), \quad (4.54)$$

$$C_{0n}^{01}(\rho) = (-1)^{n+1} (2n+1) \frac{dh_n^{(1)}(\rho)}{d\rho}, \quad (4.55)$$

$$C_{1n}^{11}(\rho) = (-1)^{n+1} \frac{2n+1}{\rho} h_n^{(1)}(\rho). \quad (4.56)$$

In these above formulas,  $C_{mn}^{ml} = 0$  if  $|m| > l$  or  $|m| > n$ .

## 4.7 Results and Discussion

In this section, we compare 4 methods SD, SM, GX and VM. The goal of these methods is to calculate and to store all axial translation coefficients  $(A_{mn}^{ml}, B_{mn}^{ml})$  with the truncation number  $N$ . The range of  $m, n, l$  is  $|m| \leq \min(n, l), 1 \leq l \leq N, 1 \leq n \leq N$ . The differences among these methods are the type of intermediate coefficients and their algorithm.

### 4.7.1 Number of coefficients

#### Comparison between SD and SM methods

The SM method by Mackowski [8, 14] has several disadvantages. First of all, from Eqn. (4.38), (4.39), SM method needs to calculate up to  $C_{NN+1}^{NN}$  to get axial translation coefficients  $(A_{NN}^{NN}, B_{NN}^{NN})$ . In addition to this, the calculation of  $C_{NN+1}^{NN}$  requires Eqn. (4.40) starts with  $C_{0n}^{00}$  calculated up to  $n = 2N+1$  because of the relationship between  $n$  and  $l$  in Eqn. (4.42). As a result, SM method calculates and stores redundant coefficients



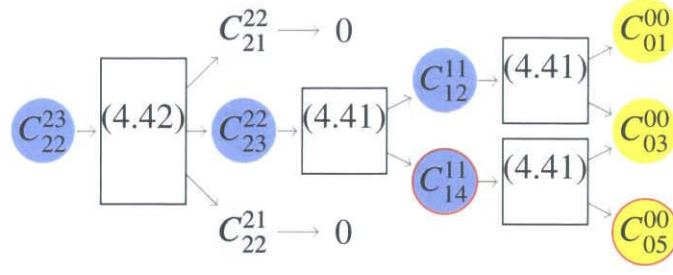


**Figure 4.2:** Computation scheme of SM method for  $C_{22}^{23}$ . The gray coefficients vanish because  $|m| > l$  or  $|m| > n$ . The yellow coefficients are initial coefficients. The blue coefficients can be resolved to lower order of  $l$  and  $m$  by Eqn. (4.41) or (4.42). All yellow and blue coefficients are required to calculate and store. The coefficients with red circle are redundant coefficients. In this case  $C_{14}^{11}$  and  $C_{05}^{00}$  are redundant coefficients.

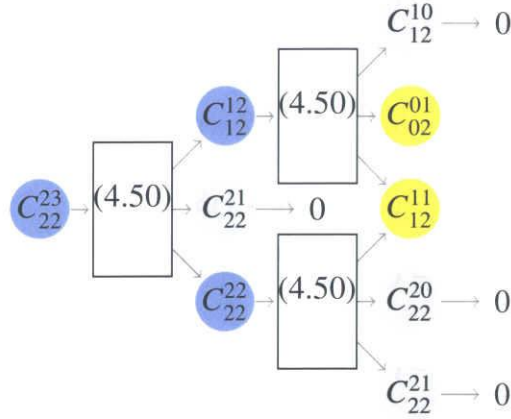


**Figure 4.3:** Computation scheme of SD method for  $C_{22}^{23}$ . The gray and yellow coefficients are the same as Fig. 4.2. The blue coefficients can be resolved to lower order of  $l$  and  $m$  by Eqn. (4.50) or (4.52). There are no redundant coefficients in SD method.

in the range of  $|m| < l, 1 \leq l \leq N, N+2 \leq n \leq 2N+1$  in the calculation process. These redundant coefficients are never used in the calculation of axial translation coefficients.

On the other hand, from Eqn. (4.43), (4.44), the SD method needs to calculate up to  $C_{NN}^{NN}$  to get axial translation coefficients  $(A_{NN}^{NN}, B_{NN}^{NN})$  (note that  $C_{mn}^{ml} = 0$  if  $|m| > l$  or  $|m| > n$ ). Also, calculation of  $C_{mn}^{ml}$  does not require any redundant coefficients because  $l$  is independent from  $n$  in Eqn. (4.50).

Fig. 4.2 and Fig. 4.3 illustrate the computation scheme of SM and SD methods for  $C_{22}^{23}$ . Fig. 4.2 and 4.3 show that SM method needs to calculate and store redundant coefficients but SD method does not need to calculate or store any redundant coefficients in computation process.

### Comparison of SD method with GX and VM methods

SD method together with GX and VM methods do not calculate or store any redundant coefficients. However, number of intermediate coefficients required in SD method is  $O(N^3)$  while that in GX and VM methods is  $O(N^4)$  (see Table 4.2).

From Eqn. (4.23), (4.24), GX method needs to calculate and store all values of  $a_q$  in the range of  $0 \leq q \leq \min(n, l)$  to get all axial translation coefficients where  $a_q = a(-m, n, m, l, p)$  and  $p = n + l - 2q$ . In other words, GX method needs to calculate and store all value of  $a(-m, n, m, l, p)$  where  $|m| \leq \min(n, l)$ ,  $1 \leq l \leq N$ ,  $1 \leq n \leq N$  and  $p = |l - n|, |l - n| + 2, \dots, l + n$ .

Similarly, from Eqn. (4.34), (4.35), VM method needs to calculate up to  $C_{NN+1}^{NN}$  to get axial translation coefficients  $(A_{NN}^{NN}, B_{NN}^{NN})$ . In turn, from Eqn. (4.36), (4.37), calculation of  $C_{NN+1}^{NN}$  requires calculating and storing all values of  $\hat{C}_{-mn, ml}^p$  where  $m, l, p$  are the same as in GX method except  $n$  in the range of  $1 \leq n \leq N + 1$ .

*Summary:* According to the range of intermediate coefficients described above, number of coefficients required for each method are shown in Table 4.2. The number of intermediate coefficients in SM and SD methods is  $O(N^3)$  while that in GX and VM methods is  $O(N^4)$ . The larger the truncation number  $N$  is, the larger the memory amount is required for storing intermediate coefficients in SM, GX and VM methods compared to SD method (see Fig. 4.4). At the truncation number of  $N = 50$ , the number of intermediate coefficients in SD method is about 1/10 that in SM method and about 1/100 that in VM and GX methods.

### 4.7.2 Execution time

We carried out extensive timing tests for SD, SM<sup>†</sup>, GX [11] and VM [10] methods on 32 bit and 64 bit Ubuntu 11.04 Core 2 duo @2GHz with 4GB Memory. The comparison of the required computing time (in seconds) for calculating all axial translation coefficients of a pair of spheres with truncation number  $N$  by SD, SM, GX and VM methods are shown in Table 4.3 (32 and 64 bit) and Fig. 4.5 (64 bit). Since the memory required for storing intermediate coefficients in SD method is smaller than that in SM, GX and VM methods, the speed of SD method is much faster than SM, GX and VM methods, especially when the truncation number  $N$  is large.

For a pair of spheres with distance  $\rho = 10$ , by comparing with SM method, SD method saves about 0.004 seconds at  $N = 25$ , 0.028 seconds at  $N = 50$  and 0.248 seconds at  $N = 100$  in 32 bit or 0.076 seconds at  $N = 25$ , 0.608 seconds at  $N = 50$  and 5.668 seconds at  $N = 100$  in 64 bit (see Table 4.3). In a multiple spheres configuration with  $N_s$  spheres (for example  $N_s = 100$ ), there are  $\frac{N_s(N_s - 1)}{2} (= 4950)$  pairs of spheres. That means, if  $N_s = 100$ , SD method saves 19.8 seconds (32 bit) or 376.2 seconds (64 bit) at  $N = 25$ , 138.6 seconds (32 bit) or 3009.6 seconds (approximate 50 minutes) (64 bit) at  $N = 50$  and 1227.6 seconds (32 bit) or 28056.6 seconds (approximate 8 hours) (64 bit) at  $N = 100$ . Therefore, we save considerable computation time when solving a multiple spheres configuration with SD method instead of other methods.

---

<sup>†</sup>The code used here is rewritten by ourselves because the original code by Mackowski is not available.

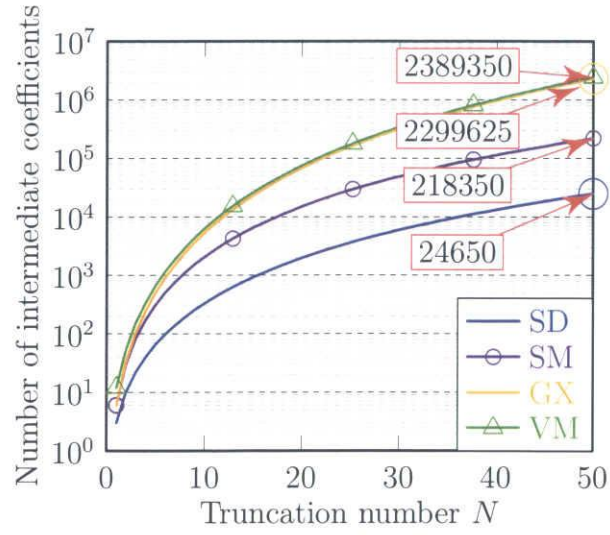


**Figure 4.4:** Number of intermediate coefficients versus truncation number in four methods.

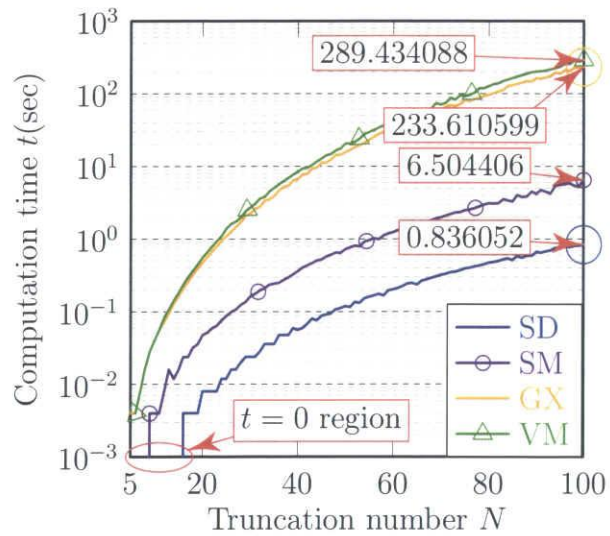


**Figure 4.5:** Computation time (in 64 bit) of all Axial Translation Coefficient needed for SD, SM, GX and VM methods.

### 4.7.3 Numerical results

Table 4.4 shows the numerical results of axial translation coefficients  $(A_{mn}^{ml}, B_{mn}^{ml})$ . The numerical results of SD, SM and GX methods are satisfactorily accurate. They agree exactly up to at least 10 digits in double precision calculations. The results also tell us that the VM method is less accurate in some circumstances, especially when  $m, l, n$  are large, although the numerical results given by all four methods are usually in good agreement.

## 4.8 Conclusion

We have discussed the improved computational method for the addition coefficients that are essential to the electromagnetic scattering by multiple spheres configurations. The new method's computation produce generally the same numerical results for axial translation coefficients as Xu [11] and Mackowski [8, 10, 14, 16]. But the numerical accuracies of these methods are not always competitive in some cases, especially for the calculation of high-degree coefficients. The proposed method reduces the required number of intermediate coefficients that improves considerably the computation speed, especially in case of large truncation number.

**Table 4.2:** Number of intermediate coefficients in four methods

Truncation number	SD	SM	GX	VM
N	$\frac{1}{6}N(N+1)(N+8)$	$\frac{1}{3}N(5N^2+12N+1)$	$\frac{1}{6}N(2N^3+10N^2+19N+5)$	$\frac{1}{3}N(N^3+7N^2+17N+11)$
1	3	6	6	12
5	65	310	500	660
20	1960	14940	67950	74340
50	24650	218350	2299625	2389350

**Table 4.3:** Execution time for SD, GX and VM methods for calculating all needed Axial Translation coefficients ( $N_{ATcoef}$ ) of a pair of spheres with distance  $\rho = 10$  in 32 bit and 64 bit.

		Computation time (sec)							
		Ubuntu 11.04: Core 2 duo @2GHz, 4GB Memory							
		32 bit				64 bit			
$N$	$N_{ATcoef}$	SD	SM	GX	VM	SD	SM	GX	VM
5	135	0.0000	0.0000	0.0000	0.0000	0.0000	0.0000	0.0040	0.0000
25	11675	0.0000	0.0040	0.0280	0.1120	0.0120	0.0880	1.1001	1.4001
50	88350	0.0120	0.0400	0.4280	1.1161	0.1200	0.7281	15.7810	20.5053
100	686700	0.1280	0.3760	5.9124	12.7008	0.8361	6.5044	233.6106	289.4341

**Table 4.4:** Numerical results for  $A_{mn}^{ml}(\rho)$  and  $B_{mn}^{ml}(\rho)$  with  $\rho = 10$ 

		$A_{mn}^{ml}$		$B_{mn}^{ml}$	
		Real part	Imaginary part	Real part	Imaginary part
$m = 5$	SD	-0.1560375861E+000	0.3148932919E+002	0.2626855449E+002	-0.1211060971E+ 000
$l = 7$	SM	-0.1560375861E+000	0.3148932919E+002	0.2626855449E+002	-0.1211060971E+000
$n = 11$	GX	-0.1560375861E+000	0.3148932919E+002	0.2626855449E+002	-01.211060971E +000
	VM	-0.1560375861E+000	0.3148932919E+002	0.2626855449E+002	-0.1211060971E+000
$m = -1$	SD	-0.2123485825E+009	-0.4758301570E-001	-0.2780633315E-002	-0.117485837 8E+008
$l = 12$	SM	-0.2123485825E+009	-0.4758301570E-001	-0.2780633315E-002	-0.1174858378E+008
$n = 15$	GX	-0.2123485825E+009	-0.4758301570E-001	-0.2780633315E-002	-0.117485837 8E+008
	VM	-0.2123485825E+009	-0.4758301570E-001	-0.2780633315E-002	-0.1174858378E+00 8
$m = 20$	SD	0.2145222716E+037	-0.3013652025E+000	0.6084982547E-001	-0.4472587576E +036
$l = 35$	SM	0.2145222716E+037	-0.3013652025E+000	0.6084982547E-001	-0.4472587576E +036
$n = 28$	GX	0.2145222716E+037	-0.3013652025E+000	0.6084982547E-001	-0.4472587576E +036
	VM	0.214 <b>4884479</b> E+037	-0.3013652025E+000	0.6084982547E-001	-0.44725 <b>73364</b> E+036
$m = 50$	SD	0.6022324113E+000	0.1197070314E+059	0.2444040581E+058	0.1203983651E+0 00
$l = 50$	SM	0.6022324113E+000	0.1197070314E+059	0.2444040581E+058	0.1203983651E+000
$n = 50$	GX	0.6022324113E+000	0.1197070314E+059	0.2444040581E+058	0.1203983651E+0 00
	VM	0.6022324113E+000	<b>-0.3048193059E+101</b>	<b>-0.3102960573E+098</b>	0.1203983651E+000

*Note:* The highlights indicate the discrepancies on the numerical values of the axial translation coefficients ( $A_{mn}^{ml}, B_{mn}^{ml}$ ) obtained by other methods compared to SD method.

*This page is intentionally left blank.*

# Chapter 5

## Scanning Near-field Optical Microscopy

### 5.1 Introduction

In the recent decades, much attention has been paid on the Scanning Near-field Optical Microscopy (SNOM or NSOM), since it is expected to be a powerful tool for the observation of microstructures and nano structures with a spatial resolution shorter than the optical wavelength [20]. SNOM provides us with eyes for the nanoworld. Among the main parameters that might be of interest for a nano structure under investigation are, besides shape and size, its chemical composition, molecular structure, as well as its dynamic properties. In order to investigate such properties, microscopes with high spatial resolution as well as high spectral and temporal resolving power are required. Present-day science and technology have an increasing need for tools that allow to characterize, generate, and manipulate structures as small as a few nanometers in size. SNOM combines the excellent spectroscopic and temporal selectivity of classical optical microscopy with a lateral resolution reaching well into the sub-100 nm regime. However, for a long time technical problems jeopardized the widespread application of SNOM. Near-field optics therefore became a focus of research and development in the field of optical microscopy in recent years [21–26]. Today, we have reached the point where SNOM represents a powerful tool for surface analysis that is technically and theoretically well understood. It is ready to be applied to a large variety of problems in physics, chemistry, and biology.

#### SNOM types

There are various types of SNOM have been proposed and put in practice. Among these, the scattering-type scanning near-field optical microscopy (s-SNOM) - often referred to as apertureless SNOM - offers a higher resolution than an apertured one [27](see Fig. 5.1).



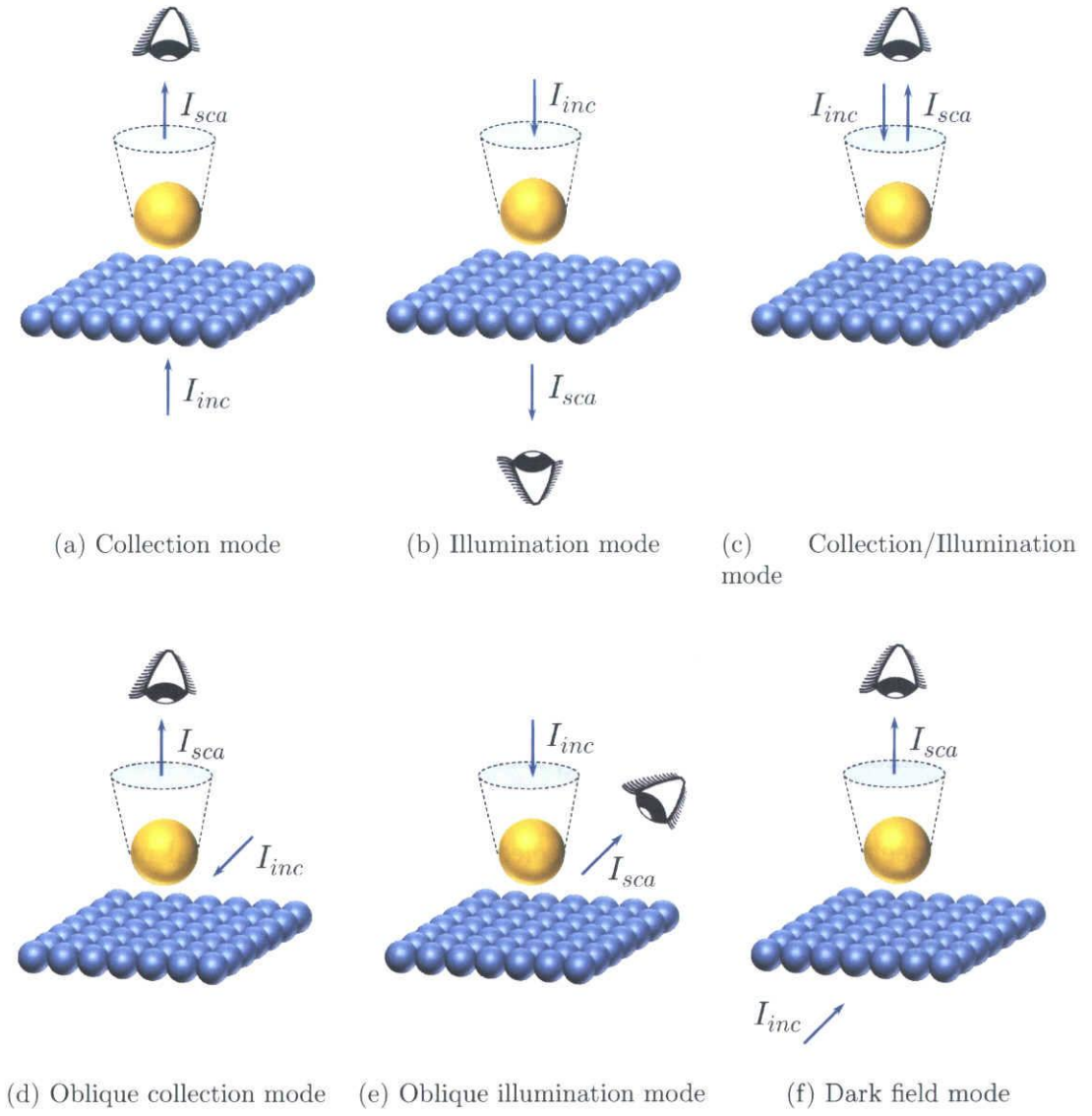


**Figure 5.1:** Six common SNOM configurations.

## Approach SNOM model

The general SNOM model with arbitrary probe and samples are solvable by numerical methods but to understand the electromagnetic phenomena of SNOM, we will simplify both probe and samples are spheres and use the analytical methods (see Figure 5.2). The analytical method we used in this dissertation can also provide solutions for the case when the sample is a multiple spheres configuration.

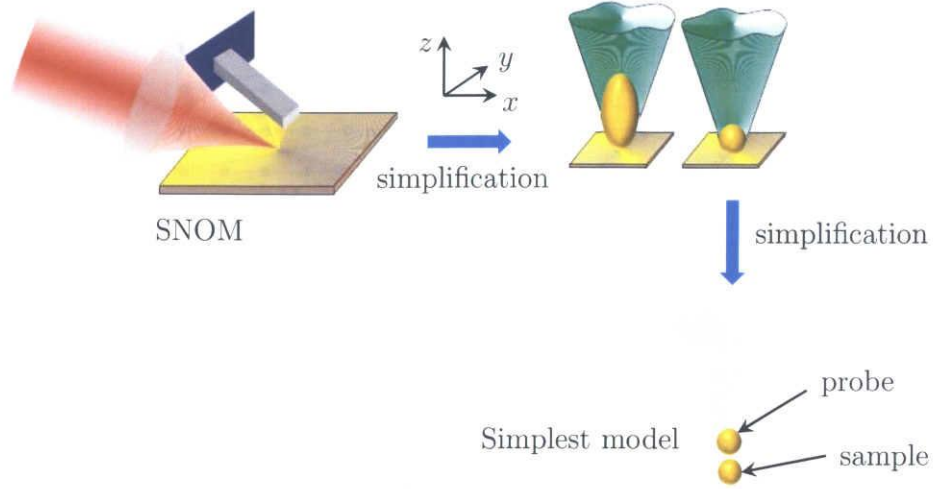


**Figure 5.2:** Scanning near-field optical microscopy models.

## 5.2 Analysis method

### 5.2.1 Formulation of problem

We propose a SNOM model with sphere-based shapes of probe and sample. The moving probe contains of  $N_{pr}$  spheres and the fixed sample contains of  $N_{sa}$  spheres. We solve the electromagnetic scattering problem of a multisphere system with  $N_s = N_{pr} + N_{sa}$  spheres, (see Fig. 5.3)

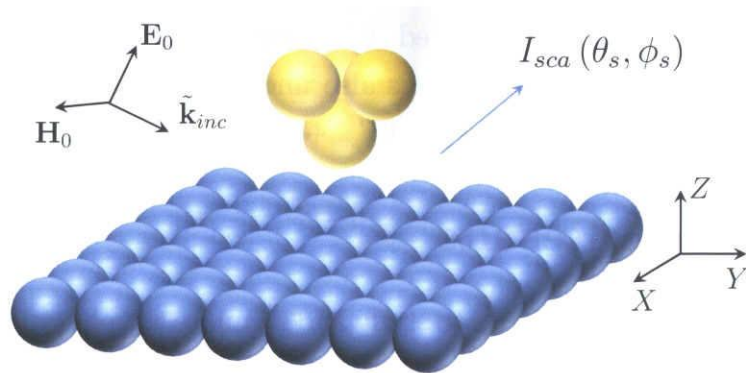


**Figure 5.3:** SNOM model.

### 5.2.2 Simulation of scanning

Assume the probe moves on the  $OXY$  plane with the scanning image size of  $L_x \times L_y$  [m<sup>2</sup>] or  $N_x \times N_y$  points (see two types of scanning in SNOM simulation in Fig. 5.4). Each state of the probe is considered as an individual scattering problem. Since the far-field properties are the time average quantities, the far-field image is independent with the probe's velocity.

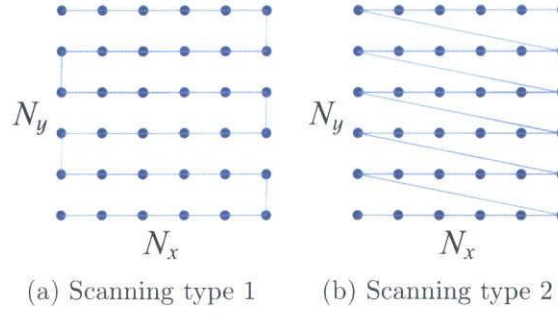


**Figure 5.4:** Two types of scanning in SNOM simulation.

### 5.2.3 Optimization of Computation

In case of scanning image with  $N_x \times N_y$  points, there are  $N_x N_y$  states of the probe. Since each state of the probe is an individual problem, we have to deal with  $N_x N_y$  problems. It is necessary to optimize the calculation of each problem. The flow chart of this calculation are shown in Fig. 5.5. The calculation of step 1 to step 8 is necessary for the first state of the probe. In step 1 of the flow chart, the Mie coefficients depend on the normalized radius and the refractive index of each sphere which is unchanged when the probe is moving. Therefore the step 1 is skipped for the next states of the probe.

The position of each sphere of the probe is modified while the probe is moving but that of the sample is fixed. Therefore in step 2 of the flow chart, we need to recalculate only the incident coefficients of each sphere of the probe for the next states of the probe.

The moving probe is rigid. It means that the relative position  $(r^{ji}, \theta^{ji}, \phi^{ji})$  between each two spheres in the probe is unchanged. Since the sample is fixed, the relative position between each two spheres in the sample is also unchanged. In other words, we need to recalculate only  $2N_{pr}N_{sa}$  instead of  $N_s^2 = (N_{pr} + N_{sa})^2$ .

## 5.3 Numerical Results

The purpose of this dissertation is to study and simulate the physical mechanism of the interaction between the probe tip and the sample in the models which contains of silver and gold spheres. The dielectric properties of the silver and gold spheres were assumed to be that of bulk material; measured bulk dielectric values reported by Johnson and Christy

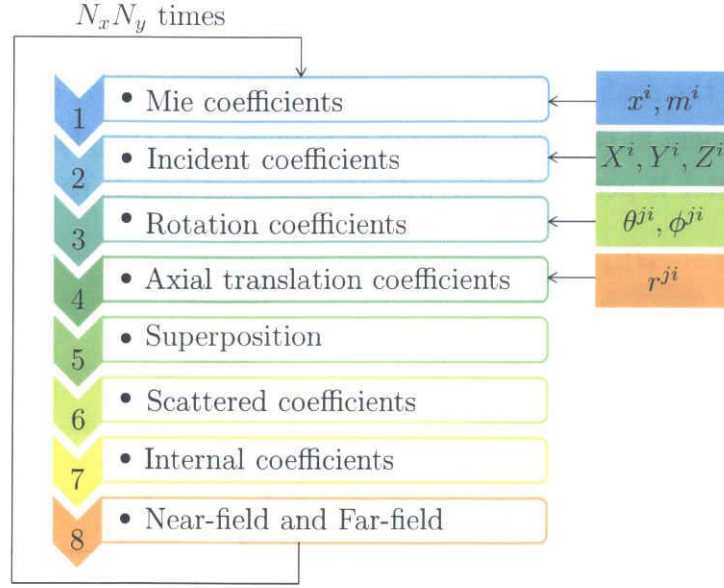


Figure 5.5: Flow chart of calculation.

[28] were used in all calculations and interpolated as needed. For example, when the wavelength  $\lambda = 628\text{nm}$ , the refractive indices of gold and silver are  $m_{Au} = 0.190 + 3.392i$  and  $m_{Ag} = 0.057 + 4.246i$ , respectively.

In this dissertation, we focus on the problem that spheres in the sample arrange in the same plane (sample plane), and the probe is one sphere (see Fig. 5.6). We assume that all the spheres in the sample have the same radius of  $r_s = 50\text{nm}$ . The receiver is put on the  $z$  direction and can measure the scattering intensity at that direction.

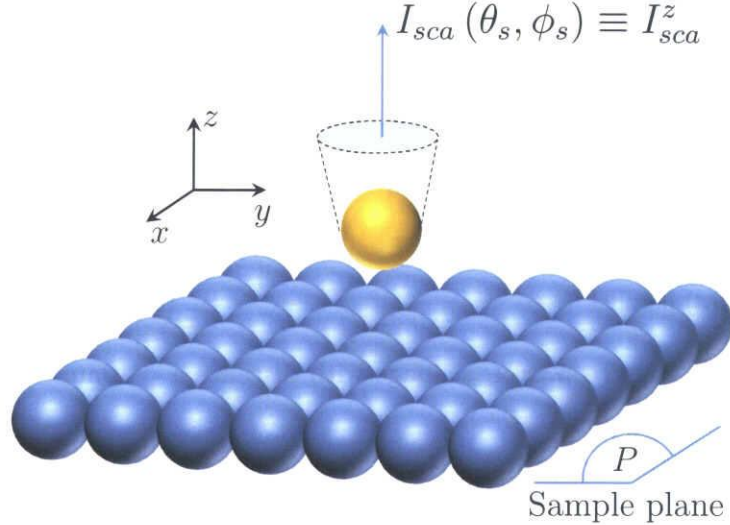


Figure 5.6: SNOM model with single sphere type probe.

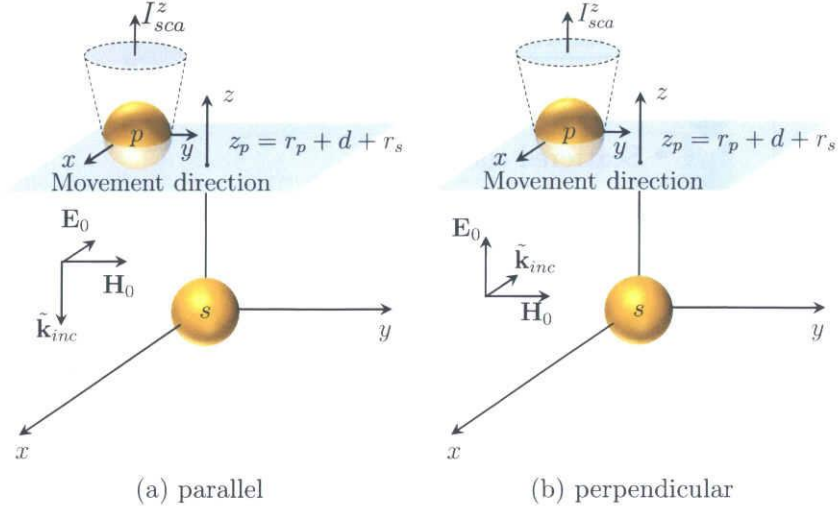
### 5.3.1 One sphere sample

The purpose of this section is choose the configuration of the incident wave and the probe.

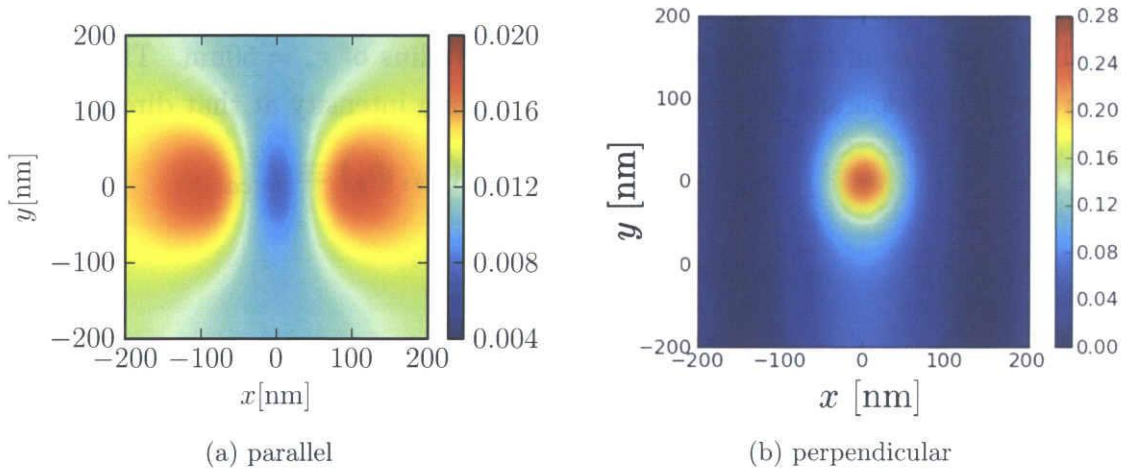


### Direction of incident wave

Fig. 5.7 shows the configuration with 2 different incident wave directions. The polarization of electric field in the first direction is parallel with the plane of sample (parallel case) while the latter is perpendicular with the plane of sample (perpendicular case).



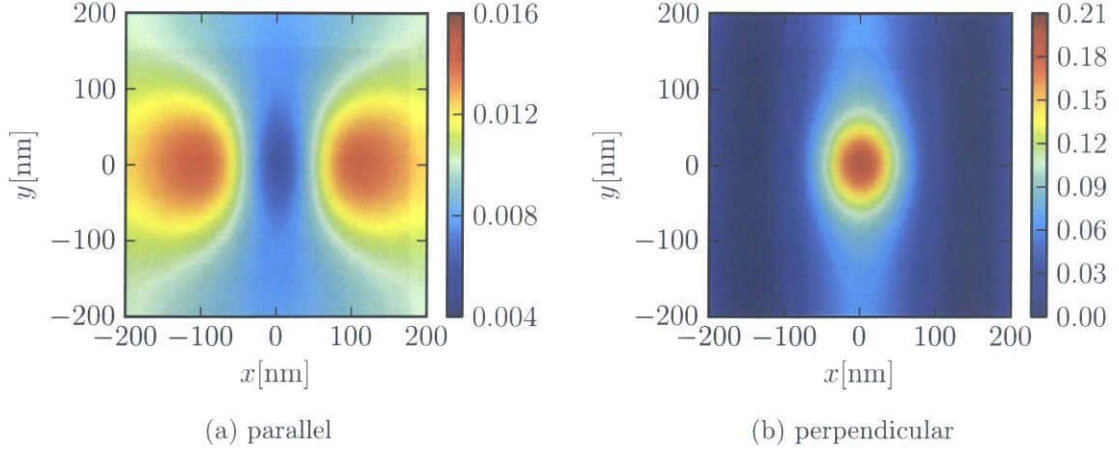
**Figure 5.7:** Direction of incident wave in 1 sphere sample model.



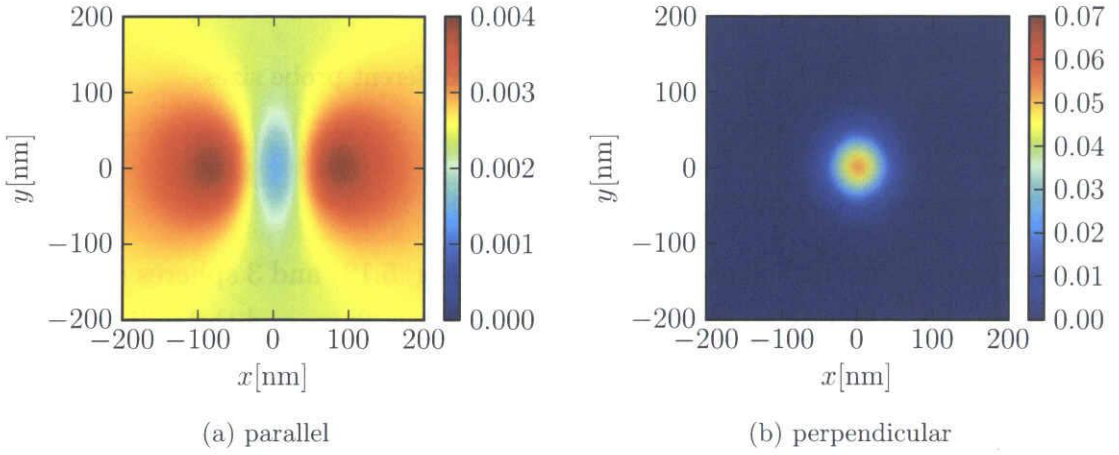
**Figure 5.8:**  $I_{sca}$  image with distance  $d = 10\text{nm}$ .

Fig. 5.8, 5.9 show the scattering intensity when the probe move in  $x$  and  $y$  directions and the distance between the probe and the sample is  $d = 10\text{nm}$ . The results show that we can not receive the true image by measuring the scattering intensity in a specific direction. The parallel case is much worse. But when we take the subtraction of  $I_{sca}$  in Fig. 5.8 and 5.9, we get Fig. 5.10. It is very easy to detect the sample in perpendicular case but we can detect nothing in parallel case.

*Conclusion:* The electric field direction of the incident wave should be perpendicular with the sample plane.



**Figure 5.9:**  $I_{sca}$  image with distance  $d = 15\text{nm}$ .



**Figure 5.10:** The difference between  $I_{sca}$  image with distance  $d = 10\text{nm}$  and  $d = 15\text{nm}$ .

### Size of the probe

Fig. 5.11 shows the intensities for four types of probe size when the distance between the probe and the sample increases. We can see that the smaller the size of probe is, the clearer the image is.

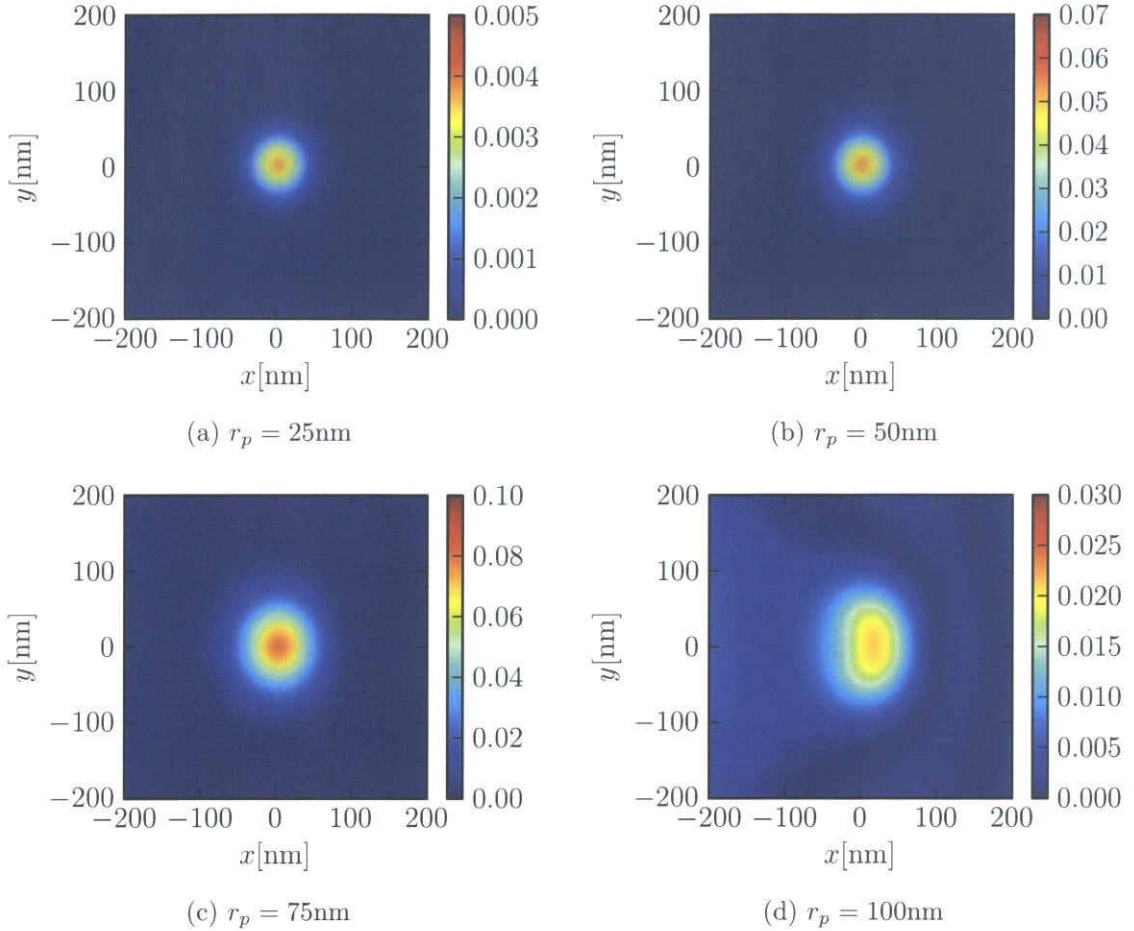


**Figure 5.11:** Far-field image with different probe sizes.

### 5.3.2 Two and three spheres sample

We can also obtain the image of sample with 2 (Fig. 5.12) and 3 spheres (Fig. 5.13) in the perpendicular case with incident wavelength of  $\lambda = 628\text{nm}$ , and the radius of probe is  $r_p = 50\text{nm}$ . Fig. 5.14 shows the image of scattering intensity when 2 spheres are ordered in x and y directions. Fig. 5.15 shows the far-field image of 3 spheres sample.

## 5.4 Conclusion

We used the analytical method to solve the problem of electromagnetic scattering by multiple spheres configuration. We apply the method to simulate the operation of SNOM models when the probe and the sample are sphere-based shape. We calculated

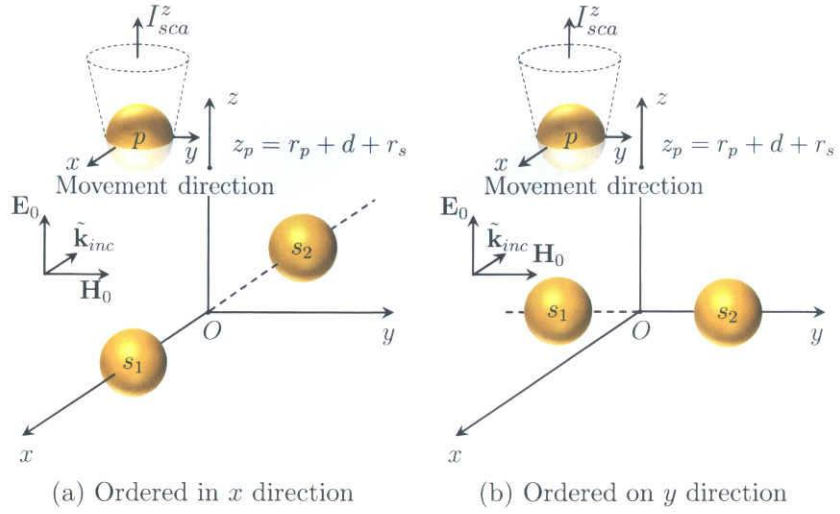


**Figure 5.12:** Direction of incident wave in 2 spheres sample model.

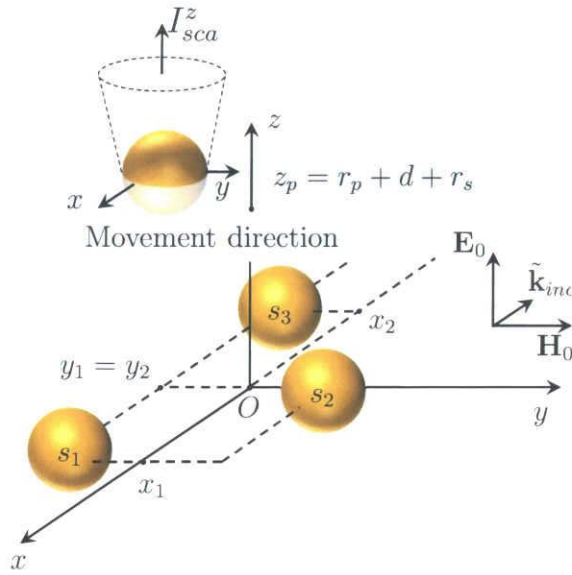


**Figure 5.13:** Direction of incident wave in 3 spheres sample model.

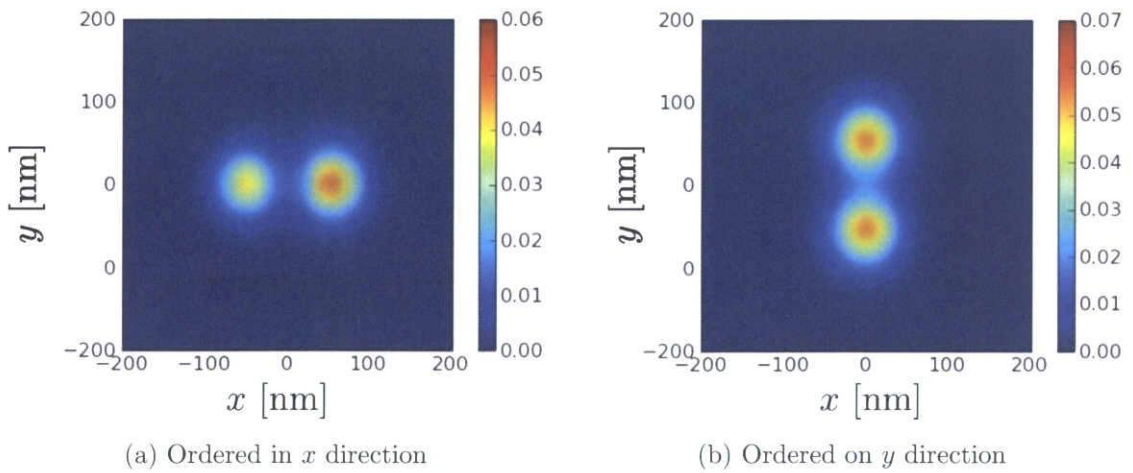


**Figure 5.14:** Far-field image of two gold spheres sample.



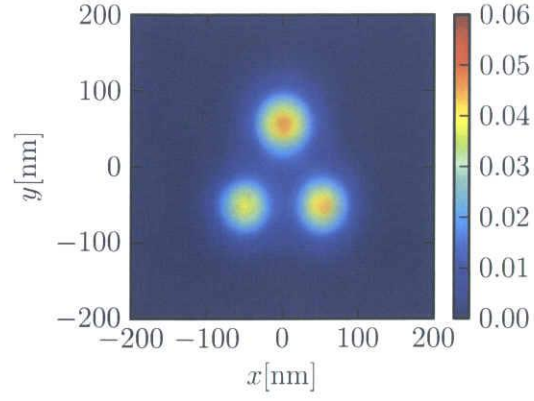


**Figure 5.15:** Far-field image of 3 gold spheres sample.

the scattering intensity at a specific direction to figure out the image of the sample. The polarization direction of electric field should be perpendicular with the sample plane. As the results, we simulate the models with gold spheres sample with the same size and on the same plane successfully.

# Chapter 6

## Rain Attenuation

### 6.1 Introduction

The attenuation by rain has received much attention [29–31] since it is closely related to the quality of communication systems. With the increasing deployment of the higher frequencies in commercial wireless networks, the accurate estimation of the rain attenuation is very important for the reliable design of a radio communication system.

The propagation of high frequency electromagnetic waves through rain are affected by two attenuating factors: absorption and scattering [32–34]. For absorption, part of its energy is absorbed by the raindrops and transformed into heat [33, 34] while the scattering aspect may introduce unwanted or interfering signals into the communication receiver that may mask the desired signal and these create several problems [34, 35]. A lot of work have been reported from the viewpoints of the change of temperature [30] and the incorporation of multiple scattering [36–39]. It is said that multiple scattering effects are small in the low frequency region but cannot be neglected at high frequencies [36]. Ishimaru et. al. [37] stated that this threshold is about 30 GHz, and that slight difference occurs between the models of first order and complete multiple scattering at 30 GHz for the rain rate more than 100 mm/h [38]. Furthermore, Roger et. al. [39] showed that the multiple scattering is negligible for frequencies up to at least 1000 GHz for coherent transmission through rain according to Twersky’s ‘free-space’ scattering formalism.

In spite of all these works dealing with multiple scattering, it is still important task to quantitatively evaluate the interaction among realistic raindrops distribution in a numerically exact manner. With regard to this, we choose a simple model with spherical raindrops [19] for exact multiple scattering solution. The solution is the result of the analysis method which builds upon the multipole expansions of electromagnetic fields, and the superposition of Mie theory [1]. In this analysis, the scattered field is expressed as a superposition of vector spherical harmonic expansions [12] written about each sphere in the configuration. The addition theorems [4] for vector spherical harmonics, which transform harmonics from one coordinate system into another, are rederived, and simple

recurrence relations for the addition coefficients are developed [19].

Apart from the dependence of rain attenuation on raindrop-size distribution, specific rain attenuation (reduction of power per unit length on the path [2]) depends upon the extinction cross section of electromagnetic wave by raindrops which are influenced by the water temperature, the water complex refractive index, the operating frequency [32].

The analytical rain attenuation models developed in this paper are limited to three different established raindrop-size distribution models. They are the negative exponential, the lognormal and the Weibull distribution model [40].

## 6.2 Raindrop Distribution Models

Let us determine the series of radii  $a^i$  as a function of rainfall intensity  $R[\text{mm/h}]$ . If  $N(a)[\text{m}^{-3}\text{mm}^{-1}]$  is the raindrop size distribution, then the integral

$$\tilde{N}(a) = \int_0^a N(a') da' [\text{m}^{-3}], \quad (6.1)$$

gives the number of drops, whose radii are less than  $a$ , per unit volume. When the number of drops taken into account in the numerical computation is  $N_s$ , the radius  $a^i[\text{mm}]$  is sampled by the rule

$$\frac{\tilde{N}(a^i)}{\tilde{N}(\infty)} = \frac{i - 1/2}{N_s}, \quad (6.2)$$

where  $\tilde{N}(\infty)$  is the total number of drops.  $N_s$  raindrops are randomly distributed inside a fictitious sphere having the volume of

$$V = \frac{N_s}{\tilde{N}(\infty)}. \quad (6.3)$$

### 6.2.1 Negative Exponential Distribution

Density function  $N(a)$  with negative exponential distribution, also known as Marshall-Palmer distribution [41], is given by

$$N(a) = N_0 \exp(-\Lambda a), \quad (6.4)$$

and

$$\Lambda = \alpha R^\beta, \quad (6.5)$$

where  $N_0$ ,  $\alpha$  and  $\beta$  are the parameters of rainfall rate which depend on the region (see Table 6.1).

From Eqn. (6.1) and Eqn. (6.4), total number of drops and drop size are derived as

$$\tilde{N}(\infty) = \frac{N_0}{\Lambda}, \quad (6.6)$$

$$a^i = -\frac{1}{\Lambda} \log \left( 1 - \frac{i - 1/2}{N_s} \right). \quad (6.7)$$

### 6.2.2 Lognormal Distribution

Density function  $N(a)$  with lognormal distribution is given by

$$N(a) = \frac{N_T}{\sigma a \sqrt{2\pi}} \exp \left\{ -\frac{1}{2} \left[ \frac{\log(2a) - \mu}{\sigma} \right]^2 \right\}, \quad (6.8)$$

and

$$N_T = a_0 R^{b_0}, \quad (6.9)$$

$$\mu = A_\mu + B_\mu \ln(R), \quad (6.10)$$

$$\sigma^2 = A_\sigma + B_\sigma \ln(R), \quad (6.11)$$

where  $N_T$ ,  $A_\mu$ ,  $B_\mu$ ,  $A_\sigma$  and  $B_\sigma$  are the parameters of rainfall rate which depend on the region (see Table 6.2).

From Eqn. (6.1) and Eqn. (6.8), total number of drops and drop size are derived as

$$\tilde{N}(\infty) = N_T, \quad (6.12)$$

$$a^i = \frac{1}{2} \exp \left[ \mu + \sqrt{2} \sigma \operatorname{erf}^{-1} \left( \frac{2i-1}{N_s} - 1 \right) \right], \quad (6.13)$$

where erf is Gaussian error function defined by

$$\operatorname{erf}(z) = \frac{2}{\sqrt{\pi}} \int_0^z \exp(-t^2) dt. \quad (6.14)$$

The inverse error function can be defined in terms of the Maclaurin series

$$\operatorname{erf}^{-1}(z) = \sum_{k=0}^{\infty} \frac{c_k}{2k+1} \left( \frac{\sqrt{\pi}}{2} z \right)^{2k+1}, \quad (6.15)$$

where  $c_0 = 1$  and

$$c_k = \sum_{m=0}^{k-1} \frac{c_m c_{k-1-m}}{(m+1)(2m+1)}. \quad (6.16)$$

### 6.2.3 Weibull Distribution

Density function  $N(a)$  with Weibull distribution [40] is given by

$$N(a) = N_0 \frac{\eta}{2\sigma} \left( \frac{a}{\sigma} \right)^{\eta-1} \exp \left[ - \left( \frac{a}{\sigma} \right)^\eta \right], \quad (6.17)$$

and

$$\eta = a_\eta R^{b_\eta}, \quad (6.18)$$

$$\sigma = a_\sigma R^{b_\sigma}, \quad (6.19)$$

where  $N_0$ ,  $a_\eta$ ,  $b_\eta$ ,  $a_\sigma$  and  $b_\sigma$  are the parameters of rainfall rate which depend on the region (see Section 6.4).

From Eqn. (6.1) and Eqn. (6.17), total number of drops and drop size are derived as

$$\tilde{N}(\infty) = N_0, \quad (6.20)$$

$$a^i = \sigma \left[ -\log \left( 1 - \frac{i - 1/2}{N_s} \right) \right]^{1/\eta}. \quad (6.21)$$

### 6.3 Specific rain attenuation

The rain attenuation is caused by scattering and absorption of electromagnetic waves by small raindrops, the specific rain attenuation in dB/km can be calculated as

$$\gamma = 10^3 \times \log_{10} e \times \int_0^{a_{max}} [C_{sca}(a) + C_{abs}(a)] N(a) da, \quad (6.22)$$

where  $C_{sca}(a)$  and  $C_{abs}(a)$  are the scattering and absorption of single sphere with radius of  $a$  ( $a$  in mm).

Since  $C_{ext} = C_{sca} + C_{abs}$ , the specific rain attenuation can be written by

$$\gamma = 10^3 \times \log_{10} e \times \int_0^{a_{max}} C_{ext}(a) N(a) da. \quad (6.23)$$

There are  $N_s$  raindrops in the volume  $V$ , we can write the specific rain attenuation as

$$\gamma = 10^3 \times \log_{10} e \times \sum_{i=1}^{N_s} C_{ext}(a^i), \quad (6.24)$$

The term  $\sum_{i=1}^{N_s} C_{ext}(a^i)$  is the summation of extinction cross sections of all individual raindrops regardless the multiple scattering. Since we propose the model with the consideration of multiple scattering, we should use the total extinction cross section  $C_{ext}$  in Eqn. (3.59) instead. Finally, the specific rain attenuation can be rewritten as

$$\gamma = 10^3 \times \log_{10} e \times \frac{C_{ext}}{V} = 4343 \frac{C_{ext}}{V}. \quad (6.25)$$

### 6.4 Numerical Results and Discussions

The refractive index of water raindrops which depends on temperature and electromagnetic frequency can be derived from [42] as Fig. 6.1.

The curve of refractive index of water shifts left in frequency when the temperature decreases.

We use the analysis method described in chapter 3 and 4 to investigate the dependence of the specific rain attenuation on frequency with various cases of temperature, rainfall intensity and number of sampled raindrops with three models: negative exponential, the lognormal and the Weibull distribution.

### 6.4.1 Negative Exponential Distribution

Table 6.1 gives the values for the parameters in Section 6.2.1 by Marshall and Palmer (M-P) [41] and other values for drizzle, widespread and thunderstorm rain types suggested by Joss et al. [43]. The rain types is classifications according to the following rainfall regimes in: drizzle ( $0 < R < 5\text{mm/h}$ ), widespread ( $5 \leq R \leq 40\text{mm/h}$ ), and thunderstorm ( $> 40\text{mm/h}$ ).

**Table 6.1:** Typical values for  $N_0$  and  $\Lambda$

Parameters	$N_0$	$\Lambda$	
		$\alpha$	$\beta$
<sup>a</sup> General (M-P)	16000	8.2	-0.21
<sup>b</sup> Joss-Drizzle	60000	11.4	-0.21
<sup>b</sup> Joss-Widespread	14000	8.2	-0.21
<sup>b</sup> Joss-Thunderstorm	2800	6	-0.21

<sup>a</sup>obtained from the studies of Marshall and Palmer [41]

<sup>b</sup>obtained from the studies of Joss et al. [43]

### 6.4.2 Lognormal Distribution

Table 6.2 are the parameters for drizzle, widespread, shower and thunderstorm rain types suggested by Ajayi and Adimula [44]. The rain types is classifications according to the following rainfall regimes in: drizzle ( $0 < R < 5\text{mm/h}$ ), widespread ( $5 \leq R \leq 10\text{mm/h}$ ), shower ( $10 \leq R \leq 40\text{mm/h}$ ), and thunderstorm ( $> 40\text{mm/h}$ ).

**Table 6.2:** Ajayi and Adimula constants for Tropical Lognormal Model [44]

Rain type	$N_T$		$\mu$		$\sigma^2$	
	$a_0$	$b_0$	$A_\mu$	$B_\mu$	$A_\sigma$	$B_\sigma$
Drizzle	718	0.399	-0.505	0.128	0.038	0.013
Widespread	264	0.232	-0.473	0.174	0.161	0.018
Shower	137	0.37	-0.414	0.234	0.223	-0.034
Thunderstorm	63	0.491	-0.718	0.195	0.209	-0.03

### 6.4.3 Weibull Distribution

Weibull distribution model with tropical region parameters suggested by Sekine [40]:  $N_0 = 1000[\text{m}^{-3}\text{mm}^{-1}]$ ,  $\eta = 0.95R^{0.14}$  and  $\sigma = 0.13R^{0.44}$ .

#### 6.4.4 Discussions

When the temperature increases, the attenuation with M-P and lognormal distribution model is almost constant at low frequencies ( $f < 30\text{GHz}$ ) and slightly decreases at higher frequencies (see Fig. 6.2 and Fig. 6.4).

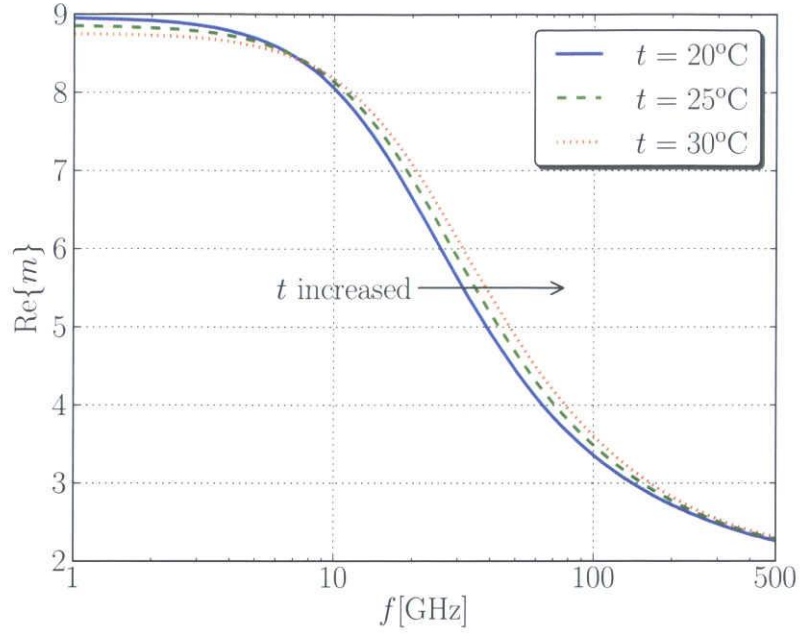
When the rainfall intensity increases, the attenuation with Joss distribution model increases, especially at the higher frequencies (see Fig. 6.3). Fig. 6.3 also shows that the attenuation with the rain type of widespread ( $R = 8\text{mm/h}$ ) is smaller than others at the frequencies over  $130\text{GHz}$ .

Fig. 6.5 shows the comparison between those distribution models. They are different because the parameters for those distributions are taken from different regions.

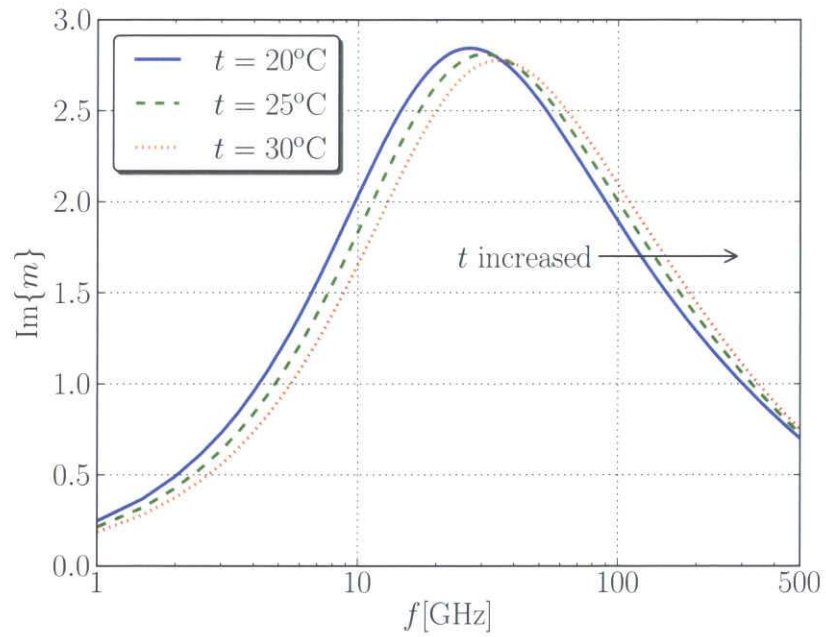
The effects of multiple scattering can be neglected at lower frequency (see Fig. 6.6) but cannot be neglected at higher frequency (see Fig. 6.6). At the frequency of  $30\text{GHz}$ , the multiple scattering effects are small with lower rainfall rate (see Fig. 6.8(a)) but are large with higher rainfall rate (see Fig. 6.8(b)).

### 6.5 Conclusion

Exact solution of electromagnetic scattering by multiple spheres configuration has been applied into the problem of calculating specific rain attenuation. We also investigate the relation of rain attenuation with temperature of the environment, frequency of the electromagnetic wave, the rainfall intensity with the consideration of multiple scattering using three distribution models: negative exponential, lognormal and Weibull. The present results and discussions will become more convincing if we deal with raindrops of realistic shape and incident wave.



(a) Real part versus frequency



(b) Imagine part versus frequency

**Figure 6.1:** Dependence of refractive index of water on temperature and frequency.



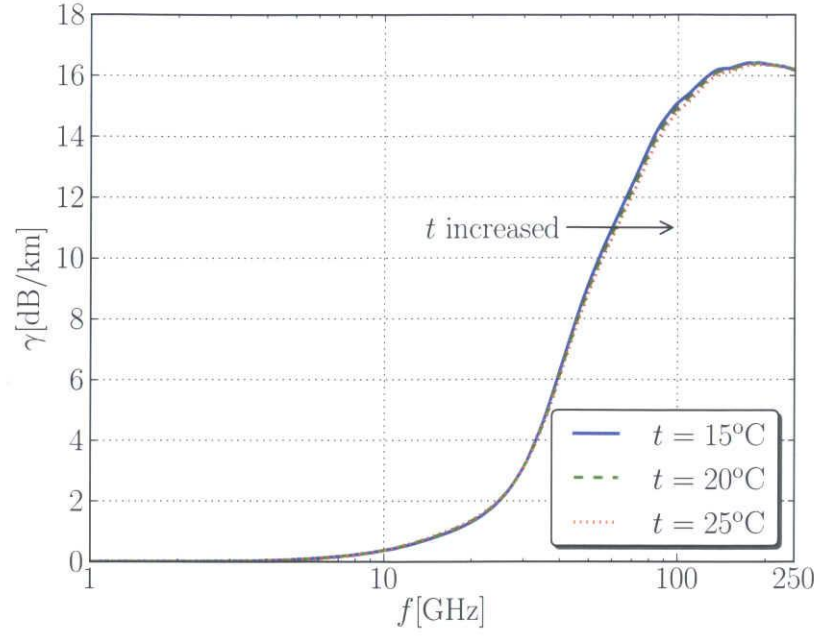


**Figure 6.2:** Negative exponential (M-P) distribution with  $N_s = 32$ ,  $R = 25$  mm/h

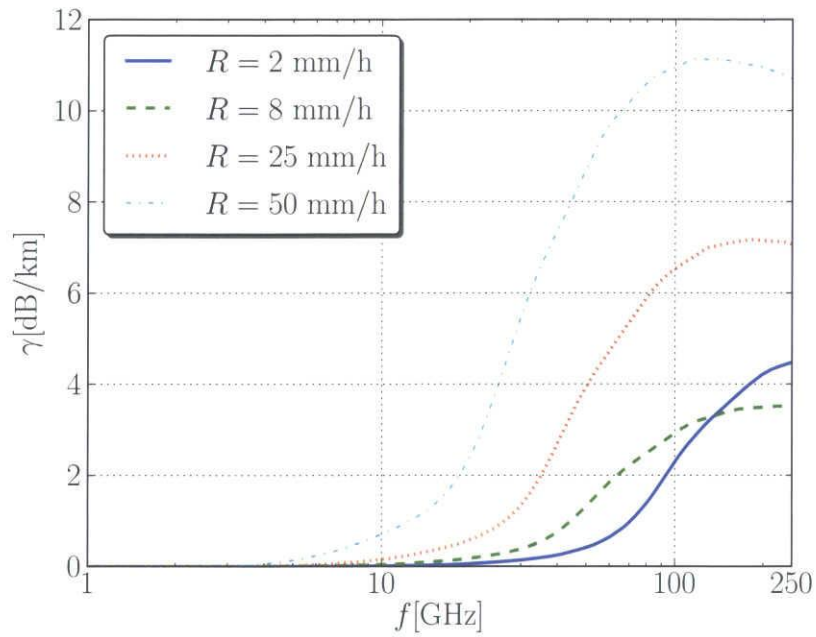


**Figure 6.3:** Negative exponential (Joss) distribution with  $N_s = 32$ ,  $t = 20^\circ\text{C}$

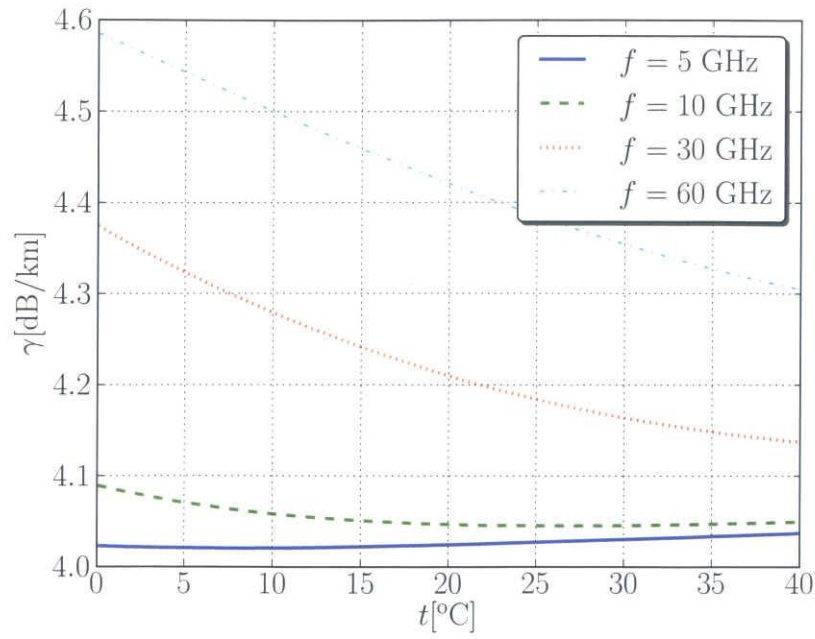


**Figure 6.4:** Lognormal distribution with  $N_s = 32$ ,  $R = 8\text{mm/h}$

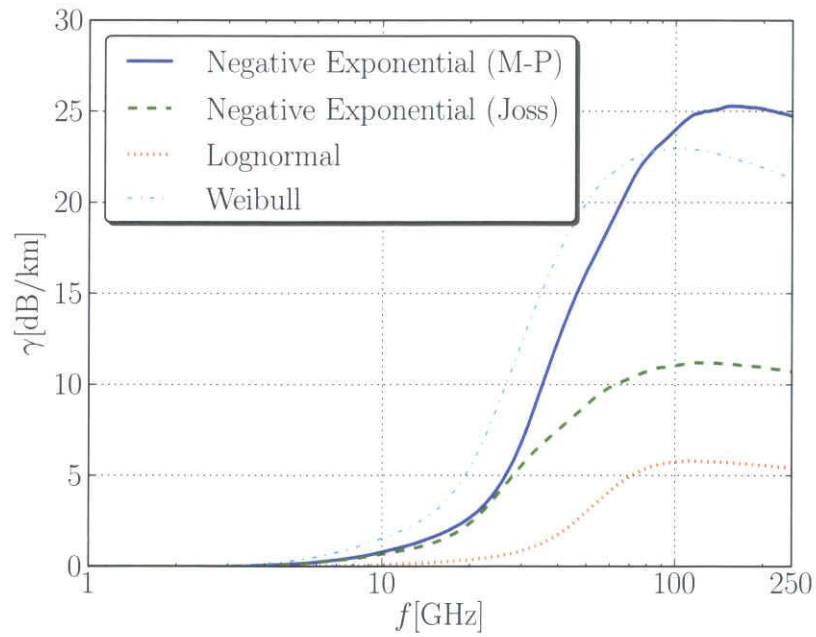


**Figure 6.5:** Comparison between distribution models with  $N_s = 32$ ,  $R = 50\text{mm/h}$  and  $t = 15^\circ\text{C}$

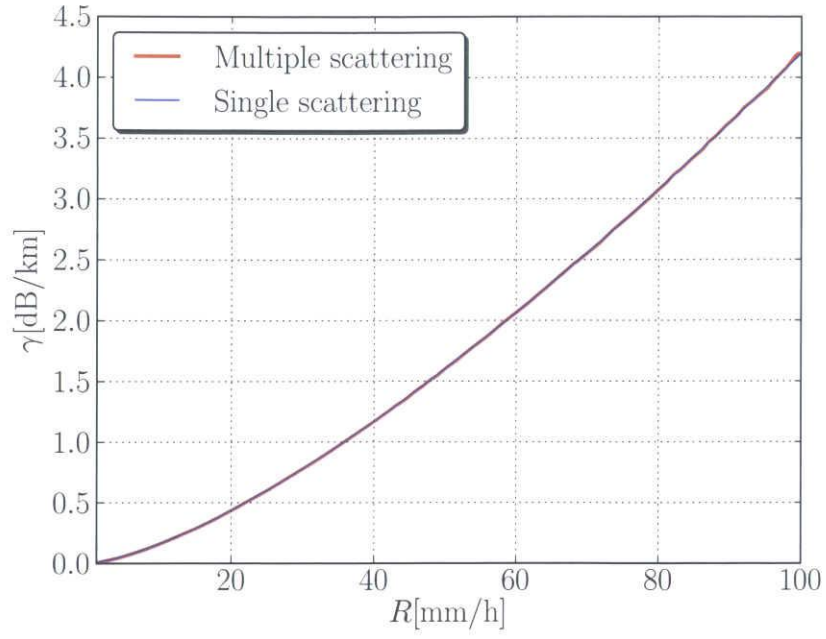


**Figure 6.6:** Dependence on multiple scattering effects with  $N_s = 32$ ,  $f = 10\text{GHz}$  and  $t = 20^\circ\text{C}$

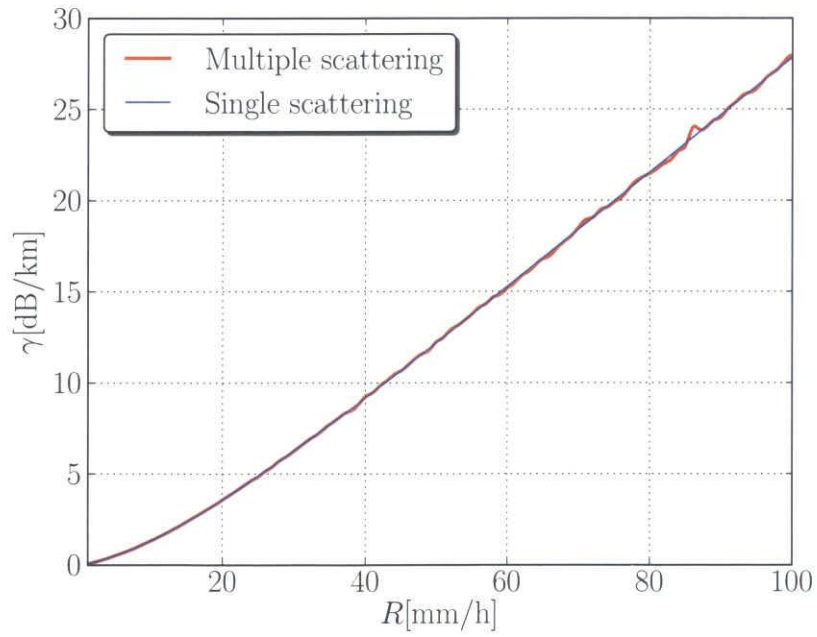


**Figure 6.7:** Dependence on multiple scattering effects with  $N_s = 32$ ,  $f = 30\text{GHz}$  and  $t = 20^\circ\text{C}$

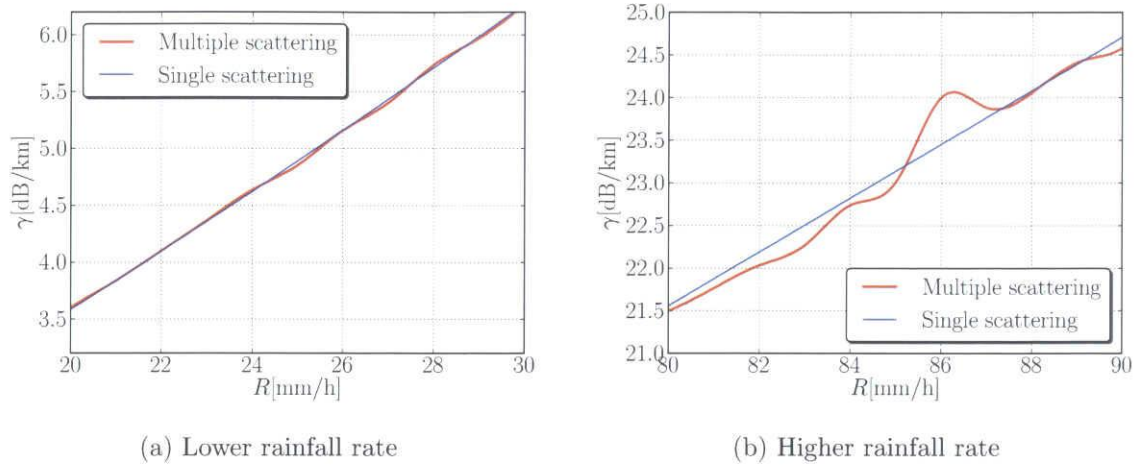


**Figure 6.8:** The effects of multiple scattering cannot be neglected at higher frequencies  $f = 30\text{GHz}$

*This page is intentionally left blank.*

# Chapter 7

## Summary

We have used the analytical method to derive the exact solution of the general problem for electromagnetic scattering by multiple spheres configuration. With this solution, we can calculate both near-field and far-field electromagnetic properties of any multiple spheres configuration even when the spheres are in contact. The results are useful when applying into its two applications on the study of Scanning Near-field Optical Microscopy (SNOM) phenomenon and on the calculation of specific rain attenuation.

In this dissertation, we started with the multipole expansions of electromagnetic wave to vector spherical harmonics by using the boundary conditions. Mie theory, which is the exact solution of one sphere configuration problem, was based on the multipole expansions of electromagnetic incident, scattered and internal fields. By applying Mie theory and the superposition theorem, the scattered field is expressed as a superposition of vector spherical harmonics written for each sphere in the configuration. The addition theorems for vector spherical harmonics, which transform harmonics from one coordinate system into another are used to calculate the addition coefficients. One of the most intractable problems in electromagnetic scattering by multiple spheres configuration is the evaluation of addition coefficients introduced by the addition theorems for vector spherical harmonics. The derivation of the analytical expressions for the addition coefficients is lengthy and complex while the computation of the addition coefficients is annoyingly time-consuming even with the reasonably fast computers available nowadays. This dissertation presents an efficient algorithm for calculating addition coefficients which is based on the recursive relation of scalar addition coefficients. Numerical results from the formulation derived in this dissertation agree with those of previous published results but the algorithm proposed here reduces the computational time considerably. This dissertation also discusses the strengths and limitations of other formulations and numerical techniques found in the literature. Once the scattered coefficients are calculated, near-field and far-field scattering properties can be derived.

Since this analytical method can be applied to multiple spheres of any size, even when they are in contact, we have used it for studying the physical mechanism of the interaction

---

between the probe tip and the sample in scanning near-field optical microscopy (SNOM) models. In these models, the probe tip is approximated to a sphere while the sample is approximated to a group of spheres with various sizes.

The method have been also used to calculate the rain attenuation via the scattering and absorption of electromagnetic waves by multiple raindrops with sphere shape. In this dissertation, we focus on the quantitative evaluations considering the change of temperature, frequency and the existence of multiple scattering effects with three raindrop-size distributions: the negative exponential, the lognormal and Weibull distribution models.

# Appendix A

## Vector Analysis

### A.1 Coordinate systems

#### A.1.1 Rectangular Cartesian coordinates

Rectangular Cartesian (or Rectangular or Cartesian) coordinates (see Figure A.1) are defined by three lines with three orthonormal unit vectors  $(\hat{\mathbf{e}}_x, \hat{\mathbf{e}}_y, \hat{\mathbf{e}}_z)$ ,

$$\hat{\mathbf{e}}_x \times \hat{\mathbf{e}}_y = \hat{\mathbf{e}}_z, \quad \hat{\mathbf{e}}_y \times \hat{\mathbf{e}}_z = \hat{\mathbf{e}}_x, \quad \hat{\mathbf{e}}_z \times \hat{\mathbf{e}}_x = \hat{\mathbf{e}}_y. \quad (\text{A.1})$$

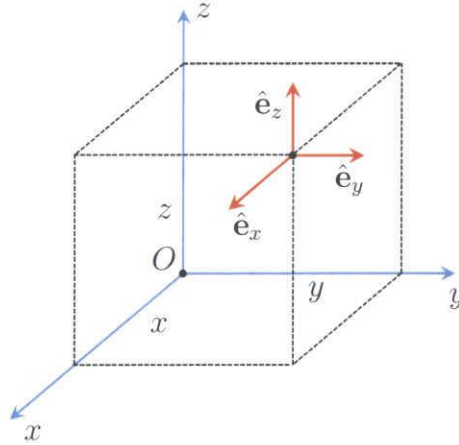


**Figure A.1:** Rectangular Cartesian coordinates.

#### A.1.2 Spherical coordinates

The transformation between spherical coordinates and Cartesian coordinates with a common origin  $(x, y, z) \rightarrow (r, \theta, \phi)$  is given by,

$$x = r \sin \theta \cos \phi, \quad y = r \sin \theta \sin \phi, \quad z = r \cos \theta, \quad (\text{A.2})$$

where  $r \geq 0$  is the distance to the point  $\mathbf{r} = (x, y, z)$  from the origin  $(0, 0, 0)$ , while  $\theta$  and  $\phi$  are spherical polar angles. At fixed  $r$  these angles can be treated as the coordinates of



the points on a sphere of radius  $r$ . Varying these angles in the range,

$$0 \leq \phi < 2\pi, \quad 0 \leq \theta \leq \pi, \quad (\text{A.3})$$

covers the whole surface of this sphere. The range of  $\phi$  and  $\theta$  can be extended to the set of all real numbers, since,

$$\begin{aligned} \mathbf{r}(r, \theta, \phi + 2\pi) &= \mathbf{r}(r, \theta, \phi), \\ \mathbf{r}(r, \theta + 2\pi, \phi) &= \mathbf{r}(r, \theta, \phi), \\ \mathbf{r}(r, -\theta, \phi + \pi) &= \mathbf{r}(r, \theta, \phi). \end{aligned} \quad (\text{A.4})$$

So any function of  $r$  should be  $2\pi$ -periodical with respect to  $\phi$  and to  $\theta$ , and further the half-period relation, expressed by the latter equation should hold. The spherical coordinates defined by transform (A.2) are orthonormal. This means that the unit vectors  $(\hat{\mathbf{e}}_r, \hat{\mathbf{e}}_\theta, \hat{\mathbf{e}}_\phi)$  form a local basis at each spatial point, where  $\hat{\mathbf{e}}_r$  is the outer normal to a sphere of radius  $r$ , while  $\hat{\mathbf{e}}_\theta$  and  $\hat{\mathbf{e}}_\phi$  are tangential vectors to this sphere (see Figure A.2). Since the basis is right-handed we have,

$$\hat{\mathbf{e}}_r \times \hat{\mathbf{e}}_\theta = \hat{\mathbf{e}}_\phi, \quad \hat{\mathbf{e}}_\theta \times \hat{\mathbf{e}}_\phi = \hat{\mathbf{e}}_r, \quad \hat{\mathbf{e}}_\phi \times \hat{\mathbf{e}}_r = \hat{\mathbf{e}}_\theta. \quad (\text{A.5})$$

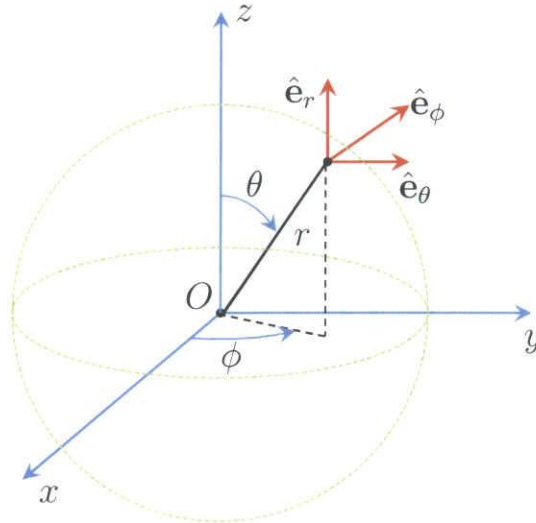


**Figure A.2:** Spherical coordinates.

### A.1.3 Conjugate coordinates

Conjugate (or Complex conjugate) coordinates,  $(x_c, y_c, z_c)$ , of any point are defined by the transformation,

$$x_c = x - iy, \quad y_c = x + iy, \quad z_c = z, \quad (\text{A.6})$$

and we have the inverse transformation,

$$x = \frac{1}{2i} (x_c - y_c), \quad y = \frac{1}{2} (x_c + y_c), \quad z = z_c. \quad (\text{A.7})$$

Since  $x$  and  $y$  are always real,  $x_c$  and  $y_c$  are always conjugate complex numbers. Some properties of Conjugate coordinates are listed here

$$\begin{aligned} (\hat{\mathbf{e}}_x - i\hat{\mathbf{e}}_y) \cdot (\hat{\mathbf{e}}_x - i\hat{\mathbf{e}}_y) &= 0, \\ (\hat{\mathbf{e}}_x + i\hat{\mathbf{e}}_y) \cdot (\hat{\mathbf{e}}_x + i\hat{\mathbf{e}}_y) &= 0, \\ (\hat{\mathbf{e}}_x - i\hat{\mathbf{e}}_y) \cdot (\hat{\mathbf{e}}_x + i\hat{\mathbf{e}}_y) &= 2, \\ (\hat{\mathbf{e}}_x - i\hat{\mathbf{e}}_y) \cdot \hat{\mathbf{e}}_z &= 0, \\ (\hat{\mathbf{e}}_x + i\hat{\mathbf{e}}_y) \cdot \hat{\mathbf{e}}_z &= 0, \\ \hat{\mathbf{e}}_z \cdot \hat{\mathbf{e}}_z &= 1. \end{aligned} \quad (\text{A.8})$$

We will use  $(\hat{\mathbf{e}}_x - i\hat{\mathbf{e}}_y, \hat{\mathbf{e}}_x + i\hat{\mathbf{e}}_y, \hat{\mathbf{e}}_z)$  instead of  $(\hat{\mathbf{e}}_{x-iy}, \hat{\mathbf{e}}_{x+iy}, \hat{\mathbf{e}}_z)$  hereafter.

$$\hat{\mathbf{e}}_{x-iy} = \frac{1}{\sqrt{2i}} (\hat{\mathbf{e}}_x - i\hat{\mathbf{e}}_y), \quad \hat{\mathbf{e}}_{x+iy} = \frac{1}{\sqrt{2i}} (\hat{\mathbf{e}}_x + i\hat{\mathbf{e}}_y), \quad \hat{\mathbf{e}}_z = \hat{\mathbf{e}}_z. \quad (\text{A.9})$$

#### A.1.4 Rotation of coordinates

##### Euler angles

Euler angles  $(\alpha, \beta, \gamma)$  of the rotation in  $z$ - $y$ - $z$  direction are shown in Figure A.3.

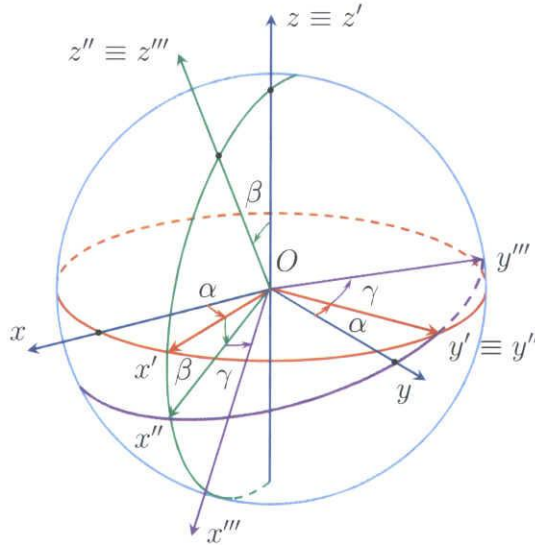


**Figure A.3:** Euler angles of rotation  $\alpha, \beta$ , and  $\gamma$ .

The relationship between the unit vectors in Cartesian coordinates in the initial and the rotated coordinate systems can be calculated as follow,

$$\begin{bmatrix} \hat{\mathbf{e}}'_x \\ \hat{\mathbf{e}}'_y \\ \hat{\mathbf{e}}'_z \end{bmatrix} = \begin{bmatrix} \cos \gamma & \sin \gamma & 0 \\ -\sin \gamma & \cos \gamma & 0 \\ 0 & 0 & 1 \end{bmatrix} \begin{bmatrix} \cos \beta & 0 & -\sin \beta \\ 0 & 1 & 0 \\ \sin \beta & 0 & \cos \beta \end{bmatrix} \begin{bmatrix} \cos \alpha & \sin \alpha & 0 \\ -\sin \alpha & \cos \alpha & 0 \\ 0 & 0 & 1 \end{bmatrix} \begin{bmatrix} \hat{\mathbf{e}}_x \\ \hat{\mathbf{e}}_y \\ \hat{\mathbf{e}}_z \end{bmatrix}, \quad (\text{A.10})$$

In the case of  $\alpha = \gamma = 0$ , the relationship between the unit vectors in Cartesian coordinates in the initial and the rotated coordinate systems can be calculated as follow,

$$\begin{bmatrix} \hat{\mathbf{e}}'_x \\ \hat{\mathbf{e}}'_y \\ \hat{\mathbf{e}}'_z \end{bmatrix} = \begin{bmatrix} \cos \beta & 0 & -\sin \beta \\ 0 & 1 & 0 \\ \sin \beta & 0 & \cos \beta \end{bmatrix} \begin{bmatrix} \hat{\mathbf{e}}_x \\ \hat{\mathbf{e}}_y \\ \hat{\mathbf{e}}_z \end{bmatrix}, \quad (\text{A.11})$$

or

$$\begin{bmatrix} \hat{\mathbf{e}}_x \\ \hat{\mathbf{e}}_y \\ \hat{\mathbf{e}}_z \end{bmatrix} = \begin{bmatrix} \cos \beta & 0 & \sin \beta \\ 0 & 1 & 0 \\ -\sin \beta & 0 & \cos \beta \end{bmatrix} \begin{bmatrix} \hat{\mathbf{e}}'_x \\ \hat{\mathbf{e}}'_y \\ \hat{\mathbf{e}}'_z \end{bmatrix}. \quad (\text{A.12})$$

Let us denote

$$\hat{\mathbf{e}}_\xi = \hat{\mathbf{e}}_x + i\hat{\mathbf{e}}_y, \quad \hat{\mathbf{e}}_\eta = \hat{\mathbf{e}}_x - i\hat{\mathbf{e}}_y. \quad (\text{A.13})$$

We will have the relation in conjugate coordinates,

$$\hat{\mathbf{e}}_\xi = \hat{\mathbf{e}}'_\xi \cos^2 \frac{\beta}{2} - \hat{\mathbf{e}}'_\eta \sin^2 \frac{\beta}{2} + \hat{\mathbf{e}}'_z \sin \beta, \quad (\text{A.14})$$

$$\hat{\mathbf{e}}_\eta = -\hat{\mathbf{e}}'_\xi \sin^2 \frac{\beta}{2} + \hat{\mathbf{e}}'_\eta \cos^2 \frac{\beta}{2} + \hat{\mathbf{e}}'_z \sin \beta, \quad (\text{A.15})$$

$$\hat{\mathbf{e}}_z = -\frac{1}{2}\hat{\mathbf{e}}'_\xi \sin \beta - \frac{1}{2}\hat{\mathbf{e}}'_\eta \sin \beta + \hat{\mathbf{e}}'_z \cos \beta. \quad (\text{A.16})$$

## A.2 Vector Transformations

### A.2.1 Rectangular to Spherical (and vice versa)

We can write that the rectangular and spherical coordinates are related by,

$$x = r \sin \theta \cos \phi, \quad y = r \sin \theta \sin \phi, \quad z = r \cos \theta, \quad (\text{A.17})$$

and the rectangular and spherical components by,

$$\begin{aligned} A_r &= A_x \sin \theta \cos \phi + A_y \sin \theta \sin \phi + A_z \cos \theta, \\ A_\theta &= A_x \cos \theta \cos \phi + A_y \cos \theta \sin \phi - A_z \sin \theta, \\ A_\phi &= -A_x \sin \phi + A_y \cos \phi. \end{aligned} \quad (\text{A.18})$$

The spherical to rectangular components related by,

$$\begin{aligned} A_x &= A_r \sin \theta \cos \phi + A_\theta \cos \theta \cos \phi - A_\phi \sin \phi, \\ A_y &= A_r \sin \theta \sin \phi + A_\theta \cos \theta \sin \phi + A_\phi \cos \phi, \\ A_z &= A_r \cos \theta - A_\theta \sin \theta. \end{aligned} \quad (\text{A.19})$$

### A.2.2 Rectangular to Conjugate (and vice versa)

In the rectangular coordinate system, we express a vector  $\mathbf{A}$  as,

$$\mathbf{A} = A_x \hat{\mathbf{e}}_x + A_y \hat{\mathbf{e}}_y + A_z \hat{\mathbf{e}}_z, \quad (\text{A.20})$$

### A.3. VECTOR DIFFERENTIAL OPERATORS

where  $\hat{\mathbf{e}}_x, \hat{\mathbf{e}}_y, \hat{\mathbf{e}}_z$  are the unit vectors and  $A_x, A_y, A_z$  are the components of the vector  $\mathbf{A}$  in the rectangular coordinate system. We will express vector  $\mathbf{A}$  in conjugate coordinate system as,

$$\mathbf{A} = \frac{1}{2}A_{x+iy}(\hat{\mathbf{e}}_x - i\hat{\mathbf{e}}_y) + \frac{1}{2}A_{x-iy}(\hat{\mathbf{e}}_x + i\hat{\mathbf{e}}_y) + A_z\hat{\mathbf{e}}_z, \quad (\text{A.21})$$

where  $A_{x+iy}, A_{x-iy}$  are defined by,

$$A_{x+iy} = A_x + iA_y, \quad A_{x-iy} = A_x - iA_y. \quad (\text{A.22})$$

#### Cross product of two vectors

Let  $\mathbf{r} = X\hat{\mathbf{e}}_x + Y\hat{\mathbf{e}}_y + Z\hat{\mathbf{e}}_z$ , and denote  $\xi = X + iY, \eta = X - iY$ , the cross product of two vectors  $\mathbf{A}$  and  $\mathbf{r}$  is,

$$\begin{aligned} \mathbf{A} \times \mathbf{r} = & \frac{1}{2}i(-ZA_{x+iy} + \xi A_z)(\hat{\mathbf{e}}_x - i\hat{\mathbf{e}}_y) \\ & + \frac{1}{2}i(ZA_{x-iy} - \eta A_z)(\hat{\mathbf{e}}_x + i\hat{\mathbf{e}}_y) + \frac{1}{2}i(\eta A_{x+iy} - \xi A_{x-iy})\hat{\mathbf{e}}_z. \end{aligned} \quad (\text{A.23})$$

## A.3 Vector differential operators

The differential operators of gradient of a scalar ( $\nabla u$ ), divergence of a vector ( $\nabla \cdot \mathbf{A}$ ), curl of a vector ( $\nabla \times \mathbf{A}$ ), Laplacian of a scalar ( $\nabla^2 u$ ), and Laplacian of a vector ( $\nabla^2 \mathbf{A}$ ) frequently encountered in electromagnetic field analysis will be listed in rectangular, spherical and mixed with conjugate coordinate systems.

### A.3.1 Rectangular coordinates

$$\nabla u = \frac{\partial u}{\partial x}\hat{\mathbf{e}}_x + \frac{\partial u}{\partial y}\hat{\mathbf{e}}_y + \frac{\partial u}{\partial z}\hat{\mathbf{e}}_z \quad (\text{A.24})$$

$$\nabla \cdot \mathbf{A} = \frac{\partial A_x}{\partial x} + \frac{\partial A_y}{\partial y} + \frac{\partial A_z}{\partial z} \quad (\text{A.25})$$

$$\nabla \times \mathbf{A} = \left(\frac{\partial A_z}{\partial y} - \frac{\partial A_y}{\partial z}\right)\hat{\mathbf{e}}_x + \left(\frac{\partial A_x}{\partial z} - \frac{\partial A_z}{\partial x}\right)\hat{\mathbf{e}}_y + \left(\frac{\partial A_y}{\partial x} - \frac{\partial A_x}{\partial y}\right)\hat{\mathbf{e}}_z \quad (\text{A.26})$$

$$\nabla \cdot \nabla u = \nabla^2 u = \frac{\partial^2 u}{\partial x^2} + \frac{\partial^2 u}{\partial y^2} + \frac{\partial^2 u}{\partial z^2} \quad (\text{A.27})$$

$$\nabla^2 \mathbf{A} = \nabla^2 A_x \hat{\mathbf{e}}_x + \nabla^2 A_y \hat{\mathbf{e}}_y + \nabla^2 A_z \hat{\mathbf{e}}_z \quad (\text{A.28})$$

### A.3.2 Spherical coordinates

$$\nabla u = \frac{\partial u}{\partial r}\hat{\mathbf{e}}_r + \frac{1}{r}\frac{\partial u}{\partial \theta}\hat{\mathbf{e}}_\theta + \frac{1}{r \sin \theta}\frac{\partial u}{\partial \phi}\hat{\mathbf{e}}_\phi \quad (\text{A.29})$$

$$\nabla \cdot \mathbf{A} = \frac{1}{r^2}\frac{\partial}{\partial r}(r^2 A_r) + \frac{1}{r \sin \theta}\frac{\partial}{\partial \theta}(A_\theta \sin \theta) + \frac{1}{r \sin \theta}\frac{\partial A_\phi}{\partial \phi} \quad (\text{A.30})$$

$$\begin{aligned}\nabla \times \mathbf{A} = & \frac{1}{r \sin \theta} \left[ \frac{\partial}{\partial \theta} (A_\phi \sin \theta) - \frac{\partial A_\theta}{\partial \phi} \right] \hat{\mathbf{e}}_r + \frac{1}{r} \left[ \frac{1}{\sin \theta} \frac{\partial A_r}{\partial \phi} - \frac{\partial}{\partial r} (r A_\phi) \right] \hat{\mathbf{e}}_\theta \\ & + \frac{1}{r} \left[ \frac{\partial}{\partial r} (r A_\theta) - \frac{\partial A_r}{\partial \theta} \right] \hat{\mathbf{e}}_\phi\end{aligned}\quad (\text{A.31})$$

$$\nabla^2 u = \frac{1}{r^2} \frac{\partial}{\partial r} \left( r^2 \frac{\partial u}{\partial r} \right) + \frac{1}{r^2 \sin \theta} \frac{\partial}{\partial \theta} \left( \sin \theta \frac{\partial u}{\partial \theta} \right) + \frac{1}{r^2 \sin^2 \theta} \frac{\partial^2 u}{\partial \phi^2} \quad (\text{A.32})$$

$$\nabla^2 \mathbf{A} = \nabla (\nabla \cdot \mathbf{A}) - \nabla \times \nabla \times \mathbf{A} \quad (\text{A.33})$$

Note that  $\nabla^2 \mathbf{A} \neq \nabla^2 A_r \hat{\mathbf{e}}_r + \nabla^2 A_\theta \hat{\mathbf{e}}_\theta + \nabla^2 A_\phi \hat{\mathbf{e}}_\phi$  since the orientation of the unit vectors  $\hat{\mathbf{e}}_r$ ,  $\hat{\mathbf{e}}_\theta$ , and  $\hat{\mathbf{e}}_\phi$  varies with the  $r$ ,  $\theta$ , and  $\phi$  coordinates.

### A.3.3 Conjugate coordinates

Some vector differential operators will be recalculated in the mixed of spherical and conjugate coordinate systems. We denote  $\cos \theta = \mu$ ,  $\sin \theta = \sqrt{1 - \mu^2}$ .

$$\begin{aligned}\nabla u = & \frac{1}{2r\sqrt{1-\mu^2}} \left[ (1-\mu^2) \left( r \frac{\partial u}{\partial r} - \mu \frac{\partial u}{\partial \mu} \right) + i \frac{\partial u}{\partial \phi} \right] (\hat{\mathbf{e}}_x - i \hat{\mathbf{e}}_y) \\ & + \frac{1}{2r\sqrt{1-\mu^2}} \left[ (1-\mu^2) \left( r \frac{\partial u}{\partial r} - \mu \frac{\partial u}{\partial \mu} \right) - i \frac{\partial u}{\partial \phi} \right] (\hat{\mathbf{e}}_x + i \hat{\mathbf{e}}_y) \\ & + \left( \mu \frac{\partial u}{\partial r} + \frac{1-\mu}{r} \frac{\partial u}{\partial \theta} \right) \hat{\mathbf{e}}_z, \quad (\text{A.34})\end{aligned}$$

$$\begin{aligned}\nabla u \times \mathbf{r} = & \frac{1}{2r\sqrt{1-\mu^2}} \left[ i(1-\mu^2) \frac{\partial u}{\partial \mu} + \mu \frac{\partial u}{\partial \phi} \right] (\hat{\mathbf{e}}_x - i \hat{\mathbf{e}}_y) \\ & + \frac{1}{2\sqrt{1-\mu^2}} \left[ -i(1-\mu^2) \frac{\partial u}{\partial \mu} + \mu \frac{\partial u}{\partial \phi} \right] (\hat{\mathbf{e}}_x + i \hat{\mathbf{e}}_y) - \frac{\partial u}{\partial \phi} \hat{\mathbf{e}}_z, \quad (\text{A.35})\end{aligned}$$

$$\begin{aligned}\nabla \times (\nabla u \times \mathbf{r}) = & \frac{1}{2} \left\{ -\frac{1}{r} \sqrt{1-\mu^2} \frac{\partial}{\partial \mu} \left[ (1-\mu^2) \frac{\partial u}{\partial \mu} \right] - \frac{1}{r\sqrt{1-\mu^2}} \frac{\partial^2 u}{\partial \phi^2} \right. \\ & \left. - \frac{\mu\sqrt{1-\mu^2}}{r} \frac{\partial}{\partial r} \left( r \frac{\partial u}{\partial \mu} \right) + \frac{i}{r\sqrt{1-\mu^2}} \frac{\partial}{\partial r} \left( r \frac{\partial u}{\partial \phi} \right) \right\} e^{i\phi} (\hat{\mathbf{e}}_x - i \hat{\mathbf{e}}_y) \\ & + \frac{1}{2} \left\{ -\frac{1}{r} \sqrt{1-\mu^2} \frac{\partial}{\partial \mu} \left[ (1-\mu^2) \frac{\partial u}{\partial \mu} \right] - \frac{1}{r\sqrt{1-\mu^2}} \frac{\partial^2 u}{\partial \phi^2} \right. \\ & \left. - \frac{\mu\sqrt{1-\mu^2}}{r} \frac{\partial}{\partial r} \left( r \frac{\partial u}{\partial \mu} \right) - \frac{i}{r\sqrt{1-\mu^2}} \frac{\partial}{\partial r} \left( r \frac{\partial u}{\partial \phi} \right) \right\} e^{-i\phi} (\hat{\mathbf{e}}_x + i \hat{\mathbf{e}}_y) \\ & + \left\{ -\frac{\mu}{r} \frac{\partial}{\partial \mu} \left[ (1-\mu^2) \frac{\partial u}{\partial \mu} \right] - \frac{\mu}{r(1-\mu^2)} \frac{\partial^2 u}{\partial \phi^2} + \frac{1-\mu^2}{r} \frac{\partial}{\partial r} \left( r \frac{\partial u}{\partial \mu} \right) \right\} \hat{\mathbf{e}}_z. \quad (\text{A.36})\end{aligned}$$

## A.4 Vector identities

### A.4.1 Addition and Multiplication

$$\mathbf{A} \cdot \mathbf{A} = |\mathbf{A}|^2 \quad (\text{A.37})$$

$$\mathbf{A} + \mathbf{B} = \mathbf{B} + \mathbf{A} \quad (\text{A.38})$$

$$\mathbf{A} \cdot \mathbf{B} = \mathbf{B} \cdot \mathbf{A} \quad (\text{A.39})$$

$$\mathbf{A} \times \mathbf{B} = -\mathbf{B} \times \mathbf{A} \quad (\text{A.40})$$

$$(\mathbf{A} + \mathbf{B}) \cdot \mathbf{C} = \mathbf{A} \cdot \mathbf{C} + \mathbf{B} \cdot \mathbf{C} \quad (\text{A.41})$$

$$(\mathbf{A} + \mathbf{B}) \times \mathbf{C} = \mathbf{A} \times \mathbf{C} + \mathbf{B} \times \mathbf{C} \quad (\text{A.42})$$

$$\mathbf{A} \cdot (\mathbf{B} \times \mathbf{C}) = \mathbf{B} \cdot (\mathbf{C} \times \mathbf{A}) = \mathbf{C} \cdot (\mathbf{A} \times \mathbf{B}) \quad (\text{A.43})$$

$$\mathbf{A} \times (\mathbf{B} \times \mathbf{C}) = (\mathbf{A} \cdot \mathbf{C})\mathbf{B} - (\mathbf{A} \cdot \mathbf{B})\mathbf{C} \quad (\text{A.44})$$

### A.4.2 Differentiation

$$\nabla \cdot (\nabla \times \mathbf{A}) = 0 \quad (\text{A.45})$$

$$\nabla \times \nabla u = 0 \quad (\text{A.46})$$

$$\nabla(u + v) = \nabla u + \nabla v \quad (\text{A.47})$$

$$\nabla(uv) = u\nabla v + v\nabla u \quad (\text{A.48})$$

$$\nabla \cdot (\mathbf{A} + \mathbf{B}) = \nabla \cdot \mathbf{A} + \nabla \cdot \mathbf{B} \quad (\text{A.49})$$

$$\nabla \times (\mathbf{A} + \mathbf{B}) = \nabla \times \mathbf{A} + \nabla \times \mathbf{B} \quad (\text{A.50})$$

$$\nabla \cdot (u\mathbf{A}) = \mathbf{A} \cdot \nabla u + u\nabla \cdot \mathbf{A} \quad (\text{A.51})$$

$$\nabla \times (u\mathbf{A}) = \nabla u \times \mathbf{A} + u\nabla \times \mathbf{A} \quad (\text{A.52})$$

$$\nabla(\mathbf{A} \cdot \mathbf{B}) = (\mathbf{A} \cdot \nabla)\mathbf{B} + (\mathbf{B} \cdot \nabla)\mathbf{A} + \mathbf{A} \times (\nabla \times \mathbf{B}) + \mathbf{B} \times (\nabla \times \mathbf{A}) \quad (\text{A.53})$$

$$\nabla \cdot (\mathbf{A} \times \mathbf{B}) = \mathbf{B} \cdot \nabla \times \mathbf{A} - \mathbf{A} \cdot \nabla \times \mathbf{B} \quad (\text{A.54})$$

$$\nabla \times (\mathbf{A} \times \mathbf{B}) = \mathbf{A}\nabla \cdot \mathbf{B} - \mathbf{B}\nabla \cdot \mathbf{A} + (\mathbf{B} \cdot \nabla)\mathbf{A} - (\mathbf{A} \cdot \nabla)\mathbf{B} \quad (\text{A.55})$$

$$\nabla \times \nabla \times \mathbf{A} = \nabla(\nabla \cdot \mathbf{A}) - \nabla^2 \mathbf{A} \quad (\text{A.56})$$

*This page is intentionally left blank.*

# Appendix B

## Special functions and their properties

### B.1 Associated Legendre functions

#### B.1.1 Definition

Associated Legendre functions  $P_n^m(\mu)$ <sup>†</sup> is defined by Stratton [12] as,

$$P_n^m \equiv \frac{1}{2^n n!} (1 - \mu^2)^{\frac{m}{2}} \frac{d^{n+m}}{d\mu^{n+m}} (\mu^2 - 1)^n. \quad (\text{B.1})$$

#### B.1.2 Properties

##### Symmetry relation

$$P_n^{-m} = (-1)^m \frac{(n-m)!}{(n+m)!} P_n^m \quad (\text{B.2})$$

##### Recursive relations

1.

$$\sqrt{1 - \mu^2} \frac{dP_n^m}{d\mu} = P_n^{m+1} - \frac{m\mu}{\sqrt{1 - \mu^2}} P_n^m \quad (\text{B.3})$$

2.

$$\sqrt{1 - \mu^2} \frac{dP_n^m}{d\mu} = -(n+m)(n-m+1) P_n^{m-1} + \frac{m\mu}{\sqrt{1 - \mu^2}} P_n^m \quad (\text{B.4})$$

3.

$$\mu P_n^m = \frac{n+m}{2n+1} P_{n-1}^m + \frac{n-m+1}{2n+1} P_{n+1}^m \quad (\text{B.5})$$

4.

$$(1 - \mu^2) \frac{dP_n^m}{d\mu} = \frac{(n+1)(n+m)}{2n+1} P_{n-1}^m - \frac{n(n+m-1)}{2n+1} P_{n+1}^m \quad (\text{B.6})$$

---

<sup>†</sup>In this appendix, we simplified  $P_n^m(\mu)$  as  $P_n^m$ .  $\mu$  is a real number and  $m, n$  are integers.



5.

$$\sqrt{1-\mu^2}P_n^m = -\frac{1}{2n+1}P_{n-1}^{m+1} + \frac{1}{2n+1}P_{n+1}^{m+1} \quad (\text{B.7})$$

6.

$$\mu\sqrt{1-\mu^2}\frac{dP_n^m}{d\mu} + \frac{mP_n^m}{\sqrt{1-\mu^2}} = \frac{n+1}{2n+1}P_{n-1}^{m+1} + \frac{n}{2n+1}P_{n+1}^{m+1} \quad (\text{B.8})$$

7.

$$\sqrt{1-\mu^2}P_n^m = \frac{(n+m+1)(n+m)}{2n+1}P_{n-1}^{m-1} - \frac{(n-m+1)(n-m+2)}{2n+1}P_{n+1}^{m-1} \quad (\text{B.9})$$

## B.2 Spherical Bessel functions

### B.2.1 Definition

#### The spherical Bessel function of the first kind

The spherical Bessel function of the first kind, denoted  $j_n(\rho)$ , is defined by,

$$j_n(\rho) \equiv \sqrt{\frac{\pi}{2\rho}}J_{n+\frac{1}{2}}(\rho), \quad (\text{B.10})$$

where  $J_n(\rho)$  is a Bessel function of the first kind<sup>‡</sup>.

#### The spherical Bessel function of the second kind

The spherical Bessel function of the second kind, denoted  $y_n(\rho)$ , is defined by,

$$y_n(\rho) \equiv \sqrt{\frac{\pi}{2\rho}}Y_{n+\frac{1}{2}}(\rho), \quad (\text{B.11})$$

where  $Y_n(\rho)$  is a Bessel function of the second kind.

#### The spherical Hankel function of the first kind

The spherical Hankel function of the first kind  $h_n^{(1)}(\rho)$  is defined by,

$$\begin{aligned} h_n^{(1)}(\rho) &\equiv \sqrt{\frac{\pi}{2\rho}}H_{n+\frac{1}{2}}^{(1)}(\rho) \\ &= j_n(\rho) + iy_n(\rho), \end{aligned} \quad (\text{B.12})$$

where  $H_{n+\frac{1}{2}}^{(1)}(\rho)$  is the Hankel function of the first kind and  $j_n(\rho)$  and  $y_n(\rho)$  are the spherical Bessel functions of the first and second kinds.

---

<sup>‡</sup>In this dissertation,  $\rho$  is a complex number and  $n$  is an integer.

### The spherical Hankel function of the second kind

The spherical Hankel function of the second kind  $h_n^{(2)}(\rho)$  is defined by,

$$\begin{aligned} h_n^{(2)}(\rho) &\equiv \sqrt{\frac{\pi}{2\rho}} H_{n+\frac{1}{2}}^{(2)}(\rho) \\ &= j_n(\rho) - iy_n(\rho), \end{aligned} \quad (\text{B.13})$$

where  $H_{n+\frac{1}{2}}^{(2)}(\rho)$  is the Hankel function of the second kind and  $j_n(\rho)$  and  $y_n(\rho)$  are the spherical Bessel functions of the first and second kinds.

## B.2.2 Properties

### Symmetry relations

1.

$$j_n(-\rho) = (-1)^n j_n(\rho) \quad (\text{B.14})$$

2.

$$y_n(-\rho) = (-1)^{n+1} y_n(\rho) \quad (\text{B.15})$$

3.

$$y_n(\rho) = (-1)^{n+1} j_{-n-1}(\rho) \quad (\text{B.16})$$

### Recursive relations

The spherical Bessel and Hankel functions satisfy many useful relations. Here we only mention the following recurrence relations, which are common to all the spherical Bessel and Hankel functions. Accordingly in the following formulas, we denote the function by  $z_n$ , which is one of  $j_n(\rho)$ ,  $y_n(\rho)$ ,  $h_n^{(1)}(\rho)$ , or  $h_n^{(2)}(\rho)$ ,

1.

$$z_{n-1} + z_{n+1} = \frac{2n+1}{\rho} z_n, \quad (\text{B.17})$$

2.

$$nz_{n-1} - (n+1)z_{n+1} = (2n+1)z'_n, \quad (\text{B.18})$$

3.

$$\frac{n+1}{\rho} z_n + z'_n = z_{n-1}, \quad (\text{B.19})$$

4.

$$\frac{n}{\rho} z_n - z'_n = z_{n+1}. \quad (\text{B.20})$$

Here the prime denotes derivative with respect to the argument.

*This page is intentionally left blank.*

# Appendix C

## Recursive relations of spherical harmonics

In this appendix, we will derive the recursive relations of scalar and vector spherical harmonics by using the recursive relations of Bessel and Legendre functions (given in Appendix B) in Conjugate coordinates (see Appendix A). Only final results are listed here.

### C.1 Scalar spherical harmonics $u_{mn}$

The scalar spherical harmonics  $u_{mn}^{(j)}$  are given by,

$$u_{mn}^{(j)} = z_n^{(j)}(r) P_n^m(\cos \theta) e^{im\phi}, \quad (\text{C.1})$$

where  $z_n^{(j)}$  is the appropriate kind of spherical Bessel functions  $j_n, y_n, h_n^{(1)}$ , and  $h_n^{(2)}$ , for  $j = 1, 2, 3$ , and 4, respectively; we used only the value of  $j = 1$  and 3 in our work;  $(r, \theta, \phi)$  are three coordinates of vector position  $\mathbf{r}$ . By taking the gradient of  $u_{mn}^{(j)}$ , resolving in the conjugate coordinates, and utilizing the recursive relations for Bessel and Legendre functions, the following equations are obtained,

$$(\hat{\mathbf{e}}_x + i\hat{\mathbf{e}}_y) \cdot \nabla u_{mn}^{(j)} = -\frac{1}{2n+1} \left( u_{m+1n-1}^{(j)} + u_{m+1n+1}^{(j)} \right), \quad (\text{C.2})$$

$$(\hat{\mathbf{e}}_x - i\hat{\mathbf{e}}_y) \cdot \nabla u_{mn}^{(j)} = \frac{1}{2n+1} \left[ (n+m-1)(n+m) u_{m-1n-1}^{(j)} + (n-m+1)(n-m+2) u_{m-1n+1}^{(j)} \right], \quad (\text{C.3})$$

$$\hat{\mathbf{e}}_z \cdot \nabla u_{mn}^{(j)} = \frac{1}{2n+1} \left[ (n+m) u_{mn-1}^{(j)} - (n-m+1) u_{mn+1}^{(j)} \right]. \quad (\text{C.4})$$

### C.2 Vector spherical harmonics $\mathbf{M}_{mn}$

We have a relation between vector spherical harmonics  $\mathbf{M}_{mn}^{(j)}$  and scalar spherical harmonics  $u_{mn}^{(j)}$ ,

$$\mathbf{M}_{mn}^{(j)} = \nabla u_{mn}^{(j)} \times \mathbf{r}, \quad (\text{C.5})$$

where  $\mathbf{r} = (r, \theta, \phi)$  is the vector position. By taking the cross product of gradient of  $u_{mn}^{(j)}$  and the vector position  $\mathbf{r}$ , the following equations are obtained,

$$(\hat{\mathbf{e}}_x + i\hat{\mathbf{e}}_y) \cdot \mathbf{M}_{mn}^{(j)} = iu_{m+1n}^{(j)}, \quad (\text{C.6})$$

$$(\hat{\mathbf{e}}_x - i\hat{\mathbf{e}}_y) \cdot \mathbf{M}_{mn}^{(j)} = i(n+m)(n-m+1)u_{m-1n}^{(j)}, \quad (\text{C.7})$$

$$\hat{\mathbf{e}}_z \cdot \mathbf{M}_{mn}^{(j)} = -imu_{mn}^{(j)}. \quad (\text{C.8})$$

### C.3 Vector spherical harmonics $\mathbf{N}_{mn}$

We have a relation between vector spherical harmonics  $\mathbf{N}_{mn}^{(j)}$  and  $\mathbf{M}_{mn}^{(j)}$ ,

$$\mathbf{N}_{mn}^{(j)} = \frac{1}{\tilde{k}} \nabla \times \mathbf{M}_{mn}^{(j)} = \frac{1}{\tilde{k}} \nabla \times (\nabla \times u_{mn}^{(j)}). \quad (\text{C.9})$$

Without loss of generality, we can use the normalized wave number  $\tilde{k} = 1$ , and we have,

$$\mathbf{N}_{mn}^{(j)} = \nabla \times \mathbf{M}_{mn}^{(j)} = \nabla \times (\nabla \times u_{mn}^{(j)}). \quad (\text{C.10})$$

By taking the curl of  $\mathbf{M}_{mn}^{(j)}$ , the following equations are obtained,

$$(\hat{\mathbf{e}}_x + i\hat{\mathbf{e}}_y) \cdot \mathbf{N}_{mn}^{(j)} = \frac{1}{2n+1} \left[ -(n+1)u_{m+1n-1}^{(j)} + nu_{m+1n+1}^{(j)} \right], \quad (\text{C.11})$$

$$\begin{aligned} (\hat{\mathbf{e}}_x - i\hat{\mathbf{e}}_y) \cdot \mathbf{N}_{mn}^{(j)} = \frac{1}{2n+1} \Big[ & (n+1)(n+m-1)(n+m)u_{m-1n-1}^{(j)} \\ & - n(n-m+1)(n-m+2)u_{m-1n+1}^{(j)} \Big], \end{aligned} \quad (\text{C.12})$$

$$\hat{\mathbf{e}}_z \cdot \mathbf{N}_{mn}^{(j)} = \frac{1}{2n+1} \left[ (n+1)(n+m)u_{mn-1}^{(j)} + n(n-m+1)u_{mn+1}^{(j)} \right]. \quad (\text{C.13})$$

# Bibliography

- [1] G. Mie, “Contributions on the optics of turbid media, particularly colloidal metal solutions (translation),” *Ann. Phys.*, vol. 330, pp. 377–445, 1908.
- [2] B. Friedman and J. Russek, “Addition theorems for spherical waves,” *Quart. Appl. Math.*, vol. 12, p. 13, 1954.
- [3] S. Stein, “Addition theorems for spherical wave functions,” *Quart. Appl. Math.*, vol. 19, p. 15, 1961.
- [4] O. R. Cruzan, “Translational addition theorems for spherical vector wave functions,” *Quart. Appl. Math.*, vol. 20, p. 33, 1962.
- [5] J. H. Bruning and Y. T. Lo, “Multiple scattering of EM waves by spheres, part I & II,” *IEEE Trans. Ant. Prop.*, vol. 19, pp. 378–390 & 391–400, 1971.
- [6] K. A. Fuller and G. W. Kattawar, “Consummate solution to the problem of classical electromagnetic scattering by ensembles of spheres. I & II,” *Opt. Lett.*, vol. 13, pp. 90–92 & 1063–1065, 1988.
- [7] F. Borghese, P. Denti, G. Toscano, and O. I. Sindoni, “Electromagnetic scattering by a cluster of spheres,” *Appl. Opt.*, vol. 18, pp. 116–120, 1979.
- [8] D. W. Mackowski, “Analysis of radiative scattering for multiple sphere configurations,” *Proc. R. Soc. Lond. A*, vol. 433, pp. 599–614, 1991.
- [9] Y. L. Xu, “Electromagnetic scattering by an aggregate of spheres,” *Appl. Opt.*, vol. 34, pp. 4573–4588, 1995.
- [10] D. W. Mackowski, K. Fuller, and M. I. Mishchenko, “Codes for Calculation of Scattering by Clusters of Spheres,” 1999.
- [11] Y. L. Xu, “Fortran codes for multi-particle light-scattering calculations,” 2003.
- [12] J. A. Stratton, *Electromagnetic Theory*. McGraw-Hill, 1941.
- [13] W. J. Wiscombe, “Improved Mie scattering algorithms,” *Appl. Opt.*, vol. 19, pp. 1505–1509, 1980.

- 
- [14] D. W. Mackowski, "Calculation of total cross sections of multiple-sphere clusters," *J. Opt. Soc. Am. A*, vol. 11, pp. 2851–2861, 1994.
  - [15] Y. L. Xu, "Calculation of the Addition Coefficients in Electromagnetic Multisphere-Scattering theory," *J. Comput. Phys.*, vol. 127, pp. 285–298, 1996.
  - [16] D. W. Mackowski and M. I. Mishchenko, "Calculation of the T matrix and the scattering matrix for ensembles of spheres," *J. Opt. Soc. Am. A*, vol. 13, pp. 2266–2278, 1996.
  - [17] W. Y. Chien and T. Szkopek, "Multiple-multipole simulation of optical nearfields in discrete metal nanosphere assemblies," *Opt Express*, vol. 16, pp. 1820–1835, 2008.
  - [18] A. R. Edmonds, *Angular momentum in quantum mechanics*. Princeton University Press, 1957.
  - [19] N. T. Dong, M. Tanaka, and K. Tanaka, "Improved Algorithms for Calculating Addition Coefficients in Electromagnetic Scattering by Multi-Sphere Systems," *IEICE TRANSACTIONS on Electronics*, vol. E95-C, no. 1, pp. 27–35, 2012.
  - [20] J. Kim and K.-B. Song, "Recent progress of nano-technology with NSOM," *Micron*, vol. 38, pp. 409–426, 2007.
  - [21] D. Pohl, "Scanning Near-field Optical Microscopy (SNOM),," *Advances in Optical and Electron Microscopy*, vol. 12, pp. 243–312, 1991.
  - [22] H. Heinzelmann and D. Pohl, "Scanning near-field optical microscopy," *Appl. Phys. A*, vol. 59, no. 2, pp. 89–101, 1994.
  - [23] B. Hecht, B. Sick, U. P. Wild, V. Deckert, R. Zenobi, O. J. F. Martin, and D. W. Pohl, "Scanning near-field optical microscopy with aperture probes: Fundamentals and applications," *J. Chem. Phys.*, vol. 112, no. 18, pp. 7761–7774, 2000.
  - [24] H. Aoki, T. Hamamatsu, and S. Ito, "Deep ultraviolet scanning near-field optical microscopy for the structural analysis of organic and biological materials," *Appl. Phys. Lett.*, vol. 84, no. 3, pp. 356–358, 2004.
  - [25] J. A. J. Backs, S. Sederberg, and A. Y. Elezzabi, "A nanoplasmonic probe for near-field imaging," *Optics Express*, vol. 19, no. 12, pp. 11280–11289, 2011.
  - [26] Y.-H. Lin and D. P. Tsai, "Near-field scanning optical microscopy using a super-resolution cover glass slip," *Optics Express*, vol. 20, no. 15, pp. 16205–16211, 2012.
  - [27] Y. Inouye and S. Kawata, "Reflection-mode near-field optical microscope with a metallic probe tip for observing fine structures in semiconductor materials," *Opt. Commun.*, vol. 134, pp. 31–35, 1996.

- [28] P. B. Johnson and R. W. Christy, "Optical Constants of the Noble Metals," *Phys. Rev. B*, vol. 6, no. 12, p. 43704379, 1972.
- [29] E. Setijadi, A. Matsushima, N. Tanaka, and G. Hendrantoro, "Effect of temperature and multiple scattering on rain attenuation of electromagnetic waves by a simple spherical model," *Progress In Electromagnetics Research*, vol. 99, pp. 339–354, 2009.
- [30] M. Bahrami, J. Rashed-Mohassel, and M. Mohammad-Taheri, "An exact solution of coherent wave propagation in rain medium with realistic raindrop shapes," *Progress In Electromagnetics Research*, vol. 79, pp. 107–118, 2008.
- [31] S. Kanellopoulos, A. Panagopoulos, and J. Kanellopoulos, "Calculation of electromagnetic scattering from a pruppacher-pitter raindrop using m.a.s. and slant path rain attenuationprediction," *International Journal of Infrared and Millimeter Waves*, vol. 26, no. 12, pp. 1783–1802, 2005.
- [32] F. Moupfouma, "A new theoretical formulation for calculation of the specific attenuation due to precipitation particles on terrestrial and satellite radio links," *Int. J. Satellite Com.*, vol. 15, pp. 89–99, 1997.
- [33] F. M. Filho, R. S. Cole, and A. Sarma, "Millimeterwave rain induced attenuation: theory and experiment," *IEE Proceedings*, vol. 133, no. 4, pp. 308–314, 1986.
- [34] D. Cermak, O. Fiser, and V. Schejbal, "Electromagnetic scattering by rain drops," *Cost 280*, 2005.
- [35] R. K. Crane, *Electromagnetic Wave Propagation through Rain*. John Wiley & Sons, New York, 1996.
- [36] W. Zhensen, Y. Yi, and C. Lihong, "Monte Carlo simulation for millimeter wave propagation and scattering in rain medium," *International Journal of Infrared and Millimeter Waves*, vol. 13, pp. 981–994, 1992.
- [37] A. Ishimaru, R. Woo, J. W. Armstrong, and D. C. Blackman, "Multiple scattering calculations of rain effects," *Radio Science*, vol. 17, no. 6, pp. 1425–1433, 1982.
- [38] A. Tsolakis and W. L. Stutzman, "Multiple scattering of electromagnetic waves by rain," *Radio Science*, vol. 17, no. 6, pp. 1495–1502, 1982.
- [39] D. V. Rogers and R. L. Olsen, "Multiple scattering in coherent radiowave propagation through rain," *COMSAT Technical Review*, vol. 13, pp. 385–401, 1983.
- [40] M. Sekine, C.-D. Chen, and T. Musha, "Rain attenuation from log-normal and Weibull raindrop-size distributions," *IEEE Trans. on Antennas and Propagation*, vol. 35, no. 3, pp. 358–359, 1987.



- [41] J. S. Marshall and W. Palmer, "The distributions of raindrop with size," *Journal of Meteorology*, vol. 5, pp. 165–166, 1948.
- [42] T. Meissner and F. Wentz, "The complex dielectric constant of pure and sea water from microwave satellite observations," *IEEE Trans Geosci Remote Sens.*, vol. 42, pp. 1836–1849, 2004.
- [43] J. Joss, J. Thams, and A. Waldvogel, "The Variation of raindrops size distribution at Locarno," *Proc. of Inter. Conf. on Cloud Physics*, pp. 369–373, 1968.
- [44] G. Ajayi and I. Adimula, "Variation in raindrop size distribution and specific attenuation due to rain in nigeria," *Ann. Telecom*, vol. 51, no. 1-2, pp. 87–93, 1996.

# List of Publications by the Author

## Journal Publications

1. Nguyen Tien Dong, Masahiro Tanaka, and Kazuo Tanaka, Improved Algorithms for Calculating Addition Coefficients in Electromagnetic Scattering by Multi-Sphere Systems, IEICE TRANSACTIONS on Electronics, vol. E95-C, no. 1, pp. 2735, 2012.

## International Conference Publications

1. Nguyen Tien Dong, Masahiro Tanaka, and Kazuo Tanaka, Analysis and computation of electromagnetic scattering by multiple spheres configuration, in Third International Conference on Communications and Electronics (ICCE2010), Nha Trang, Vietnam, 2010.
2. Nguyen Tien Dong, Masahiro Tanaka, and Kazuo Tanaka, Electromagnetic scattering by multiple spheres configuration, in 2010 Asia-Pacific Radio Science Conference (AP-RASC10), Toyama, Japan, B1-2, 2010.
3. Nguyen Tien Dong, Masahiro Tanaka, and Kazuo Tanaka, Electromagnetic scattering by multi-spheres systems and its application for calculating rain attenuation, in International Symposium on Antennas and Propagation (ISAP2012), Nagoya, Japan, P0359, 2012.

## Domestic Conference Publications

1. Nguyen Tien Dong, Masahiro Tanaka, Kazuo Tanaka, and Tran Trong Minh, The calculation of far-field scattering properties by multiple spheres configuration, in IEICE Society Conference, Niigata, Japan, C1-12, 2009.
2. Nguyen Tien Dong, Masahiro Tanaka, Kazuo Tanaka, and Tran Trong Minh, Analysis of electromagnetic scattering from multiple spheres configuration, in The paper of Technical Meeting on Electromagnetic Theory, IEE Japan, Okinawa, Japan, EMT-09-102, 2009.

3. Nguyen Tien Dong, Masahiro Tanaka, and Kazuo Tanaka, Numerical analysis of electromagnetic scattering from multiple spheres configuration, in The paper of Technical Meeting on Electromagnetic Theory, IEE Japan, Tokyo, Japan, EMT-10- 058, 2010.
4. Nguyen Tien Dong, Masahiro Tanaka, and Kazuo Tanaka, Analysis of scanning near-field optical microscopy with simple models, in The paper of Technical Meeting on Electromagnetic Theory, IEE Japan, Fukushima, Japan, EMT-10-148, 2010.
5. Nguyen Tien Dong, Masahiro Tanaka, and Kazuo Tanaka, Improved algorithm for calculating addition coefficients in electromagnetic scattering by multiple spheres configuration, in The paper of Technical Meeting on Electromagnetic Theory, IEE Japan, Tokyo, Japan, EMT-11-056, 2011.
6. Nguyen Tien Dong, Masahiro Tanaka, and Kazuo Tanaka, Electromagnetic scattering of gaussian beams by multiple spheres configuration, in The paper of Technical Meeting on Electromagnetic Theory, IEE Japan, Toyama, Japan, EMT-11-140, 2011.
7. Nguyen Tien Dong, Masahiro Tanaka, and Kazuo Tanaka, Analysis of electromagnetic scattering by multiple spheres configuration and its application for SNOM models, in 2012 IEICE General Conference, Okayama, Japan, C-1-17, 2012.
8. Nguyen Tien Dong, Masahiro Tanaka, and Kazuo Tanaka, Rain attenuation of electromagnetic waves by multiple spheres model, in The paper of Technical Meeting on Electromagnetic Theory, IEE Japan, Hokkaido, Japan, EMT-12-081, 2012.
9. Nguyen Tien Dong, Masahiro Tanaka, and Kazuo Tanaka, Rain attenuation of electromagnetic waves by multiple spheres model with various raindrop-size distributions, in The paper of Technical Meeting on Electromagnetic Theory, IEE Japan, Kyushu, Japan, EMT-12-141, 2012.